LEADING EDGE REVIEW

High temperature shape memory alloys

J. Ma[1], I. Karaman*[1,2] and R. D. Noebe[3]

Shape memory alloys (SMAs) with high transformation temperatures can enable simplifications and improvements in operating efficiency of many mechanical components designed to operate at temperatures above 100°C, potentially impacting the automotive, aerospace, manufacturing and energy exploration industries. A wide range of these SMAs exists and can be categorised in three groups based on their martensitic transformation temperatures: group I, transformation temperatures in the range of 100–400°C; group II, in the range of 400–700°C; and group III, above 700°C. In addition to the high transformation temperatures, potential high temperature shape memory alloys (HTSMAs) must also exhibit acceptable recoverable transformation strain levels, long term stability, resistance to plastic deformation and creep, and adequate environmental resistance. These criteria become increasingly more difficult to satisfy as their operating temperatures increase, due to greater involvement of thermally activated mechanisms in their thermomechanical responses. Moreover, poor workability, due to the ordered intermetallic structure of many HTSMA systems, and high material costs pose additional problems for the commercialisation of HTSMAs. In spite of these challenges, progress has been made through compositional control, alloying, and the application of various thermomechanical processing techniques to the point that several likely applications have been demonstrated in alloys such as Ti–Ni–Pd and Ti–Ni–Pt. In the present work, a comprehensive review of potential HTSMA systems are presented in terms of physical and thermomechanical properties, processing techniques, challenges and applications.

Keywords: High temperature shape memory alloys, Intermetallics, Thermomechanical processing, Shape memory effect, Superelasticity, Martensitic transformation

I. Introduction

Since the discovery of shape memory alloys (SMAs), much progress has been made both in the scientific understanding and application of these multifunctional materials. Owing to the unique behaviours of shape memory effect and superelasticity, SMAs have become a major materials class of choice in the biomedical industry and are beginning to permeate into other technological areas. However, the complexity of their governing microstructural mechanisms and physical behaviours have rendered sporadic commercial interest in these materials. Nevertheless, there is a recent revitalisation of interest in SMAs, driven primarily by the aerospace and automotive industries, for their potential to operate as solid state actuators.

Shape memory effect is a phenomenon whereby a deformed material could recover its predeformed shape after being heated. When this procedure is performed against some biasing force, the material is capable of doing work from its shape change. Superelasticity is an isothermal phenomenon where the material is able to recover high amounts of strain (up to more than 20% in a few single crystalline alloys) triggered by mechanical stress. These two behaviours are the result of reversible martensitic transformation – a diffusionless solid state phase transformation mechanism that can be activated by temperature, stress and magnetic field.

Current practical uses for SMAs are, however, limited to temperatures below 100°C. This is the transformation temperature limit of the two most commercially successful SMA systems: the near equiatomic Ni–Ti binary and Cu based ternary alloys. During thermomechanical processes required to produce stable shape memory or superelastic behaviour, the transformation temperatures are further reduced.[1] Naturally, such limitation hinders the utility of SMAs in high temperature applications, and necessitates design modifications for SMA containing components in order to reduce operating temperatures to below 100°C, or completely abandon their use. On the other hand, the unique properties of SMAs become even more beneficial at high temperatures, since it is preferable to adopt single piece adaptive and multifunctional components over more complex multicomponent assemblies due to the higher

[1]Department of Mechanical Eng., Texas A&M University, College Station, TX 77843 3123, USA
[2]Materials Science and Eng. Interdisciplinary Graduate Program, Texas A&M University, College Station, TX 77843 3003, USA
[3]NASA Glenn Research Center, MS 49–3, Cleveland, OH 44135, USA

*Corresponding author, email ikaraman@tamu.edu

Published by Maney for the Institute and ASM International
DOI 10.1179/09506601OX12646898728363

likelihood of wear or damage and the greater weight and volume required by the latter. These issues have triggered several studies on possible SMAs with transformation temperatures above 100°C. This class of materials is simply referred to as high temperature shape memory alloys (HTSMAs). As of now, despite intensive research efforts in recent years, HTSMAs have yet to be utilised commercially in appreciable amounts due to a number of unresolved issues.

Several recent reviews on HTSMAs are available,[2–7] but the majority is restricted in scope to the basic metallurgical properties of reported materials and/or focus on only a few alloy systems. The present work seeks to provide a more comprehensive coverage of the possible alloy systems that display high temperature shape memory and superelastic behaviours, as well as processing techniques and the potential applications of HTSMAs. In addition, we intend to provide a resource for industry and facilitate the introduction of SMAs into commercial high temperature applications. The primary target of this article is centred upon thermomechanical properties of SMAs, namely the transformation temperatures, shape memory and superelastic behaviours, and the bulk of the discussion on individual alloy systems will focus on the quantification of these properties, processes that have been shown to improve them, and governing microstructural phenomena in their operation. Topics such as physics, thermodynamics and crystallographic theory of martensitic transformation will not be addressed in detail.

First, a brief introductory discussion of SMAs is included for readers unfamiliar with these materials in Section II. Section II.1 is designed to provide a basic understanding of SMAs for non-experts in this field. The section evolves around the stress–temperature phase diagram where transformation temperatures are plotted as a function of applied stress. Various phenomena related to SMAs, such as shape memory and superelastic behaviour, are described based on the deformation temperature relative to the transformation temperatures, and microstructural changes that take place during these behaviours. The origin of two way shape memory effect and processes that create it are also discussed.

Following this, the focus is shifted toward important engineering properties of shape memory and superelastic behaviour, such as recoverable strain, irrecoverable strain, thermal and stress hysteresis, and work output. In Section II.2, primary factors that affect these properties are discussed. These topics include effects on shape memory and superelastic behaviour from conventional processing techniques – work hardening and precipitation hardening, the role of crystallographic texture, the effect of martensite/austenite structure, and variables unique to HTSMAs, such as oxidation and creep. In essence, this section addresses the question of how one may be able to improve shape memory and superelastic behaviour.

Section III provides detailed information on individual HTSMA systems based on the following temperature ranges: 100–400°C, 400–700°C and above 700°C. These temperature ranges were chosen based on temperature ranges of potential applications. The critical characteristic transformation temperatures of the alloys will be used for their classification, i.e. martensite finish temperature M_f will be used for alloys studied for shape memory effect and austenitic finish temperature A_f will be used for those studied for superelastic behaviour. Unconventional processing techniques such as rapid solidification, physical vapour deposition and severe plastic deformation will also be discussed in subsections for each alloy system. Finally, some proposed applications of HTSMAs will be summarised in Section IV and the present article will conclude by recapping some major problems and challenges facing the development and commercialisation of HTSMAs.

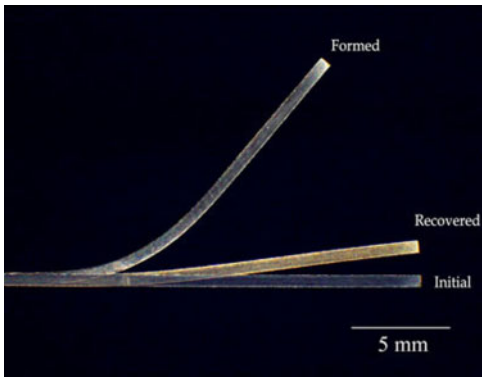

1 The one way shape memory effect: the initial SMA strip is deformed to the 'formed' state, but upon heating, the strip is able to return to its nearly undeformed shape.[7] (Reproduced with permission from The Taylor & Francis Group)

II. Basics of SMAs and issues at high temperatures

II.1. Brief introduction to SMAs

For readers less familiar with SMAs, a brief overview of these materials is provided here. Since the present article is focused primarily on the thermomechanical behaviours of HTSMAs such as shape memory effect and superelasticity, a detailed description of these behaviors and the underlying microstructural mechanisms are reviewed.

One way shape memory effect and superelasticity are the most frequently utilised SMA behaviours in applications. One way shape memory effect refers to the ability of an SMA deformed at a low temperature to recover the deformation when heated to a higher temperature. In other words, the material is able to memorise its undeformed shape (Fig. 1). Superelasticity refers to the ability of SMAs to recover large amounts of stress induced inelastic deformation immediately upon unloading. Both behaviours are a consequence of the reversible martensitic transformation.

II.1·1. Mechanisms of shape memory effect and superelasticity

Martensitic transformation is a solid to solid phase transformation that occurs through a coordinated shear movement of atoms over very short (on the order of angstroms) distances where atoms retain close relationship with one another, as opposed to random long range diffusion of atoms. The high temperature phase, austenite, transforms to a low temperature phase, martensite, upon cooling. Because the crystal structure of austenite is different than that of martensite, it is

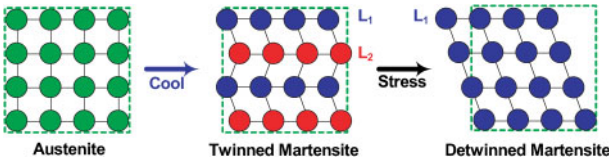

2 A simplified illustration of the austenite and martensite structures. In the absence of stress, austenite transforms to twinned martensite upon cooling in order to accommodate strain caused by a change in crystal structure. The twinned martensite is composed of multiple (usually two) twin related lattice correspondence variants, labelled L_1 and L_2 in this figure. When stress is applied, the martensite may detwin, resulting in a single lattice correspondence variant structure and a net shape change

possible to introduce a macroscopic shape change that accompanies the transformation.

When martensite forms in austenite, the difference in their crystal structures generates large amounts of local strain. This strain is large enough so that it cannot be purely accommodated elastically. Instead in SMAs, which undergo reversible martensitic phase transformation, the strain is accommodated by producing a twinned martensite structure (see Fig. 2). When the higher symmetry austenite transforms to the lower symmetry martensite, it may do so in several 'ways', called martensite lattice correspondence variants. The number of such variants that can be formed is determined by the symmetry of martensite and austenite; for example, there are 12 lattice correspondence variants of a monoclinic martensite to a cubic austenite.[8] In essence, each lattice correspondence variant is a 'variation' of the martensite with a different orientation relationship to the austenite, but they are all energetically equivalent to one another under stress free conditions. By forming a structure of twin related lattice correspondence variants, the martensite is able to accommodate a significant portion of the strain associated with the change in crystal structure, as shown in Fig. 2. These twin related lattice correspondence variants are collectively referred to as a habit plane variant, and several different habit plane variants can then be formed in such a way that together, they reduce the remaining strain of the transformation. This means that the transformation from austenite to martensite can be made to produce nearly no macroscopic shape change, and the resulting structure of the martensite phase that accomplishes this is then considered to be 'self-accommodated', as seen in Fig. 3. Under an external biasing stress, certain habit plane variants become energetically favoured and form/grow at the expense of others in a process known as martensite reorientation. In addition, the martensite may also detwin, where analogously, the lattice correspondence variant favoured under stress grows at the expense of others. Both martensite reorientation and detwinning results in a macroscopic shape change, and give rise to the shape memory behaviour and superelasticity. More details can be found in the literature regarding the nature of martensitic transformation,[9–11] structural description of twinning in martensite,[12–18] and self-accommodation.[19–25] For the sake of simplicity, detwinning and martensite reorientation will be treated as the same mechanism in this introductory section.

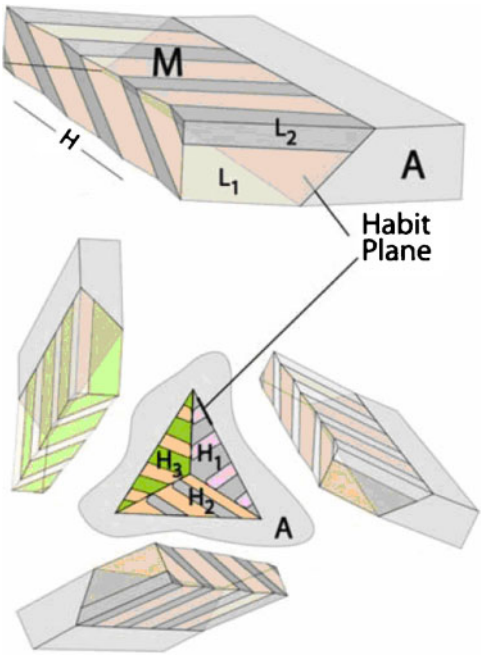

3 Process of self-accommodation in martensite;[13] L_1 and L_2 are two different lattice correspondence variants. Under no stress, pairs of twin related lattice correspondence variants form a habit plane variant (H_1, H_2 and H_3), shown in top figure, and several habit plane variants can then arrange themselves in such a way that results in no net shear, and approximate no volume change from the transformation, shown in the middle triangle. When external stress is applied, the degeneracy of the various habit plane variants and lattice correspondence variants are lifted, and the most favourable variant – the one most available to accommodate the desired strain – is formed at the expense of others. Reproduced with permission from Springer Science and Business Media

The martensitic transformation can be induced both thermally and through the application of external stress. In other words, application of stress and reduction in temperature both act as driving forces for the austenite→martensite transformation. In fact, there is a linear relationship between the two. This relationship is derived from the thermodynamics relationships of phase transformation and is called the Clausius–Clapeyron relationship. Roughly, it states that $d\sigma/dT$ =constant, and the transformation temperature is a straight line in the $\sigma-T$ space seen in Fig. 4.

The transformation process, however, is somewhat more complicated than that illustrated in Fig. 4. In general, the transformation is not completed immediately at a single temperature, but occurs gradually over a range of temperature. The temperature during cooling at which the transformation from austenite to martensite, or the forward transformation, first begins is called the martensite start temperature, M_s. The temperature at which the forward transformation reaches completion is called the martensite finish temperature, M_f. Conversely, upon heating above the austenite start temperature, A_s, the martensite begins to transform back to austenite – the reverse transformation. The temperature at which reverse transformation is completed is the austenite finish temperature, A_f. Each of these temperatures approximately

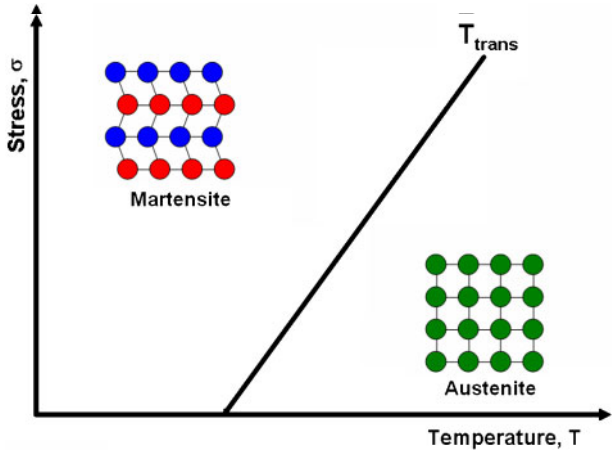

4 **The linear relationship between transformation temperature and applied stress: an increase in applied stress results in a corresponding increase in transformation temperature**

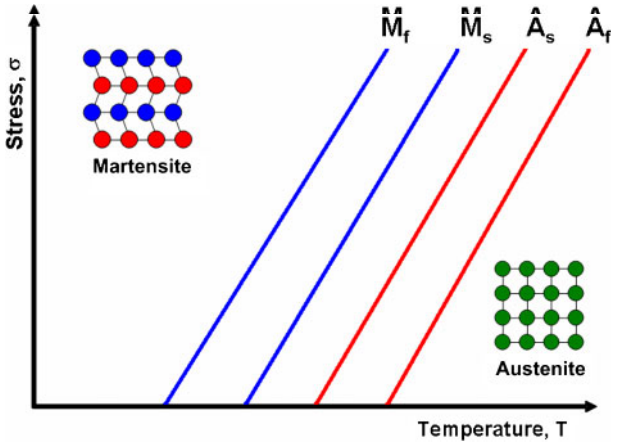

5 **A σ–T phase diagram of SMAs undergoing martensitic transformation. Above A_f, the specimen is fully in the austenite state, and below M_f, the material is fully martensitic**

follows a Clausius–Clapeyron relationship, and by plotting all four of these temperatures on the same σ–T diagram, a shape memory phase diagram is obtained (Fig. 5). However in reality, the slopes of the σ–T relationship of each transformation temperature are generally not the same, and may not even be a straight line due to the effect of microstructural features such as grain size, and microstructural mechanisms such as dislocation slip. Nevertheless, idealised versions are used here for simplicity and to convey the important parameters/mechanisms for clear introduction of thermomechanical behaviours of HTSMAs in the following sections.

The deformation response of SMAs depends on the temperature relative to the transformation temperatures (M_s, M_f, A_s and A_f) of the alloy. If the material is deformed below M_f in a self-accommodated martensite structure (Fig. 3), then the strain is accommodated by the growth of one variant favoured by the stress at the expense of others, as well as detwinning (Fig. 6). Since all martensite variants are equally stable thermodynamically in the absence of external and internal stresses, the martensite stays in the reoriented and detwinned state, and the material remains in the deformed shape after unloading. When heated above A_f after unloading, all martensite transforms back to austenite. When the austenite is once again cooled below M_f, the martensite will again form in a self-accommodated state, and all deformations from detwinning are recovered in the absence of plasticity; this is known as the shape memory effect (Fig. 6).

If deformation takes place above A_f where the alloy is fully austenitic, the material may deform by stress induced martensitic transformation and possibly detwinning of the transformed martensite. Upon unloading, the stress induced martensite is unstable at that temperature, and will completely transform back to

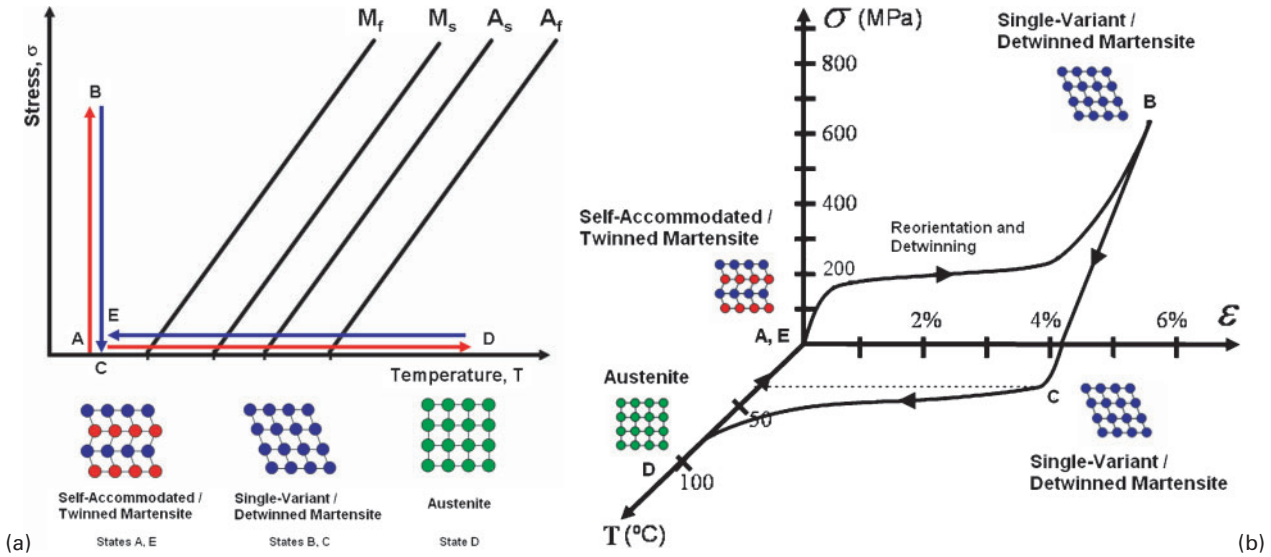

6 ***a*** **demonstration of the shape memory effect using σ–T phase diagram. An initially twinned (self-accommodated) martensite (state A) is deformed at a temperature below M_f, causing it to detwin (state B) and remain in the detwinned state after unloading (state C). This leads to an external shape change (shown in *b*). Upon heating to above A_f, the detwinned martensite transforms fully back into austenite (state D), which again transforms to twinned (self-accommodated) martensite when cooled below M_f, restoring the initial shape; *b* demonstration of the shape memory effect on a σ–ε diagram**

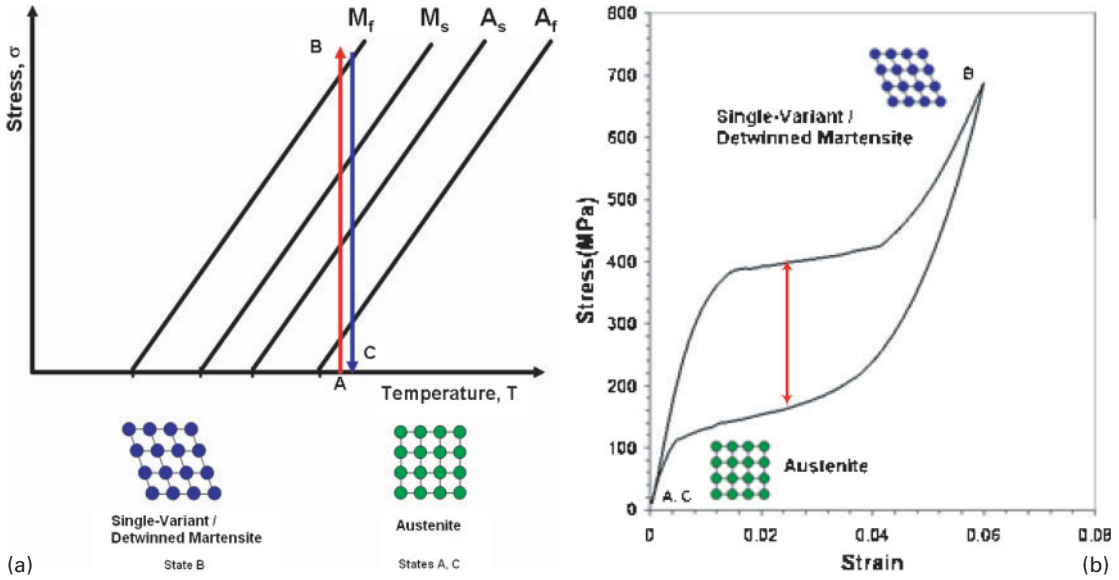

7 ***a*** **demonstration of superelasticity using a** $\sigma-T$ **phase diagram. Initial austenite (state A) is deformed at temperatures above** A_f**, and with sufficient stress, becomes fully martensite in detwinned state (state B). When stress is removed upon unloading, the specimen returns to a fully austenite state and recovers all imposed deformation immediately (state C).** ***b*** **demonstration of superelasticity on a** $\sigma-\varepsilon$ **diagram**

austenite and as a consequence, the deformation is recovered. This behaviour is known as superelasticity (Fig. 7).

II.1·2. Characteristics of shape memory and superelastic behaviour

For any application of SMAs, there are several important properties other than transformation temperatures. Primarily, these properties can be condensed into the following characteristics: the magnitude (in terms of strain) of shape memory or superelastic behaviour and their reversibility. The former is represented by the recoverable strain ε_{rec}, and the latter by the irrecoverable strain ε_{irr} and recovery rate. The recoverable strain is the total amount of strain that can be recovered after a complete shape memory or superelastic cycle. It is important to note that ε_{rec} depends on how the characterisation experiment is carried out and the experimental conditions such as applied stress level and temperature. In terms of shape memory behaviour evaluated from stress free shape recovery experiments as seen in Fig. 6, ε_{rec} is the sum of the elastic recovery from unloading and the strain recovery corresponding to detwinned martensite transforming first to austenite upon heating and then to twinned martensite upon cooling. For superelasticity (Fig. 7), ε_{rec} is the total recovery upon unloading and contains a combination of elastic recovery and strain recovery upon reverse transformation from stress induced martensite to austenite. This topic will be addressed in further detail in the corresponding subsections of Section II.1·4.

Clearly, ε_{rec} contains two components: elastic strain and shape strain. Shape strain may come from either detwinning/reorientation of martensite for the shape memory effect, ε_{sme}, or the transformation from austenite to martensite, as in superelasticity, ε_{SE}. Observed shape strains also depend on the experimental conditions, for example, whether the experiment is conducted in tension or compression, because of the anisotropic nature of SMAs (see Sections II.2·2 and II.2·3). In this review article, we have chosen to use ε_{rec} as the main measurement of the magnitude of recovery, and its definition from different experiments is elaborated upon in Section III.1·4.

Reversibility of shape memory and superelastic behaviours is a measure of the magnitude of recovery relative to the magnitude of initial deformation. For example, if an SMA is deformed to 5% strain at a temperature below M_f, and recovers 4·5% strain from shape memory effect after unloading and heating, there is a 0·5% strain that is left over and not recovered. This 0·5% strain is then considered to be ε_{irr} and therefore permanent. The recovery rate is the ratio of ε_{rec} to the applied deformation, and would be 90% in this example. Irreversibility in SMAs is normally considered to be generated by the creation and movement of dislocations, but can also be caused by stabilised martensite that does not transform to austenite even after heating above A_f. While the former is truly irreversible, the retained martensite in the latter case may be recovered by heating to even higher temperatures. However, it is not easily possible to know the contribution of each to the total ε_{irr} without specifically testing for them. Such type of experiments have not in general been carried out in HTSMA studies, and the readers are advised to bear in mind that reported ε_{irr} most likely contains contributions from both mechanisms, and possibly from additional mechanisms that may play a role only at high temperatures. These additional mechanisms will be discussed in Section II.3·1.

During martensitic transformation, some of the driving force for the transformation is lost to the environment through non-reversible mechanisms. The magnitude of the associated energy loss or dissipation, is reflected in the thermal (ΔT) or stress hysteresis ($\Delta\sigma$ in Fig. 7) of a full transformation cycle. Dissipation during the transformation can be due to several mecahnisms, including the creation of defects, emission of acoustic waves, and generation of heat due to internal friction at the phase interfaces. In actuator type applications,

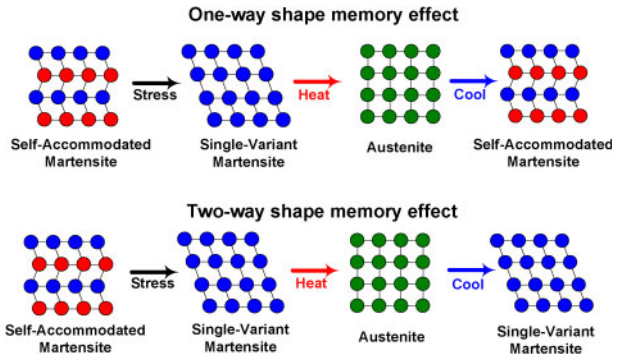

8 Demonstration of one way and two way shape memory effects. Whereas the martensite normally returns to a self-accommodated structure after cooling from austenite in the one way shape memory effect, the TWSME causes the martensite to adopt a more 'single variant' configuration. Owing to local oriented internal stresses or other reasons, certain habit plane variants become favoured, and the martensite changes shape upon cooling from austenite

dissipation negatively impacts the efficiency of SMA devices. In thermally driven SMA devices, a large hysteresis means a larger heating and cooling range, and thus, higher energy cost and power demands are required for the operation of the device. Fortunately, hysteresis can be reduced through thermomechanical training (Section II.2·1), structural (Section II.2·2) and orientation/texture (Section II.2·3) manipulations, and controlling the thermoelastic nature of the transformation through alloying (Section II.2·4). Furthermore, alloys with large hysteresis can be utilised for damping or energy absorption applications.

Finally, in actuation applications, work output is an important parameter. Work output can be simply defined as $\sigma \times \varepsilon$, where ε is ε_{rec} and σ is the applied stress. The evaluation of work output is performed using constant stress thermal cycling experiments (also referred to as isobaric thermal cycling experiments). In these experiments, SMAs are cycled through their transformation temperatures under constant applied stress, so that the total ε_{rec} from each of these cycles is multiplied by the stress at that cycle to yield work output. This type of experiment is described in more detail in Section II.1·4.

When individual HTSMA systems are discussed in Section III, their shape memory and superelastic behaviours will be reported in terms of the properties discussed in this subsection (ε_{rec}, ε_{irr}, recovery rate, ΔT and work output). This allows comparison to be made among the different systems. Unfortunately, for many alloy systems, several of these properties have not been reported in literature.

II.1·3. Other shape memory related behaviours

The shape memory effect described in previous sections is mainly one-way shape memory behaviour because only the austenite shape is 'memorised'. The only shape that the martensite is capable of remembering is the same shape as the austenite due to self-accommodated structure of martensite variants. There is another shape memory behaviour where it is also possible to memorise a martensite shape different from the austenite shape. This behaviour is called the two way shape memory effect (TWSME): when the SMA is cooled from austenite to martensite, instead of adapting to a self-accommodated structure, some variants

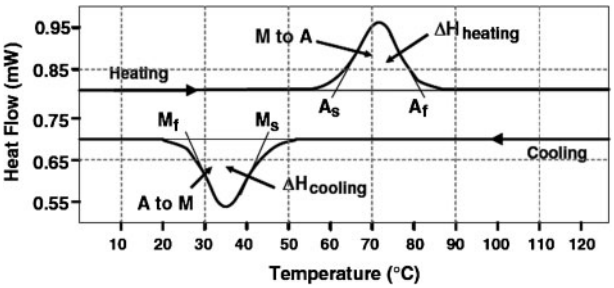

9 Determination of transformation temperatures via DSC measurements

of the martensite are favoured and the martensite adopts a shape different from that of the self-accommodated structure as seen in Fig. 8. Two way shape memory effect is considered to be caused by internal stresses that develop in the SMA from plastic deformation in martensite,[25–27] superelastic cycles,[28] aging for precipitation under stress and/or under constraint.[29–31] The internal stresses generated from these mechanisms are anisotropic, which may be created by directionally organised dislocations or retained martensite from prior thermomechanical training[25–28] or by aligned coherent precipitates.[29–31] The symmetry and arrangement of point defects has also been suggested as a possible explanation for TWSME,[32] and this mechanism will be discussed in more detail in Section II.2·2.

In practice, TWSME is not used as commonly as the one-way shape memory effect. The reason behind this is that ε_{rec} from TWSME is generally smaller,[12] and because it depends on internal stress, two way shape memory strain tends to deteriorate at higher temperatures. Currently, reported TWSME in HTSMA systems are small and very unstable. For this reason, while TWSME is reported whenever available in this review article, it will not be subjected to the same attention and discussion as for the one way shape memory behaviour.

Another unique behaviour of SMAs is called 'rubber-like behaviour'. It is similar to superelasticity in austenite, where deformation is recovered immediately upon unloading. However, rubber-like behaviour occurs completely in martensite. It is suggested that the behaviour stems from symmetry-conforming short-range order of point defects in martensite.[32,33] In HTSMA literature, rubber-like behaviour has not been reported. Thus, it will be excluded from the present article.

II.1·4. Evaluation of shape memory properties

Characterisation of shape memory and superelastic behaviour in SMAs require a different set of evaluation techniques than those used for ordinary engineering materials. In this section, some of these techniques and important material parameters and properties, that such techniques are designed to determine, will be summarised.

II.1·4.a. Transformation temperatures

Transformation temperatures can be directly measured through many techniques including differential scanning calorimetry (DSC), electrical resistivity measurement as a function of temperature, and dilatometry. They can also be measured indirectly through extrapolation of transformation temperatures as a function of stress (similar to Fig. 5) from a series of constant stress thermal cycling experiments.

In Fig. 9, transformation temperatures are defined on a DSC plot. Two peaks are shown, marking the forward

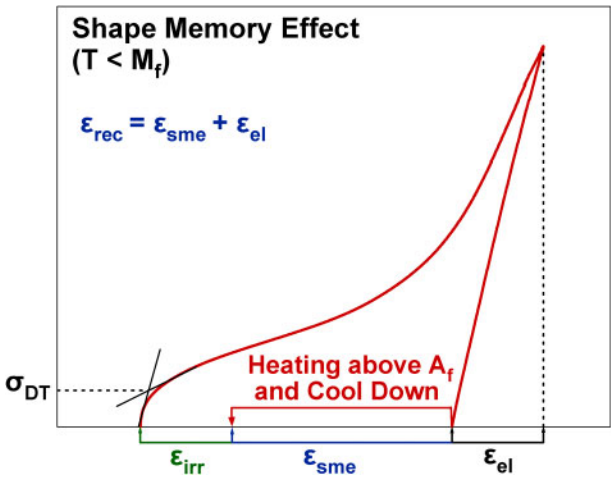

10 **Shape memory properties from a one way shape memory experiment. Detwinning/reorientation stress is denoted by σ_{DT}, while irrecoverable strain, shape memory strain, and elastic strain are denoted by ε_{irr}, ε_{sme} and ε_{el}, respectively**

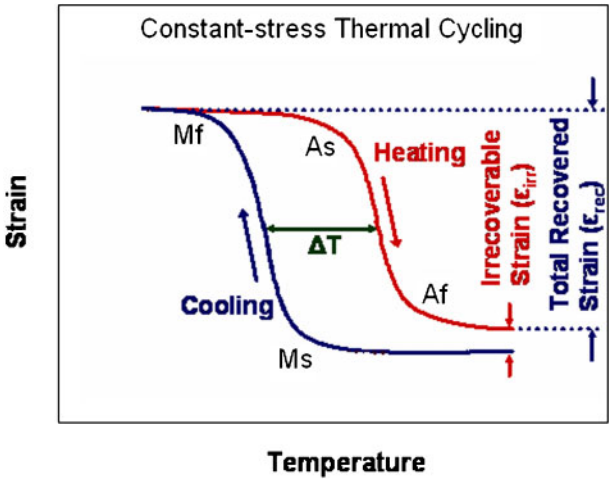

11 **Representative strain versus temperature response of an SMA in constant stress thermal cycling experiments. Important shape memory characteristics are also shown, such as transformation temperatures, irrecoverable strain ε_{irr}, total recovered strain ε_{rec} and transformation thermal hysteresis ΔT**

and reverse transformations. The forward transformation is exothermic, and the reverse transformation endothermic. The temperatures at the peaks of the forward and reverse transformations are known as martensite peak temperature M_p and austenitic peak temperature A_p, respectively. The difference between A_p and M_p ($A_p - M_p$) is a measure of ΔT.

Another technique for measuring transformation temperatures is electrical resistivity measurement as a function of temperature. The temperature dependence of electrical resistivity is different for austenite and martensite due to their structural differences. Transformation temperatures are indicated by an abrupt change in resistivity versus temperature slope during heating and cooling. Other techniques such as dilatometry can be used if there is a significant volume change between martensite and austenite, but the volume change in thermoelastic martensitic transformations is generally very small. *In situ* X-ray, neutron and electron diffraction can also be used to detect transformation temperatures by observing the temperatures at which diffraction corresponding to martensite or austenite appears or disappears. The indirect measurement of transformation temperatures via constant stress thermal cycling experiments is discussed in the next subsection.

II.1·4.b. Shape memory properties

In most studies, shape memory behaviour is characterised by stress free recovery experiments where the specimen is deformed in martensite, unloaded, and then allowed to recover its shape upon heating under no external stress. This type of experiment is described in Fig. 6, and the corresponding properties are defined in Fig. 10.

In actuation applications, however, the shape memory behaviour is never used in this fashion. Instead, an external biasing force always exists on SMA actuators during thermal cycling. During transformation, the associated shape change causes SMA to push against the biasing force, thus doing mechanical work. For characterisation of shape memory behaviour under this condition, constant stress thermal cycling experiments, as shown in Fig. 11, are used. A series of such thermal cycling experiments at various stress levels are usually conducted as shown in Fig. 12*a*. The analysis of the

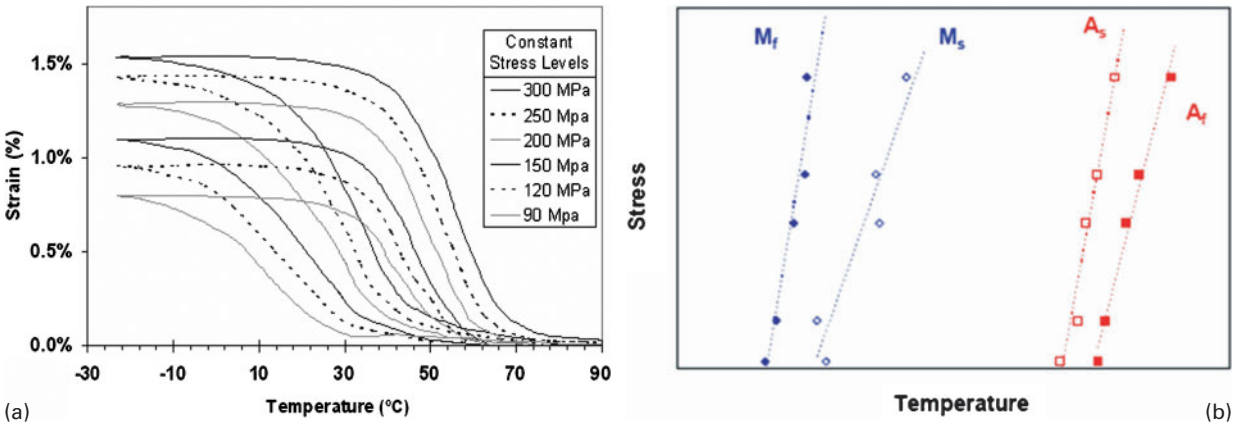

12 **Construction of stress versus temperature phase diagram *b* for an SMA using constant stress thermal cycling experiments in *a*. The lines for each transformation temperature in *b* can be extrapolated down to zero stress to determine the stress free transformation temperatures.**

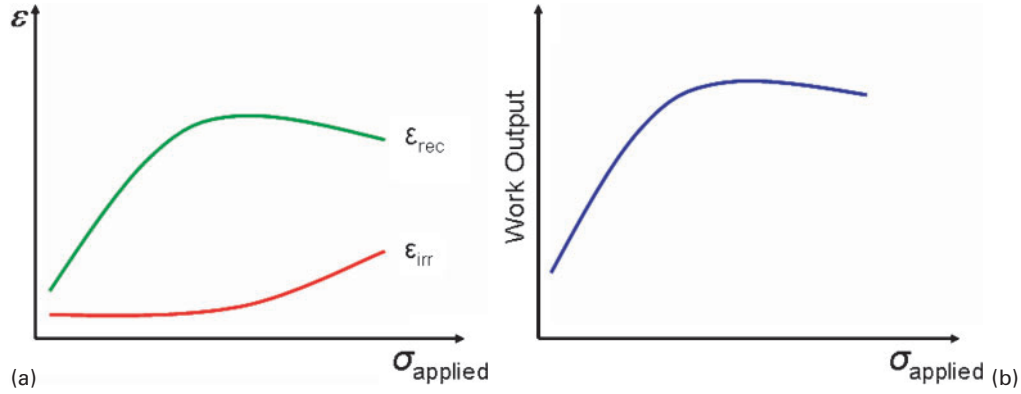

13 ***a*** **ε_{rec}, ε_{irr} and** ***b*** **work output as a function of applied stress. The curves are constructed using the data extracted from constant stress thermal cycling experiments in Fig. 12*a***

strain versus temperature responses from these experiments and determination of transformation temperatures at each stress level lead to the construction of the stress–temperature phase diagrams in Fig. 12*b*. Using the stress–temperature relationships in Fig. 12*b*, transformation temperatures at stress free condition can be extrapolated[34].

Constant stress thermal cycling experiments are also used to determine the evolution of ε_{rec}, ε_{irr}, ΔT and work output of the material as a function of applied stress. Plotting ε_{rec} from each thermal cycle as a function of applied stress level generates a plot similar to Fig. 13*a*. In this figure, ε_{rec} increases initially with increasing stress, but eventually reaches a maximum before decreasing rapidly. At the same time, ε_{irr} is usually small up to a certain applied stress level, and then, increases monotonically with increasing stress. Multiplying the ε_{rec} at each stress level with the stress, a plot for the variation of work output with the stress (Fig. 13*b*) is created. Similar to ε_{rec}, the work output also increases with increasing stress up to a certain level, reaches a maximum and then decreases with further increase in stress. Not surprisingly, the maximum work output corresponds closely to the maximum ε_{rec}.

II.1·4.c. Superelastic properties

Superelastic properties can be evaluated from the loading–unloading experiments shown in Fig. 14 at different temperatures. However, the temperature at which superelastic experiments are conducted relative to A_f is critical. The larger the difference between the test temperature and A_f, the greater the driving force will be required to initiate stress induced transformation which results in inferior superelasticity. Above a certain temperature, called M_d, stress induced martensitic transformation becomes impossible because plastic deformation will occur first. It is, therefore, a good practice to conduct superelastic characterisation experiments at a consistent deformation temperature of A_f+X, where X is a constant and A_f depends on the alloy, in order to compare the superelastic properties of different alloys and the same alloys with different microstructures.

Important superelastic properties, as shown in Fig. 14, are similar to those for the shape memory behaviour (Fig. 10), namely ε_{irr}, ε_{rec} and σ_{SIM}. Recoverable strain includes elastic recovery and recoverable shape change from the stress induced martensitic transformation and possibly also martensite detwinning. With increasing applied strain, both ε_{rec} and ε_{irr} tend to increase. Similar to the shape memory behaviour, ε_{rec} reaches a maximum at some strain level while ε_{irr} increases monotonically.

Not only can shape memory and superelastic experiments be performed through different experiment types, they can also be conducted under different stress states, such as in tension, compression, torsion or bending. Deformation modes in SMAs are highly orientation dependent, especially in martensite, so whether a specimen is deformed in tension or compression can play a significant role on the outcome of shape memory or superelastic properties. This is illustrated by the differences in the tensile and compressive behaviour of an SMA shown in Fig. 15. The fundamental reason behind this has to do with the structures of and lattice correspondences between martensite and austenite, and crystallographic texture of the sample. This issue will be discussed in Section II.2·3. However, we mention this effect here because in many HTSMA studies, the evaluation of shape memory and superelastic effects are performed in different conditions without a unified standard. Some researchers conduct experiments in

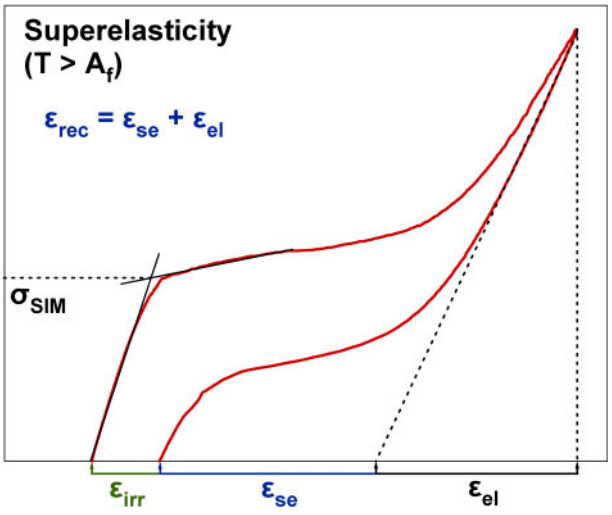

14 Superelastic properties from a typical experiment: σ_{SIM} denotes the critical stress for stress induced martensitic transformation; ε_{irr}, ε_{se} and ε_{el} represent irrecoverable strain, superelastic shape strain and elastic strain, respectively. Total strain recovery, ε_{rec}, during superelastic behavior is the sum of ε_{se} and ε_{el}

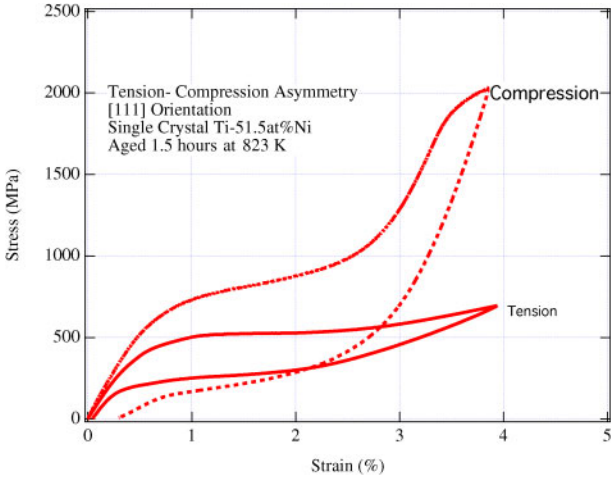

15 The tension compression asymmetry in a polycrystalline Ni rich Ni–Ti SMA. The superelastic behaviours in tension and compression are notably different in the same sample.[35] (Reproduced with permission from Springer Science and Business Media)

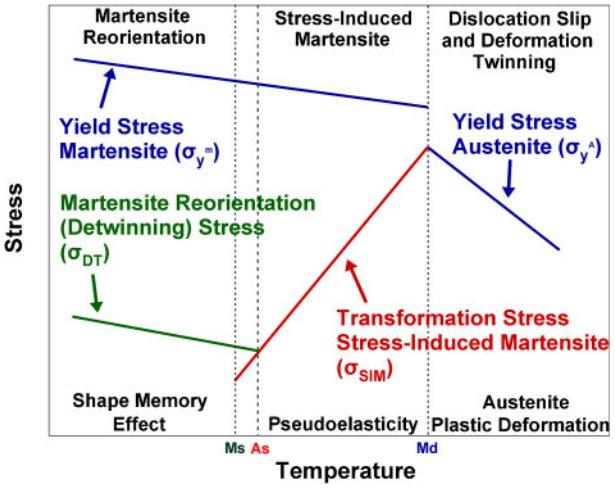

16 A model for the critical stresses of various deformation modes as a function of temperature in SMAs. If the yield stresses are above reorientation/detwinning stress σ_{DT} and stress induced transformation stress σ_{SIM}, one expects good reversibility and repeatability of shape memory and superelastic behaviours. However, all of these critical stresses depend on alloy type and composition, microstructure and crystal orientations/textures. For many alloys, σ_y is very close to σ_{DT} and σ_{SIM}, making reversible transformations exceedingly difficult. Above M_d, plasticity sets in and stress induced martensitic transformation is no longer possible

tension, while others in compression or bending. As a result, reported shape memory properties of the exact same material often vary significantly. In this article, the mode of deformation as well as the temperature at which deformation takes place will always be reported alongside the shape memory or superelastic properties.

II.2. Factors affecting shape memory and superelastic behaviours

Shape memory and superelastic behaviours are functions of a large number of factors that include both inherent microstructural and structural features of the alloy as well as external influences such as applied stress and temperature. The complexity causes difficulty in characterisation and the comparisons between the properties of various materials since it is difficult to isolate the effects of a single factor on shape memory and superelastic behaviour. This problem has been encountered in a large number of published studies on HTSMAs, where a change in shape memory or superelastic behaviour is ascribed to a single factor, even though some others were not held constant at the same time. Such instances will be alluded to in discussions on alloy systems in Section III.

A few of these factors will be discussed in this subsection. While the list is by no means exhaustive, the selected topics are considered, by the authors, to possess the greatest influence on shape memory and superelastic behaviour. These factors apply to all SMAs, but they are especially important for HTSMAs because the constraint of excess thermal energy at high temperatures causes a general deterioration of shape memory and superelastic properties, making their improvements through some factors less effective and increasing the importance of the ability to influence them through alternative methods.

In Section II.3, we will address the topics that concern explicitly with issues at high temperatures, both in terms of shape memory and superelastic behaviour and metallic alloys in general. It is important to realise that not all of the issues in Sections II.2 and II.3 have been addressed by HTSMA researchers. In fact, a great deal is completely missing in certain alloy systems. The goal of Sections II.2 and II.3 is both to highlight these issues relevant to HTSMAs and to note missing points in current research literature and topics that have yet to be studied. These topics are echoed whenever possible during discussions on individual alloy systems in Section III, and revisited in Section IV.

II.2·1. Plastic deformation and strengthening of SMAs

The factor that most greatly influences the level of irrecoverable strain ε_{irr} in SMAs is considered to be the ability of the material to resist plastic deformation, or its yield strength σ_y. During martensitic transformation, local internal stresses can often become several times higher than external the applied stresses, and the alloy may deform plastically even though the applied stress level does not exceed σ_y. For this reason, higher σ_y generally results in lower ε_{irr} and more stable shape memory and superelastic behaviours. Additionally, instead of considering σ_y alone, it is helpful to compare the difference between σ_y and the critical stress of the mechanism responsible for the shape memory σ_{DT} or superelastic behaviours σ_{SIM}, as seen in Fig. 16.

Shape memory behaviour occurs through reorientation and/or detwinning of martensite. The associated critical stress for their onset is usually called the reorientation or detwinning stress. We will not differentiate between the two here, and will simply refer to the critical stress shown in Fig. 10 as σ_{DT}. Superelasticity is activated by stress induced martensitic transformation, and the corresponding critical stress is σ_{SIM}. In general, σ_y in both martensite and austenite decreases with increasing temperature (Fig. 16), but this is not necessarily true for σ_{DT} and σ_{SIM}. Depending on the alloy system, σ_{DT} may increase or decrease with increasing temperature. On the other hand, σ_{SIM} always increases with temperature because austenite is stabilised by increasing deformation temperature.

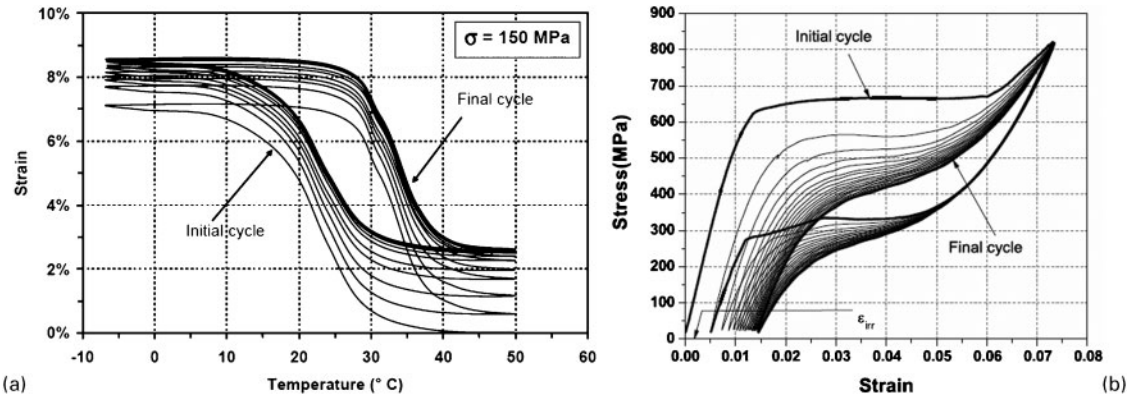

17 Thermomechanical training of SMAs through *a* constant stress thermal cycling (shape memory training) and *b* constant temperature superelastic cycling (superelastic training)

Classical work hardening methods, such as cold working, effectively increase σ_y of ductile SMAs. Cold working improves the shape memory behaviour by increasing σ_y, thereby decreasing ε_{irr} and allowing higher values of recovered transformation strain ε_{rec} to be reached. As a rule of thumb for SMAs, cold working in a phase will stabilise it, and for HTSMAs, the room temperature phase is martensite. Cold working at room temperature should therefore stabilise martensite and increase reverse transformation temperatures. In some alloy systems, hard precipitate phases can be produced by aging at relatively low temperatures around 300–500°C, and the combination of precipitation hardening and work hardening can further improve shape memory and superelastic properties. Unfortunately, a large number of prospective HTSMA systems are intermetallics with very limited ductility at room temperature, making them very difficult to process. Precipitates that can be used for strengthening usually cause further deterioration in ductility in these alloys.

It is also possible to improve shape memory and superelastic behaviour of SMAs through training. In this process, SMAs are thermally or mechanically cycled between the austenite and martensite a number of times. During training, some level of irrecoverable deformation takes place, but gradually saturates as the number of cycles increases. On one hand, the process acts somewhat as work hardening, but more importantly, dislocations or remnant martensite are generated through the transformation process itself, and are therefore located at the 'correct' places leading to favourable oriented internal stresses and strengthening. These dislocations and remnant martensite decrease the dissipation during transformation and discourage further dislocation creation upon subsequent cycles. Training is most commonly performed by temperature cycling under stress (shape memory training) or through stress–strain cycling at constant temperature (superelastic training), both of which are demonstrated in Fig. 17. Most SMAs can be trained, but desirable results often require a large number of training cycles. It is, however, difficult to train SMAs with limited ductility or poor fatigue resistance.

The aforementioned processes for increasing σ_y are very widely used because they are relatively easy to conduct, but in many HTSMA systems, the lack of ductility, phase instability and the high operating temperatures prevents these conventional techniques from being carried out, or limits their effectiveness.

II.2·2. Structure of transforming phases in SMAs

Structural factors of austenite and martensite, such as their crystal symmetry and lattice parameters, are central to the understanding of shape memory and superelastic behaviour of SMAs. Structural parameters define maximum capabilities of a transforming system, such as maximum transformation strain achievable. Although these maximum capabilities are often unreachable in practice, they provide an upper limit for shape memory and superelastic properties.

II.2·2.a. Structural restrictions for martensitic transformation

Crystal structure of martensitically transforming phases dictates whether shape memory and superelastic behaviour can occur at all between the two phases. According to Bhattacharya *et al.*,[36,37] transforming phases must have a group–subgroup relationship in order for shape memory behaviour to exist. Since martensite has a lower symmetry structure than austenite, the martensite must always be a subgroup of austenite. This explains why there are no thermoelastic martensitic transformations between a bcc austenite and an hcp martensite, since they are excluded by the theory.

Another important role of structures of transforming phases is that they control the maximum possible transformation strain, ε_{tr}^{max}. At the most basic level, the maximum shape strain possible between austenite and martensite is determined by the magnitude of the shear required to go from one structure to the other. As a rule of thumb, the greater the magnitude of this shear, the greater the maximum transformation strain.[37] Of course, the maximum transformation strain is rarely reached in practice, but it is generally observed that for a given austenite structure, the less symmetrical martensite phases (such as monoclinic B19′ martensite) produce, the greater ε_{tr}^{max} than the martensite phases with higher symmetry (such as orthorhombic B19 martensite).[37] In addition, a greater distortion of martensite from austenite often results in higher transformation strains. For example, transformation strain in the Ni–Mn–Ga system with tetragonal martensite increases when the c/a axis ratio of the martensite unit cell deviates further away from 1, because a c/a ratio far from 1 signifies a greater distortion from the cubic austenite.[38]

II.2·2.b. Symmetry of point defects

Otsuka and Ren[32,33] proposed a symmetry conforming short range ordering (SC-SRO) process to explain the nature of martensite/austenite stabilisation, TWSME, as well as the 'rubber-like' pseudoelastic behaviour observed in some martensite. In this theory, the equilibrium arrangement of point defects is assumed to be identical to the underlying crystallographic symmetry of the respective phases. That is, equilibrium defects will adhere to an 'orthorhombic arrangement' if the crystallographic structure of martensite is orthorhombic. Since martensite and austenite possess different crystal symmetries, the equilibrium arrangement of point defects will be different in each phase. Upon transformation from austenite to martensite, the defect arrangement of austenite is inherited, but this arrangement is not favourable in martensite, and the defects will attempt to rearrange themselves into a new equilibrium arrangement based on the martensite structure through short range diffusion processes. A similar rearrangement of defects will have to take place once again on the reverse transformation from martensite to austenite.

If defect structure is allowed to reach equilibrium in a phase mimicking the symmetry of that phase, the phase would be stabilised; if, for example, this occurs in martensite, A_s and A_f would increase. Otsuka and Ren[32,33] concluded that such a phenomenon is present in all martensitic transformations and its kinetics can be predicted by considering the reduced homologous melting temperature (M_s/T_m), where T_m is the melting temperature of the alloy. For a ratio of under 0·2, kinetics (aging) is too slow for this phenomenon to produce any measurable changes, and for a ratio above 0·6 it occurs almost instantaneously. For a reduced temperature between 0·2 and 0·6, aging occurs gradually and is manifested as a time dependent change in transformation characteristics.

This type of martensitic aging is one of the prime contributors to time dependent instabilities in SMAs, particularly those that operate at high temperatures. The effect of martensitic aging on shape memory properties is reflected in the change in transformation temperatures during prolonged exposure at high temperatures. Since it is a diffusion mechanism, the time scale at which this change in transformation temperatures occurs depends on the temperature at which the SMA is held. In the range of transformation temperatures of many HTSMAs, the reduced melting temperatures are in the range of 0·2 to 0·6, and thus, martensitic aging occurs gradually. A gradual change in transformation temperatures occurring during the lifetime of an SMA makes its use difficult in applications requiring precise control of transformation temperatures. These issues will be discussed in greater detail in Section III.3·2.

II.2·2.c. Role of structure on transformation hysteresis

Structure and lattice parameters of transforming phases also play a role in determining the energy dissipation during transformation, and thus, transformation thermal hysteresis, ΔT, and stress hysteresis, $\Delta\sigma$. Martensitic transformation between two phases can be described by a transformation stretch tensor which describes the lattice and orientation relationships between the austenite and martensite. For example, the transformation stretch tensor between a bcc austenite and one particular

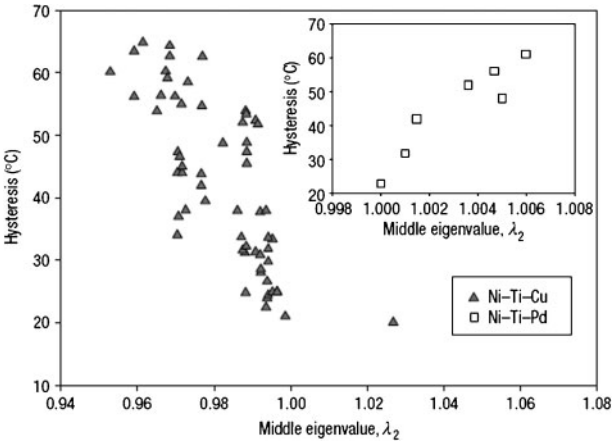

18 Variation of transformation thermal hysteresis, ΔT, with the middle eigenvalue of the transformation stretch tensor in the Ni–Ti–X alloy systems. ΔT appears to be minimised when the middle eigenvalue approaches one.[39] (Reproduced with permission from Macmillan Publishers and the Nature Publishing Group)

lattice correspondence variant of an orthorhombic martensite is[39]

$$U_1 = \begin{bmatrix} \beta & 0 & 0 \\ 0 & \dfrac{\alpha+\gamma}{2} & \dfrac{\alpha-\gamma}{2} \\ 0 & \dfrac{\alpha-\gamma}{2} & \dfrac{\alpha+\gamma}{2} \end{bmatrix}$$

where $\beta=b/a_0$, $\alpha=a/a_0$ and $\gamma=c/a_0$ (where a_0 is the lattice parameter of the austenite, and a, b, c are the lattice parameters of the martensite). According to Cui *et al.*,[39] the energy dissipation, in the form of thermal hysteresis, can be minimised by maximising the compatibility between martensite and austenite. This compatibility could be measured using the middle eigenvalue (the second largest/smallest eigenvalue) of the transformation stretch tensor: the closer the middle eigenvalue is to one, the better the compatibility between austenite and martensite. Figure 18 shows experimental data from the Ni–Ti–X alloy systems, and it certainly appears that ΔT reaches a minimum when the middle eigenvalue approaches unity.

II.2·3. Effects of crystallographic orientation and texture: single crystals and polycrystals

II.2·3.a. Single crystal orientation

ε_{tr}^{max} of an SMA depends not only on the structures of the transforming phases, but also on the orientation relationship between the crystal and the axis of the applied stress along which the transformation strain is to be determined. This is because a martensitic transformation can be considered as a deformation mode, and activate only along certain crystallographic directions on certain crystallographic planes, similar to deformation slip and twinning. Any directionally applied stress can be resolved into a shear component and a normal component on the deformation plane, and these can be further decomposed into deformation directions (according to the shear and dilatation components of the transformation). Based on the orientation relationship between the direction of the applied stress and a particular habit plane variant, described by its unique pair of twinning plane and transformation shear direction, it is possible to calculate a

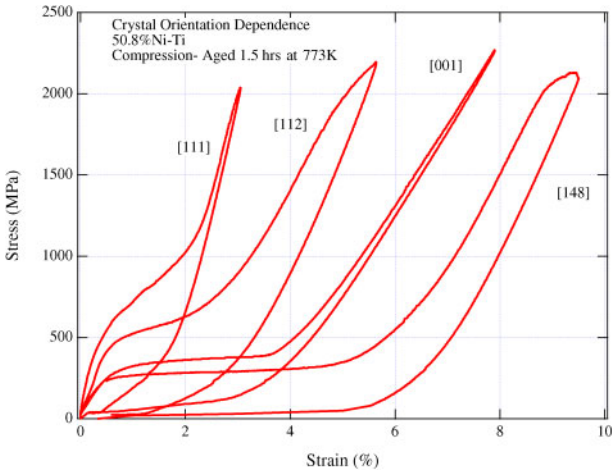

19 Crystal orientation dependence of superelastic behaviour in a series of single crystalline Ni rich Ni–Ti SMA samples under compression: σ_{SIM}, ε_{rec} and $\Delta\sigma$ are all strongly affected by the single crystal orientation.[35] (Reproduced with permission from Springer Science and Business Media)

'resolved shear stress factor' (RSSF) for this variant.[18] The greater the RSSF factor for a variant, the more likely that variant will be activated/favoured.

In a single crystal, the RSSF of each habit plane variant can be found for a given applied stress state, and the σ_{SIM} and ε_{tr}^{max} of that single crystal is dictated by the variants most favoured by that particular stress state.[18] This is indeed the case, as seen in Fig. 19, where σ_{SIM} of single crystals loaded along different orientations are indeed different. This effect is a consequence of a higher RSSF in those orientations with lower σ_{SIM}. Moreover, ε_{rec} is greater in orientations that have lower σ_{SIM}, the reasons of which are described below. In addition, $\Delta\sigma$ is also crystallographic orientation dependent as seen in the figure; however, the mechanisms responsible for such dependence will not be discussed here for the sake of brevity, more details can be found in work by Hamilton *et al.*[40]

Similarly in single crystals, it is possible to calculate the ε_{tr}^{max} expected along the known crystallographic direction of any uniaxially applied stress. One approach for such calculations is the energy minimisation theory developed by Ball and James.[23] The calculations can be conducted with the assumptions of either full detwinning of martensite or no detwinning,[18] while the real ε_{tr}^{max} is likely to be somewhere in between the values obtained from these two methods. These calculations can be performed for all orientations within the stereographic triangle for a cubic austenite, for instance, and plotted as transformation strain contours, if the lattice parameters and crystallographic structures of austenite and martensite are known.[18] One such example is shown in Fig. 20 for a Ni rich NiTi SMA.[41] It is clear that single crystal orientations along which external stress is applied have a significant effect on ε_{tr}^{max}. In addition, the sense of loading (i.e. tension versus compression) has notable effect on ε_{tr}^{max} as seen in the figure. This is because of the fact that martensitic transformation shear is unidirectional, similar to conventional deformation twinning shear observed in many metals and alloys with hcp and fcc structures. Likewise, the detwinning process in martensite variants is also unidirectional, ease of detwinning under tension may not necessarily indicate easy detwinning under compression. Thus, tension and compression loadings favour different martensite variants and degree of detwinning, and consequently, lead to remarkably different transformation strains.[18,35,41,42]

II.2·3.b. Polycrystalline texture

It is reasonable to expect that orientation effects in single crystals would similarly be applicable to polycrystals. This is indeed true, and shape memory and superelastic behaviours of polycrystalline SMAs is dependent on orientation distribution of the grains in the material, also known as texture. In polycrystalline SMAs, materials with strong texture in a particular orientation would be expected to have similar behaviour as a single crystal of that orientation. If the texture is nearly random, the behaviour of the polycrystal approximately becomes an average of the behaviour of single crystals of all orientations. Therefore, if shape memory and superelastic behaviours are known for single crystals of different orientations, then one can

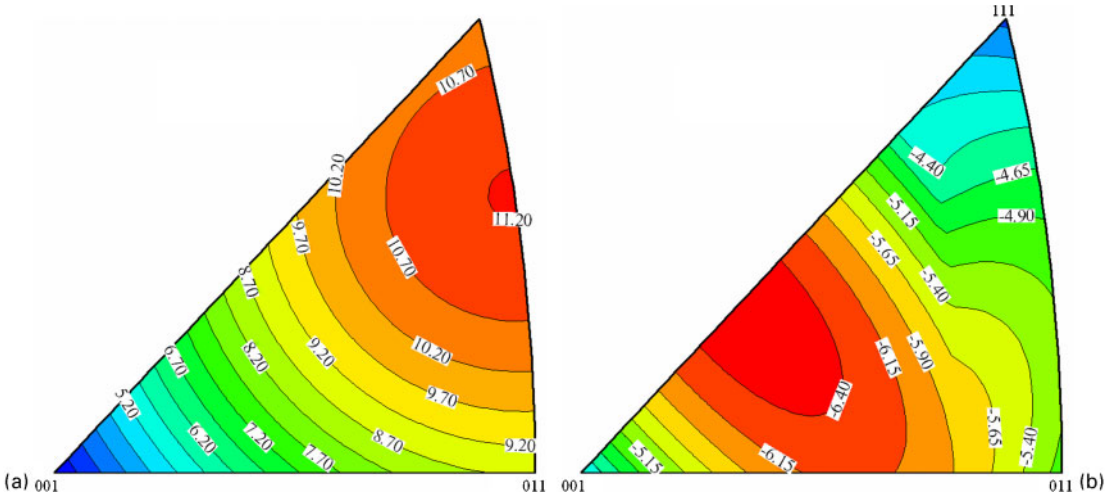

20 Maximum transformation strains as a function of the crystallographic direction of uniaxially applied stress in a Ni rich NiTi SMA under *a* tension and *b* compression[41] calculated using the energy minimisation theory.[23] Note the large difference between the orientation with the highest ε_{tr}^{max} (11·2% in tension), and that with the lowest ε_{tr}^{max} (essentially 3·0% in tension). Reproduced with permission from Springer Science and Business Media

attempt to process a polycrystalline SMA to achieve strong texture close to the orientation exhibiting the best sets of shape memory or superelastic properties. Texture can be introduced by traditional cold working techniques such as cold rolling, and the specimens can be cut at certain angles to achieve the desired texture. Nevertheless, it is difficult to control texture precisely using these methods. Texture evolution under a given stress state and strain level is dictated by the available plastic deformation mechanisms limiting the achievable textures using conventional processing techniques. Recently developed severe plastic deformation techniques such as equal channel angular extrusion (ECAE) can expand the attainable texture space and provide more precise texture control.[43–45]

The exact response of polycrystalline SMAs with weak texture is, however, complicated due to the required geometrical accommodation across the grain boundaries. It is known that based on the Taylor Criteria, a minimum of five independent deformation systems are needed for general deformation to occur in randomly textured polycrystals. Martensitic transformation is a deformation mode, and the number of independent deformation systems is analogous to the number of martensite lattice correspondence variants for the transformation.[37] The number of lattice correspondence variants, of course, depends on the structures of martensite and austenite. Assuming a cubic austenite, the transformation will not have the required five martensite variants to satisfy the Taylor Criteria if martensite has tetragonal or trigonal structure. On the other hand, both orthorhombic and monoclinic martensites possess more than five variants if they are transformed from a cubic austenite. For this reason, completely recoverable martensitic transformation would be extremely difficult to achieve in non-textured polycrystalline SMAs with cubic austenite and tetragonal or trigonal martensite.[37] More importantly, repeated transformation cycles can lead to intergranular fracture due to the strain incompatibility across grain boundaries limiting cyclic deformation of this kind of SMAs.[37] Published data on polycrystalline HTSMAs are in accord with these observations in conventional SMAs. Polycrystalline HTSMAs with cubic austenite to tetragonal martensite transformation, such as Ni–Al, Ni–Mn and Ni–Mn–Ga have shape memory behaviour with very poor recoverability.

From experiments, large and highly reversible shape memory and superelastic behaviours have been found in $\langle 100 \rangle$ single crystal SMAs with tetragonal martensite, for example, the Co–Ni–Al/Ga SMAs discussed in Section III.1·4. Thus it would appear that obtaining the $\langle 100 \rangle$ texture in polycrystalline form of these alloys would be the most important step for improving shape memory behaviour. While exceptions exist, the potential for good shape memory behaviour from tetragonal martensite appears to be problematic in general.

II.2·4. Thermoelastic martensitic transformation

Martensitic transformations can be classified as thermoelastic or non-thermoelastic. In thermoelastic transformations, the interfacial boundary between martensite and austenite is very mobile, and interfacial strain between the two phases is converted into elastic lattice strain instead of being relieved through generation of defects such as dislocations. During the reverse transformation, the stored lattice strain simply causes a reversion of austenite back to the original martensite. On the other hand, non-thermoelastic transformation requires nucleation of austenite during the reverse transformation. Therefore, non-thermoelastic transformation is in general not reversible, and SMAs are normally associated with thermoelastic martensitic transformation. However, some materials with non-thermoelastic transformations are somewhat reversible, such as some cobalt and iron based alloys, and are also considered to be SMAs. In general, the thermoelastic nature of martensitic transformations is reflected in the thermal hysteresis, ΔT. Non-thermoelastic transformations possess large ΔT up to several hundred degrees Celsius, while ΔT of thermoelastic transformations is typically less than 100°C. In certain systems, the transformation can be made more thermoelastic through alloying, and is generally accompanied by a reduction in ΔT and improvement in the reversibility of the shape memory behaviour.

II.3. Additional factors at high temperature

In addition to the factors mentioned in Section II.2, several others affecting SMAs uniquely in the high temperature regime are now considered. As many such factors are not exclusive to SMAs, only those directly impacting shape memory properties, such as transformation temperatures and ε_{rec}, will be discussed in detail.

II.3·1. Mechanical behaviours at high temperatures

II.3·1.a. Effects of temperature on yield strength

Deformation behaviour of HTSMAs is complicated by the availability of thermal energy at high temperatures. A common challenge for SMAs is to minimise ε_{irr} because of plastic deformation that occurs during phase transformation. This problem is exacerbated at high temperatures due to the reduction of σ_y in both austenite and martensite. The impact of this reduction is practically much more significant on superelasticity than on the shape memory effect since the former requires the deformation temperature to be above A_f (see Fig. 16). As σ_{SIM} increases with temperature, the difference between σ_{SIM} and σ_y of austenite or martensite quickly diminishes, and slip becomes the dominant deformation mechanism. This is one reason for the scarcity of high temperature superelastic alloys, even though many alloys are capable of showing high temperature shape memory behaviour.

Figure 16 describes only the general trends in critical stresses for each deformation mechanism, but not their relative magnitudes. In materials that show shape memory or superelastic behaviour, σ_y is assumed to be above σ_{DT} and σ_{SIM}, respectively, but the relative magnitude of these stresses depends on deformation temperature, composition, and processing conditions of the material, which dictate transformation temperatures. Detwinning and martensitic reorientation are diffusionless processes, so while σ_{DT} may decrease with increasing temperature as indicated, its dependence on temperature should be weaker than the temperature dependence of dislocation processes. In other words, as temperature increases, the decrease in σ_y should be much larger than the decrease in σ_{DT}. As a result, HTSMA systems designed to operate at moderate to high temperature (above 400°C) seldom show appreciable shape memory and superelastic behaviour, and even in alloys that do, full recovery at any applied strain level is rarely

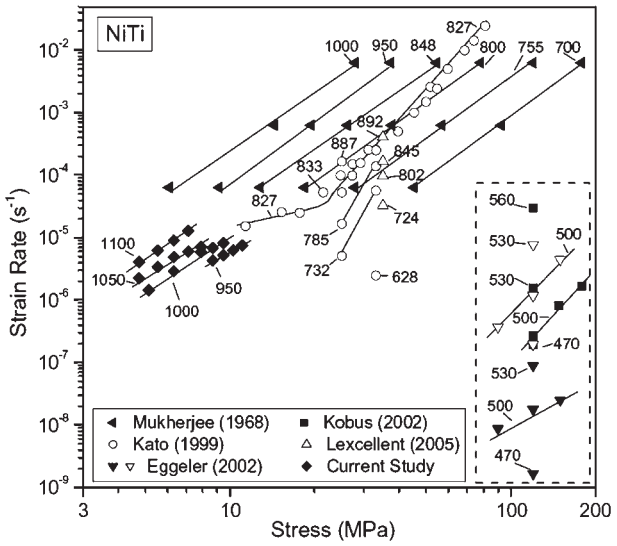

21 Creep data for binary Ni–Ti; reproduced with permission. 'Current Study' refers to the results of Oppenheimer *et al.*[53] Reproduced with permission from Elsevier

observed. Strategies for combating these problems were discussed in Section II.2.

II.3·1.b. Creep

The effects of creep are important for HTSMAs with very high transformation temperatures (above ~400°C). Although creep is probably not a vital deformation mechanism during the operation of HTSMA components with lower transformation temperatures, its effects are still important during high temperature processing and forming of the material. Creep manifests itself in many forms, such as diffusional creep, power law creep based on dislocation climb, and low temperature creep based on viscous effects of solute atmospheres.[46] A detailed description of the creep mechanisms will not be provided here, and interested readers are referred to Refs. 46–48.

There are only a limited number of studies on the creep behaviour of SMAs, and most of them have focused on the binary Ni–Ti SMA.[49–53] A summary of the results, plotted for the creep rate as a function of applied stress and creep temperature, is shown in Fig. 21. There is some incongruity in the results, as seen in the difference in the measured creep rates between the studies of Oppenheimer *et al.*,[53] Mukherjee,[51] Lexcellent,[50] and Kato[52] at relatively high temperatures. Oppenheimer *et al.*[53] attributed these differences to four possible reasons:

(i) tension compression asymmetry: with the exception of Oppenheimer *et al.*, who carried out experiments in compression, experiments in all other cited works were performed in tension
(ii) differences in grain sizes of materials used in each study
(iii) deviation of alloy composition from stoichiometry
(iv) a possible change in creep mechanism over the temperature range where the experiments were performed.

Possible effect of texture was also mentioned as an explanation for the discrepancies among different studies. Regardless, the exact reason for the discrepancies is not yet known, and indicates the need for further detailed studies. Nevertheless, for operation of Ni–Ti SMAs below 500°C, creep does not appear to be an issue even at stress levels near 200 MPa.

For creep responses of HTSMAS, however, the studies mentioned serve only as a starting point. Phase transformation often generates local stresses much higher than macroscopic stress, and it is anticipated that creep resistance will be worse when the SMA undergoes transformation cycles at high temperatures compared to static creep. If the high operating strain/stress levels are required for HTSMA components, creep would become a problem even at intermediate temperatures (~500°C). It is necessary to directly test how phase transformation will affect creep resistance, as well as how creep affects shape memory properties. This type of information has not been reported in most HTSMA systems.

II.3·2. Microstructural instability

Transforming phases in many SMAs are non-equilibrium phases. Given sufficient aging time at a high temperature, the equilibrium phase will often form. If the temperature at which precipitation of stable phases takes place is far above the operating temperature range of the alloy, controlled precipitation can be used to improve the properties of many SMAs. For example, strong precipitates are often used to improve the shape memory properties. In some brittle SMAs, ductile equilibrium phases are often created from aging in order to improve ductility of the alloy.

Unfortunately for HTSMAs, the formation of equilibrium phases may not be quite controllable. If the operating temperature range of the HTSMA is high enough for precipitation to occur at a sufficient rate, then precipitation will cause a continuous change in the shape memory properties of the alloy due to composition change of the matrix. These changes, such as in transformation temperatures, will eventually reach a degree such that the HTSMA component will no longer perform the designed function, i.e. the HTSMA effectively has a lifetime controlled by precipitation. For example, in nickel rich Ni–Ti binary SMAs, Ti_3Ni_4 precipitation occurs during aging at temperatures above 300°C. These alloys are usually heat treated to a 'peak aged' condition such that nanosized coherent precipitates provide the best hardening and thus, stability in the transformation behaviour of the alloy. However, if a similar Ni–Ti SMA is to be used at temperatures near 300°C, the precipitation process will continue during the operation of the alloy, the precipitates will grow larger in size and become incoherent, and the precipitation hardening effect will be diminished. The only effect remaining will be the compositional change of the matrix. This is a particular problem for certain Cu based and Ni based HTSMAs, which will be discussed in Sections III.1·3 and III.1·6 respectively.

Many HTSMA systems depend on work hardening or training to improve and stabilise their shape memory behaviour, but at a sufficiently high temperature, dislocation recovery will become significant enough that the effect of work hardening and training will be gradually lost over some period of time. Recovery is a thermal phenomenon, so the critical temperature at which the impact of recovery on the shape memory behaviour becomes unacceptable depends on the

expected time the SMA component will be exposed to the temperature of interest during its lifetime. The rate at which it occurs at a particular temperature depends on the melting point and microstructure of the alloy. Similarly, recrystallisation also has a negative effect on most SMAs. The temperature at which recrystallisation becomes a serious problem is usually high, but its onset renders strengthening by grain refinement impossible. These two temperatures become an upper limit for alloys strengthened by conventional methods.

Finally, water quenching required after homogenisation or solution heat treatments of many HTSMA systems cause some disordering of crystal structures and high levels of non-equilibrium vacancy concentrations. If self-diffusion is fast enough, the reordering process can drastically change the transformation temperatures, such as in the case of Cu based HTSMAs during repeated martensitic transformation as discussed in Section III.1·3.

II.3·3. Oxidation

Alloys exposed to the atmosphere at high temperatures will inevitably react with oxygen and other gaseous species. As a result, metal oxide products can form at the sample surface. If the reaction is not stopped and sufficient amount of oxygen is available, which is usually the case in an uncontrolled atmosphere, then the alloy will continue to lose more of its mass to oxide products. Fortunately, oxide formation at the surface slows down the diffusion of metal ions and oxygen and controls the rate of oxidation. Therefore, in addition to temperature, oxidation rate is determined by the permeability of the oxide layer. Alloys designed to operate at high temperatures, such as the nickel based superalloys, are capable of forming a stable and impermeable oxide layer to prevent further oxidation once a critical oxide layer thickness is formed.

An oxidation problem unique to SMAs is that unlike high temperature structural metals, even a slight change in the matrix composition may become unacceptable for SMAs. Transformation temperatures in SMAs such as Ti–Ni and Ni–Al are very sensitive to composition, and often change more than 100°C with each atomic percentage variation in composition.[54–56] Frequently, the oxide layer of an alloy is composed of mostly the oxide of a single element, thus reducing its concentration in the matrix. The oxidation effect of SMAs is most often studied on Ti–Ni alloys, and it was found that the sample surface consists of mostly titanium oxide, which results in a nickel rich layer immediately below the surface significantly reducing local transformation temperatures.[57–62] Thickness of the oxide layer from aging increases sharply when oxidation temperature exceeds 700–800°C,[57–61,63] such that the oxide layer formed from 1 h oxidation at 500°C is about 275 nm thick, whereas the thickness of the layer formed at 1 h oxidation at 700°C exceeds 70 μm.[58]

Further details on oxidation of Ti–Ni and other conventional SMAs are beyond the scope of this article; however, it is interesting to point out the reported effects of oxidation on their shape memory properties. Kim *et al.*[60] observed a decrease in all transformation temperatures in $Ti_{49·6}Ni_{50·6}$ sheets with thickness of 0·8 mm after oxidisation in air at 900°C for 1 h when compared to the transformation temperatures of non-oxidised specimens. The decrease in M_s was only ~5°C, but A_f and M_f decreased by 10–15°C, and A_s by ~25°C. The authors attributed this effect to a nickel rich layer that forms immediately beneath the titanium oxide surface layer. On the other hand, Nam *et al.*[58] found an increase in both M_s and A_f as dry air oxidation temperature is increased from 450 to 850°C while duration is held constant at 10 min in $Ti_{51}Ni_{49}$ wire with diameter of 1·7 mm. This increase is attributed by the authors to the compressive stress exerted by the oxide surface on the matrix beneath. This compressive stress is believed to be hydrostatic, so that it acts in the normal direction to the habit planes of the martensitic transformation. Theoretically, a hydrostatic stress acts normal to the habit plane of martensites, and will assist the transformation (increase transformation temperatures) if the volume change from the austenite→martensite transformation carries the same sign as the hydrostatic stress applied, where compressive stress is negative.[64] This is indeed the case for the Ti–Ni alloys.[64,65] Nam *et al.* suggest that the compressive stress is increased with an increase in the oxidation temperature, mostly likely because of the thickening of the oxide layer and the change in its structure as oxidation temperature is increased. However, large hydrostatic pressure is needed to significantly impact transformation temperatures since the volume change of martensitic transformation associated with thermoelastic SMAs is small. The stress at the matrix/oxide interface is not known, and it is not clear why compressive stress at the interface would be expected to increase when oxide layer thickens. More experimental data is needed to determine whether the compressive stress alone sufficiently explains the increase in transformation temperature during oxidation.

While the results of the two reports appear to be conflicting, this is not necessarily the case. The specimens used in the study by Kim *et al.*[60] are already nickel rich, so any additional decrease in the titanium concentration immediately causes immediate reduction in transformation temperatures.[54] The specimens in the study by Nam *et al.*[58] are titanium rich. In the titanium rich region, transformation temperatures are not sensitive to small changes in composition. As oxidation temperature is increased, the reduction of titanium content in the matrix right below the oxide layer becomes larger as titanium oxide is formed at the surface. However, the titanium rich composition of the alloy means that a certain amount of titanium must be depleted first before the transformation temperatures could decrease due to the compositional change. In the meantime, other mechanisms, such as possibly the compressive stress from the oxide layer, can cause an increase in transformation temperatures instead. Further evidence lies in the specimens oxidised at 1000°C for 10 min in the study by Nam *et al.*[58] Even though the transformation temperatures from DSC in this condition were not reported directly, the composition of the matrix was changed to $Ti_{48·2}Ni_{51·8}$ from the initial composition of $Ti_{51}Ni_{49}$. It was also shown that M_s of the specimen oxidised at 1000°C was lower as compared to that aged at 850°C in a set of constant stress heating cooling curves reproduced in Fig. 22.

The study by Nam *et al.*[58] also addressed the effects of oxidation on the shape memory behaviour of $Ti_{51}Ni_{49}$ alloy from thermal cycling experiments under constant tensile stress of 60 MPa. As oxidation temperature increased, both ε_{rec} and ε_{irr} remain constant up to an

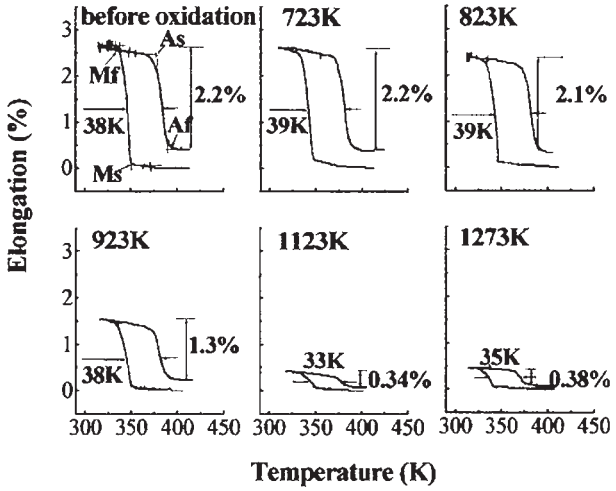

22 Tensile thermal cycling curves under 60 MPa for $Ti_{51}Ni_{49}$ SMA oxidised for 10 min at various temperatures. At temperatures above 823 K (550°C), both ε_{rec} and ε_{irr} are reduced. Reproduced with permission.[58] Reproduced with permission from Springer Science and Business Media

oxidation temperature of 550°C. However, if oxidation temperature is increased further, both ε_{rec} and ε_{irr} are reduced as shown in Fig. 22. The authors did not provide an explanation for these observations. However, the reduction of ε_{rec} at high oxidation temperature should not necessarily be related to a deterioration of the shape memory effect. Reduction of both ε_{rec} and ε_{irr} at a constant stress level is often observed in a work hardened or precipitation strengthened material, because while the strengthening mechanism suppresses plastic deformation, it also poses a barrier to martensitic transformation. Therefore, a greater applied stress is needed to achieve the same level of ε_{rec}. Thus it is possible that if applied stress is increased beyond 60 MPa, ε_{rec} would increase in specimens oxidised at higher temperatures. Also, since the oxide layer does not transform, the compressive stress imposed by it may act against the applied tensile stress. Therefore, the actual stress experienced by the matrix near the oxide matrix interface is smaller than the applied stress, resulting in a more self-accommodated martensite structure in this area and reducing ε_{rec}.

From these results, it would appear that the rate of oxidation is too low to be considered as an issue for Ni–Ti–X based HTSMAs designed to operate at lower temperatures (about 200–300°C), however, it becomes a more serious problem at higher temperature. Finally, the unique problem to SMAs is the transformation temperature sensitivity to compositional changes due to oxidation, which limits both the maximum temperature and exposure time of the SMA components. Shape change associated with the transformation of the matrix may also cause cracking in the brittle oxide layer, making the development of a stable oxide layer difficult even in alloys normally with good oxidation resistance.

III. Potential HTSMA systems

III.1. Alloys with characteristic transformation temperatures between 100 and 400°C

Following the vast amount of research performed on SMAs operating near room temperature, most work performed on HTSMAs has been within the 100–400°C temperature range for a number of reasons including:

(i) the availability of numerous alloy systems with transformation temperatures in this range
(ii) the similarity in processing of these materials to the thermomechanical processing of current commercial alloys
(iii) the temperature range being comparatively low and thus, the relative ease in experimentation.

At this temperature range, it may be expected that thermally activated processes would not have a significant effect on shape memory behaviour, but this has not necessarily been the case. Even so, in the short term, the best chance for developing a new family of commercial HTSMAs is expected to originate from the alloy systems described in this section.

III.1·1. Ti–Ni–(Pd,Pt) system

Interest in the Ti–Ni–Pd and Ti–Ni–Pt systems as potential HTSMAs was derived from three sets of studies: the comprehensive study of phase transformations in binary B2 titanium alloys,[66] the discovery of high transformation temperatures in the Ti–Pd and Ti–Pt binary systems by Donkersloot,[67] and the discovery of ternary alloying effects on the transformation temperatures of binary Ni–Ti SMAs by Eckelmeyer.[68] Based on the results from these studies, palladium and platinum were added to the Ti–Ni system in order to increase transformation temperatures, and nickel to the Ti–Pd and Ti–Pt systems to improve shape memory behaviour.

III.1·1.a. Ti–Ni–Pd alloys

Ti–Ni–Pd HTSMAs have received the most rigorous attention over the years. Initial focus was centred on improving their high temperature shape memory behaviour, but more recently, the focus has shifted towards improving their work output, as well as dimensional and microstructural stability. In this system, transformation temperatures can be altered by replacing nickel with palladium. If the concentration of titanium is held constant at nearly 50 at-%, the relationship between the transformation temperatures and relative concentration of nickel and palladium is parabolic, as shown in Fig. 23. A minimum in transformation temperatures occurs at approximately 10 at-%Pd, although the exact composition of this minimum is still subjected to debate.[66,69,70] In compositions with palladium concentrations greater than the palladium concentration at this minimum, replacing nickel with palladium increases transformation temperatures by approximately 15°C/at-%.[69,71–73] On the other hand, if the concentration of palladium is lower than the composition at the minimum, replacing nickel with palladium actually lowers the transformation temperatures by 4°C/at-%.[69] This parabolic dependence of the transformation temperatures on composition stems from the change in the structure of martensite. On the higher palladium concentration side of the minimum, B2 austenite transforms to B19 orthorhombic martensite, and at the lower palladium concentration side, it transforms to B19′ monoclinic martensite or R phase. The composition at which the transformation temperatures are at a minimum corresponds to the point of the structure transition. Because of the complete mutual miscibility of the Ti–Ni and Ti–Pd systems, the relationships between

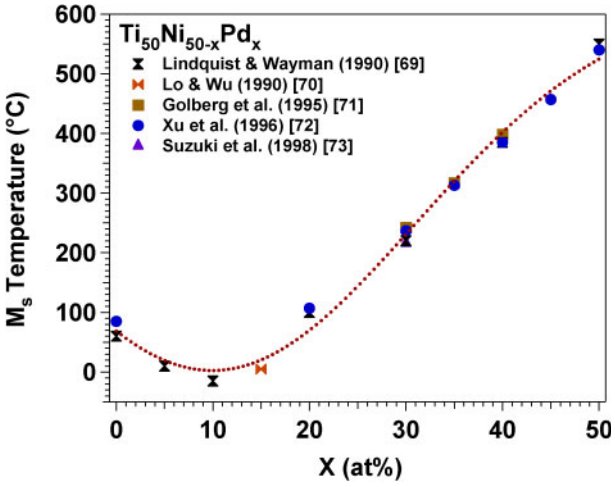

23 Martensite start temperature, M_s, as a function of the palladium content in quasi-equiatomic $Ti–Ni_{50-x}Pd_x$ alloys. Transformation temperatures increase linearly with the Pd content for alloys containing greater than approximately 10–15 at-%. The trendline is a fit through all data points

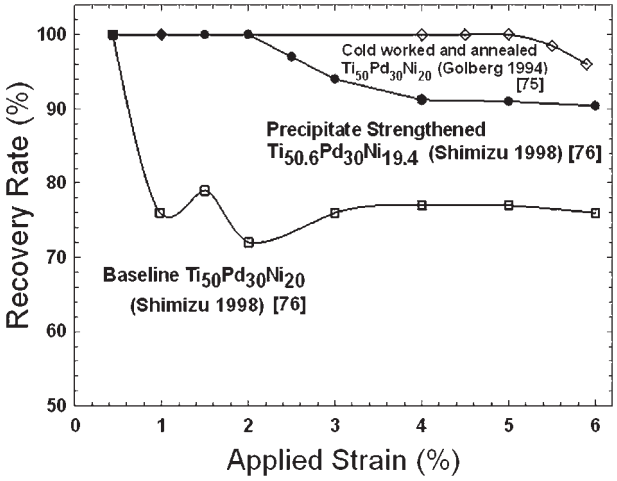

24 Effect of processing on the recovery rate of Ti–Ni–Pd alloys: all specimens were deformed in tension slightly below M_f: 170°C,[75] and 200°C.[76] Figure reproduced with permission from The Taylor & Francis Group[7]

transformation temperatures and composition hold over all ranges of palladium concentration. This enables the access to a continuous range of transformation temperatures from room temperature to over 500°C by adjusting the amount of palladium in the alloy.

Otsuka *et al.*[74] reported poor shape recovery of binary $Ti_{50}Pd_{50}$ HTSMA, concluding that this was primarily caused by the low σ_y of both austenite and martensite. They proposed three possible solutions to improve its shape memory behaviour by strengthening the material through:

(i) solid solution hardening via ternary alloying
(ii) thermomechanical processing
(iii) precipitation hardening or some combination of these approaches.

As the following discussion demonstrates, these solutions have met with varying degrees of success.

While the main effect of nickel addition to Ti–Pd alloys is the reduction in transformation temperatures, it also has an indirect effect of improving shape memory behaviour by lowering the temperature range at which the alloy would be used. At a lower temperature, σ_y is at a higher level. Khachin[66] observed full recovery of 4% applied strain in high temperature torsion experiments on $Ti_{50}Ni_{13}Pd_{37}$. However, Lindquist and Wayman[69] studied the same alloy at room temperature under tension, and were only able to obtain 40% recovery of 6% applied strain. The reason for this discrepancy was not resolved, but it is likely due to the differences in the way the materials were processed and tested, which can have a remarkable effect on recovery rate in Ti–Ni–Pd alloys as shown in Fig. 24.

Although the σ_y of Ti–Pd alloys can be raised indirectly through nickel addition, it is still too low for perfect shape recovery. Several researchers addressed the issue of low σ_y in Ti–Ni–Pd HTSMAs by further solid solution strengthening. Suzuki *et al.*[73] and Yang *et al.*[77] added small amounts of boron to $Ti_{50}Pd_{30}Ni_{20}$ and $Ti_{50\cdot7}Ni_{22\cdot3}Pd_{27}$ alloys, respectively, but neither caused a notable reduction in ε_{irr} with boron additions of up to 0·2 at-%. Micrometre sized Ti_2B particles were found along the grain boundaries, but they were too large and non-uniformly distributed to possibly function as particles for precipitate hardening.[73] Instead, boron acted as a grain refiner by reducing the grain growth rate in these alloys.[73] In identically solution treated or hot rolled specimens, 0·12 at-% boron reduced the grain size from ~40 μm down to 10 μm in the $Ti_{50\cdot7}Ni_{22\cdot3}Pd_{27}$ HTSMA.[77] Presumably for the same reason, 0·2 at-% boron addition to $Ti_{50}Ni_{30}Pd_{20}$ doubled the room temperature tensile elongation to failure from 8 to 16% strain,[73] and increased the ultimate tensile strength from 460 to 800 MPa for a sample deformed in martensite at a temperature of 170°C.[78] It is not clear why the grain refinement effect of boron did not improve the shape memory behaviour, since σ_y increases with grain size refinement. In other studies on solid solution hardening, 5 at-% gold or platinum replacing palladium in $Ti_{50\cdot5}Ni_{19\cdot5}Pd_{30}$ increased σ_y and mildly enhanced cyclic stability, but had little effect on total recoverable strain.[78] From these results,[73,78] it appears that increasing σ_y alone will not necessarily always result in improvements in shape memory behaviour. Another recent study similarly observed little impact on the shape memory recovery rate after alloying $Ti_{50\cdot6}Ni_{19\cdot4}Pd_{30}$ with 1 wt-% cerium,[79] no reason for this observation was given.

Although boron and cesium do not appear to improve the shape memory behaviour, a recent study by Atli *et al.*[80] showed that 0·5 at-% scandium addition to $Ti_{50\cdot5}Ni_{24\cdot5}Pd_{25}$, replacing titanium, was more effective in this aspect. Although the scandium lowered transformation temperatures by about 6–10°C, it was able to reduce ε_{irr} from constant stress thermal cycling experiments under tension by half at stress levels above 200 MPa without adversely affecting ε_{rec}. This improvement was believed to be caused by the solution hardening effect of scandium, but the effect of scandium on the σ_y of martensite and austenite was not explicitly shown. Additionally, scandium addition also reduced ΔT and improved cyclic stability. After 10 thermal cycles at 200 MPa, the cumulative ε_{irr} was reduced by ~20% in the scandium containing specimen.

Golberg *et al.*[71,75,81] investigated the effects of thermomechanical treatments on the shape memory

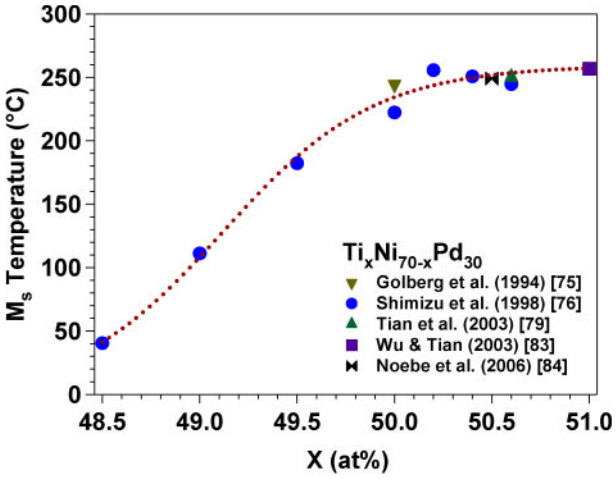

25 Dependence of the martensite start temperature, M_s, on the Ti/(Ni,Pd) ratio. M_s remains fairly constant on the Ti rich side of stoichiometry but drops off precipitously on the (Ni,Pd) rich side. The trendline is a fit through all data points

behaviour of Ti–Ni–Pd HTSMAs. Cold rolling up to 24·5% reduction in thickness followed by annealing at 400°C for 1 h proved effective in increasing σ_y levels of martensite in $Ti_{50}Ni_{20}Pd_{30}$ at 170°C from ~200 to 400 MPa, such that up to 5·3% applied strain was fully recovered by heating above A_f (~250°C) after tensile deformation at 170°C. This was a significant improvement over the solution treated alloy where only 2·5% strain could be fully recovered under the same testing conditions. Cold rolling and subsequent annealing, however, decreased the transformation temperatures by about 20–30°C as compared to that of the solution treated specimens, as expected from the observations on binary Ni–Ti SMAs.[82] On the other hand, while superelasticity exists in the cold rolled and annealed alloy tested above A_f, the strain recovery after unloading was incomplete. The authors concluded that the strength of the parent phase was still too low as compared to the high σ_{SIM} levels, and ε_{irr} was caused by plasticity.[71]

Investigating $Ti_xPd_{30}Ni_{70-x}$ (x=48·5 to 51·0 at-%) alloys encompassing both sides of the equiatomic composition, Shimizu *et al.*[76] realised (Fig. 25) that with decreasing titanium content, transformation temperatures decrease only slightly in Ti rich compositions, but drops off dramatically on the Ni/Pd rich side, such that M_s declines to room temperature in a $Ti_{48·5}Pd_{30}Ni_{21·5}$ alloy. This is similar to the composition dependence of transformation temperatures in binary Ni–Ti SMAs, and is rationalised by the solubility of excess titanium or nickel atoms near the equiatomic composition. Solubility for extra titanium atoms in near equiatomic Ni–Ti is almost negligible, and although the solubility for extra nickel atoms is also small, it is possible to accommodate excess Ni concentrations under 1 at-% in solution. Therefore, in titanium rich compositions, the extra titanium atoms tend to immediately form second phases, and do not affect the composition of the matrix and thus the transformation temperatures of the alloy. However, a small concentration of extra nickel atoms can dissolve in the matrix, changing its composition and transformation temperatures. Utilising precipitates in Ti rich compositions after proper heat treatments, Shimizu *et al.*[76] (Fig. 24) were able to demonstrate that $Ti_{50·6}Pd_{30}Ni_{19·4}$ outperformed the equiatomic $Ti_{50}Pd_{30}Ni_{20}$ alloys with a recovery rate of 90% versus 78% respectively, on samples deformed to 6% applied strain at 200°C under tension. The improvements were attributed to the homogeneous distribution of fine Ti_2(Ni,Pd) type precipitates formed during the annealing process.

Shirakawa *et al.*[85] and Nagasako *et al.*[86] studied the phase transformations in the (Ni,Pd) rich Ti–Ni–Pd alloys, and compensated for the decrease in transformation temperature from the nickel rich matrix by increasing the palladium content. While the two way shape memory behaviour of a $Ti_{48}Pd_{31}Ni_{21}$ alloy annealed at 400°C was qualitatively described, no quantitative data on either one way or two way shape memory behaviour were available.[85] Furthermore, it should also be possible to maintain reasonably high transformation temperatures in nickel rich compositions without increasing Pd content by applying appropriate heat treatments. The reported precipitates are nickel rich in nickel rich compositions, and were identified to be $Ti_2(Ni,Pd)_3$ and $Ti_3(Ni,Pd)_4$ types,[86] so as these precipitates grow, nickel content in the matrix should be reduced, thereby increasing transformation temperatures. Even though no published studies have explicitly demonstrated this in Ti–Ni–Pd alloys, this technique has been used in Ni–Ti–Hf (see Section III.1·2) alloys with some success.[87]

The combined effect of thermomechanical treatment and precipitate hardening through Ti_2(Ni,Pd) particles was investigated by Tian and Wu.[83,88,89] Tian *et al.*[88] claim that deformation in tension at room temperature followed by heating above A_f produced full recovery of up to 7·2% strain and up to 95% recovery at 11% applied strain in a 9% cold rolled $Ti_{50·6}Pd_{30}Ni_{19·4}$ alloy annealed for 1 h at 400°C. However, these experiments were conducted without an extensometer, and from the published figures, the elastic modulus of martensite and austenite were calculated to be 9 and 15 GPa respectively. This indicates that the strain measurements are not quantitatively reliable. Nevertheless, there is useful information to be taken away from the work: when the specimen is deformed at 270°C (above A_f), it does not initially show superelasticity, but exhibits shape memory behaviour instead with a recovery rate of ~90% after reheating to ~400°C. If this deform heat process is repeated about five times, a fully recoverable superelastic behaviour appears which is likely caused by the strengthening effect of training.[88] Owing to the uncertainty in the strain measurement, this superelastic behaviour cannot be quantified.

Martensite reorientation, and thus the shape memory behaviour was absent in 21–29% cold rolled $Ti_{50}Pd_{30}Ni_{20}$ alloy during subsequent deformation at 173°C when post-rolling annealing temperatures were below A_s.[81] Moreover, shape memory behaviour deteriorated if the post-rolling annealing temperatures were very high. Golberg *et al.*[81] concluded that annealing at a temperature below A_s does not allow the preferentially oriented martensite inherited from the rolling process to reset to a self-accommodated martensitic morphology. Conversely, annealing far above A_f initiated microstructural recovery, destroying the work hardening effects of cold rolling. An ideal post-rolling annealing temperature

was proposed to be above A_s but below the recrystallisation temperature.[81] A follow-up study by Xu *et al.*[72] examined the recovery and recrystallisation processes over a full range of cold rolled and annealed $Ti_{50}(Ni,Pd)_{50}$ alloys with palladium contents ranging from 0 to 50 at-%. They observed that recovery started at 450°C in $Ti_{50}Pd_{30}Ni_{20}$ alloy and recrystallisation began at 550°C in $Ti_{50}Pd_{40}Ni_{10}$ alloy. Physically, these diffusion driven mechanisms reduce ε_{rec} by increasing grain size and reducing dislocation density from cold working.[90] If recrystallisation takes place in martensite, reverse transformation temperatures (A_s and A_f)[91] increase due to the loss of internal twins in the martensite. This occurs because during phase transformation, elastic energy is stored in the internal twins of martensite as elastic strain. Recrystallisation replaces these martensites with the 'new' strain free martensite, and the stored elastic energy is lost. Since stored energy is a driving force for the reverse transformation, its loss results in the increase in A_s and A_f. In particular, recovery and recrystallisation temperatures in the range of 450–600°C prevent effective thermomechanical treatment of alloys with high Pd contents and high transformation temperatures since recovery would occur within the operational temperature range of the alloy. Recovery should also cause thermomechanical training and TWSMEs in these HTSMAs to be almost impossible. This factor has severely limited the development of higher temperature Ti–Ni–Pd HTSMAs with Pd contents beyond about 35 at-%.

Similarly, thermal cycling can also affect the stability and properties of SMAs either by introducing a buildup of internal stresses or through their relaxation. For example, thermal cycling of $Ti_{50\cdot6}Pd_{30}Ni_{19\cdot4}$ under 200 MPa increased transformation temperatures by up to 16°C,[92] and stabilised after about 30 cycles. In contrast, thermal cycling under no stress reduced transformation temperatures by 5–10°C, with alloys of higher Pd content exhibiting a greater shift in transformation temperatures during cycling.[91] It was suggested that dislocations introduced during cycling suppressed the martensitic transformation during stress free thermal cycling, but the oriented internal stress fields generated from isobaric thermal cycling assisted the external applied stress, increasing transformation temperatures.[92]

Another mechanism of thermal and time dependent instability in the Ti–Ni–Pd HTSMAs and many other HTSMAs in general is the martensite aging behaviour, whereby transformation temperatures increase with increasing aging time in the martensitic state. In alloys with less than 30 at-%Pd, this effect is very small; however at higher Pd concentrations, a two stage increase in transformation temperatures with increasing aging time was evident in cold worked and annealed samples.[91] Initially, a rapid increase in transformation temperatures with up to 20 h aging at 240°C occurred, and was believed to be a consequence of the SC-SRO phenomenon of point defects,[33] while a more sluggish recovery process was responsible for the second stage. This behaviour is absent at lower Pd compositions because of lower aging temperatures and lower M_s/T_m ratio of near 0·2 in these alloys. This ratio was shown by Ren and Otsuka to be too low for martensitic aging by the SC-SRO mechanism to proceed.[3] In contrast, the M_s/T_m ratio is higher (0·3–0·4) in alloys with higher Pd concentrations, and allows for martensite aging to dominate the initial stages where transformation temperatures can rapidly increase.

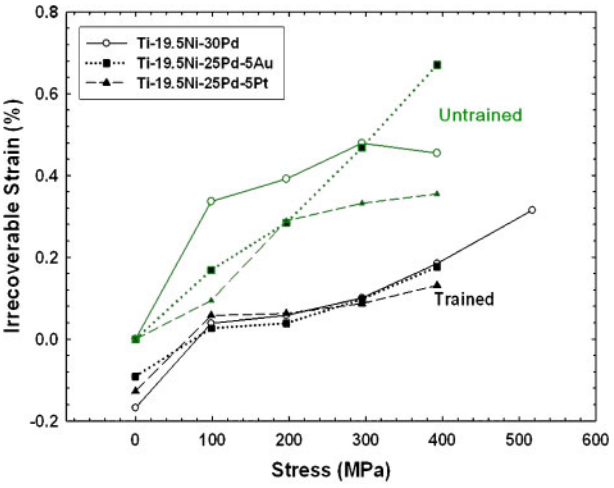

26 Effect of thermomechanical processing and alloying on ε_{irr} of Ti–Ni–Pd–X alloys[94] (Reproduced with permission from the SPIE)

While a significant body of data exists concerning transformation temperatures and shape memory responses of Ti–Ni–Pd HTSMAs, the major physical property discussed up to this point has been the stress free shape memory response seen in Fig. 10. In reality, few applications actually would use the alloy in that fashion. Instead, HTSMAs offer more potential as solid state replacements for conventional actuation systems such as solenoids, motors, or pneumatic and hydraulic systems and for use as the major motive force in adaptive and reconfigurable components for aircraft and other related applications. Therefore, the main interest is the shape memory response of the alloy, not under stress free conditions, but acting against some kind of biasing force. Consequently, the most recent research on Ti–Ni–Pd alloys has focused on the load biased or constant stress thermal cycling response.

The constant stress thermal cycling response of a typical SMA was shown Figs. 11 and 12. The properties measured from this type of tests that are critical for applications are ε_{irr} and ε_{rec} at a given stress level. Another useful property is the work output (Fig. 13*b*), which is the product of ε_{rec} and applied stress. It is desirable in actuator applications for HTSMA components to be dimensionally stable (small ε_{irr}) while possessing a large 'stroke' (large ε_{rec}) under as high a stress level as possible.

Ti–Ni–Pd alloys containing less than ~35 at-%Pd have acceptable work characteristics but tend to suffer from rather high ε_{irr} during thermal cycling under load. This irreversibility worsens with increasing applied stress[78] and increasing Pd concentration at constant stress.[93] Therefore, a significant focus of the recent research on Ti–Ni–Pd alloys has been in pursuit of mechanisms that reduce ε_{irr}. In particular, Bigelow *et al.*[94] have found that alloying with Pt or Au reduced ε_{irr} considerably in the absence of thermomechanical training as summarised in Fig. 26, but no significant reduction of ε_{irr} from these alloying elements occurred in trained specimens. Thermomechanical training alone also reduced ε_{irr} significantly as seen in Fig. 26. Not only

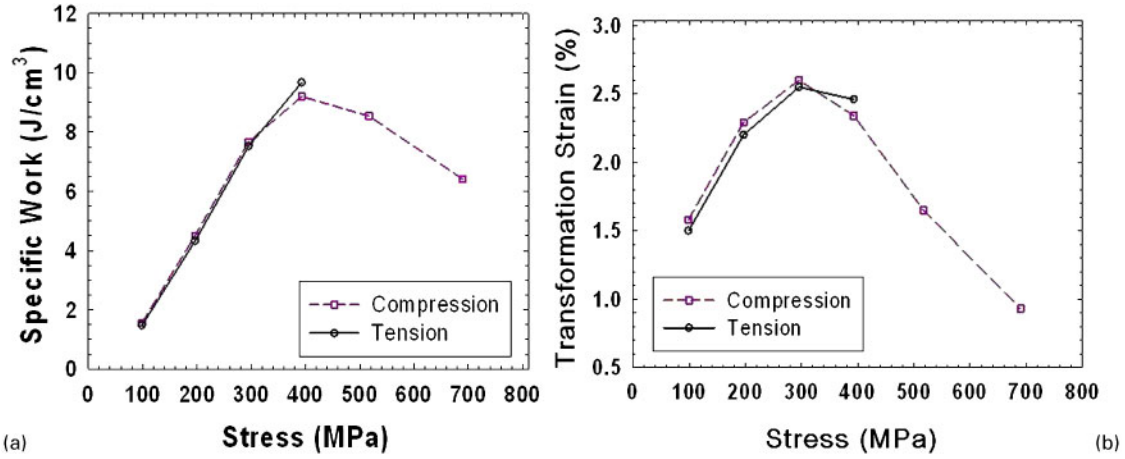

27 ***a*** **specific work output for a $Ti_{50\cdot5}Ni_{19\cdot5}Pd_{30}$ alloy as a function of applied stress loaded in both tension and compression and** ***b*** **the corresponding transformation strain versus applied stress.[84] (Reproduced with permission from the SPIE)**

are these approaches useful in reducing ε_{irr} in Ti–Ni–Pd alloys, they also have no detrimental effect on recoverable strain and thus relative work output for these materials.

The amount ε_{irr} for a given alloy and stress level increases as the maximum temperature to which the sample is thermally cycled increases, with all other considerations being constant,[94] thus placing another criterion on the upper temperature limit for these materials. However, certain alloying additions such as 5 at-%Pt increases the maximum temperature capability of Ti–Ni–Pd alloys by $\sim$30°C,[94] thus providing some measure of protection against overheating.[95]

Similar to conventional Ni–Ti SMAs,[96,97] the work output for Ti–Ni–Pd alloys peaks at some optimum stress level[84] as shown in Fig. 27*a*. This peak in work output is a result of competing factors. As the stress level increases, more martensite variants become favourably aligned and detwinned, forming more single variant morphology and accommodating larger strains. At the same time, the increasing stress level approaches σ_y of the alloy and causes irrecoverable deformation to occur instead of martensitic transformation, and negatively affects the recoverability of martensite. Consequently, these factors cause ε_{rec} to reach a maximum and then rapidly decrease with increasing stress as shown in Fig. 27*b* for the $Ti_{50\cdot5}Ni_{19\cdot5}Pd_{30}$ alloy. Therefore, even though the applied stress continues to increase, ε_{rec} diminishes and its product with applies stress, which is work output, reaches a maximum at a particular stress level as well.

The maximum work output for various Ti–Ni–Pd alloys as a function of the transformation temperatures range, such that the full range over which the transformation occurs (M_f to A_f) for each alloy is clearly indicated,[98] is shown in Fig. 28. Large and consistent work output of between 8 and 11 J cm^{-3} is achieved for alloys with transformation temperatures between 100 and 300°C. However, for alloys with transformation temperatures above this range, the work output drops off almost catastrophically so that alloys with transformation temperatures in the neighbourhood of 500°C are capable of essentially zero work output, placing another limit on the viability of HTSMAs beyond just the need for a high transformation temperature. This is a natural consequence of the reduction of σ_y at higher temperatures and the onset of creep deformation.[99]

Most of the behaviours just described for the Ti–Ni–Pd alloys, such as generally poor recoverable strain capability and the sharp decline in work output beyond $\sim$300°C, can be explained by comparing the deformation characteristics of the individual martensite and austenite phases. To demonstrate this point, Bigelow *et al.*[93] determined σ_y of austenite, stress levels for martensite reorientation/detwinning, and σ_y of martensite for a series of Ti–Ni–Pd alloys containing 15 to 46 at-%Pd which are shown in Fig. 29. For each composition, one sample was loaded at a temperature of M_f-50°C and then thermally recovered under stress-free conditions. This experiment resulted in a value for σ_{DT} of martensite, and σ_y of the martensite. Another sample was then loaded at A_f+50°C to determine σ_y of austenite. At around 37 at-%Pd, the reorientation stress and σ_y of austenite cross. At lower Pd contents than this crossover composition, work is possible because an applied stress results predominantly in martensite

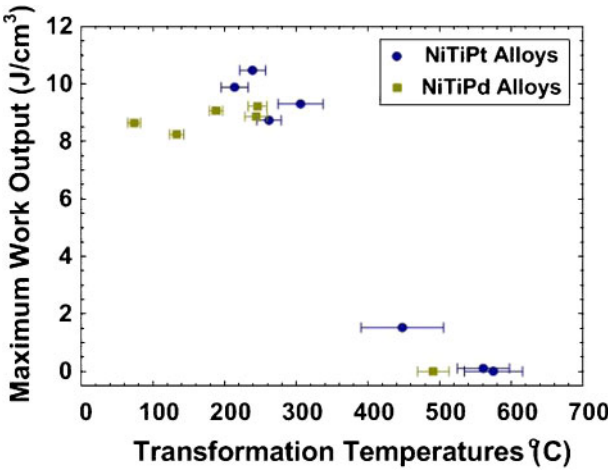

28 Work output for a series of Ti–Ni–Pd and Ti–Ni–Pt alloys as function of the transformation temperature range (M_f to A_f).[98] Alloys containing ternary additions producing transformation temperatures greater than about 400°C show almost no usable work output. (Reproduced with permission from the SPIE)

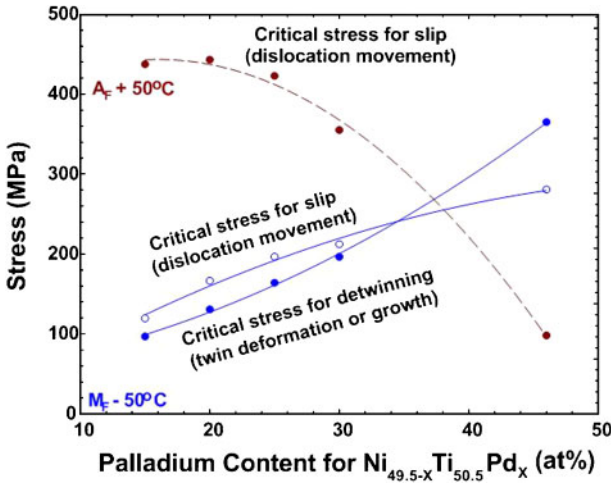

29 Critical stress data for Ti–Ni–Pd alloys determined from monotonic tensile tests and strain recovery behaviour.[93] (Reproduced with permission from the SPIE)

reorientation before or occurring concurrently with slip in the martensite, but does not result in permanent deformation of the austenite. At the highest Pd content studied, which corresponds to an alloy with ~500°C transformation temperature in Fig. 28, any stress high enough to cause reorientation in the martensite also produces a much greater amount of slip in the austenite when the alloy is cycled through the transformation.

Furthermore, while the amount of ε_{irr} increases in an approximately linear fashion with increasing Pd content between 15 and 30 at-%Pd,[93] some amount of unrecovered deformation occurs at every stress level, even in the alloy with the lowest Pd content. Based on Fig. 29, although the σ_{DT} is lower than σ_y of martensite over this range of composition, their difference is only ~20 MPa, and it is very likely for plastic deformation to take place. However, it is also possible that some of the unrecovered deformation in lower Pd compositions may be caused by remnant martensite that did not transform back to austenite upon heating. Although strain from remnant martensite can be recovered by heating to a higher temperature, this is often impractical in applications, where the range of temperature cycles is generally fixed. In alloys with a high Pd content (greater than ~37 at-%), permanent deformation of both the martensite and austenite occurs well before martensite reorientation; therefore there is little to no recoverable deformation that can occur to produce work, and large amounts of non-recoverable permanent deformation accumulate when thermally cycled under load. In addition, creep begins to have a noticeable effect near 400°C, and will likely cause more irreversible deformation during the thermal cycling of alloys with a high Pd content.[99]

The experiments by Bigelow *et al.*[78,93,94] are very useful in revealing the critical factors that would lead to the development of superior alloys for actuator type applications. These are: a low σ_{DT}; a high σ_y to any types of slip or other processes that would lead to irreversible deformation of the martensite phase, and a high σ_y of austenite. Therefore, the key to developing dimensionally stable HTSMAs with good work output is to prevent the plastic deformation processes while not greatly affecting reorientation/detwinning stress. The primary methods for accomplishing this are the same as those originally suggested Otsuka *et al.*[74] for improving the stress free shape memory behaviour of Ti–Pd alloys, namely: solid solution hardening, the use of thermo-mechanical processing, and precipitate strengthening.

Finally, the only study on the direct effect of creep on the shape memory behaviour was carried out on $Ti_{50}Ni_{10}Pd_{40}$ alloy with M_s of 388°C and A_f of 411°C.[99] Significant amount of ε_{irr} was accumulated during tensile thermal cycles between 300 and 520°C under 200 MPa. When the heating cooling rate was decreased from 20 to 2°C min^{-1}, ε_{irr} after one heating cooling cycle almost doubled (Fig. 30), an indication of high creep activity. When the stress level was reduced to 100 MPa for heating cooling cycles conducted within the same temperature range, ε_{irr} levels were much lower, and

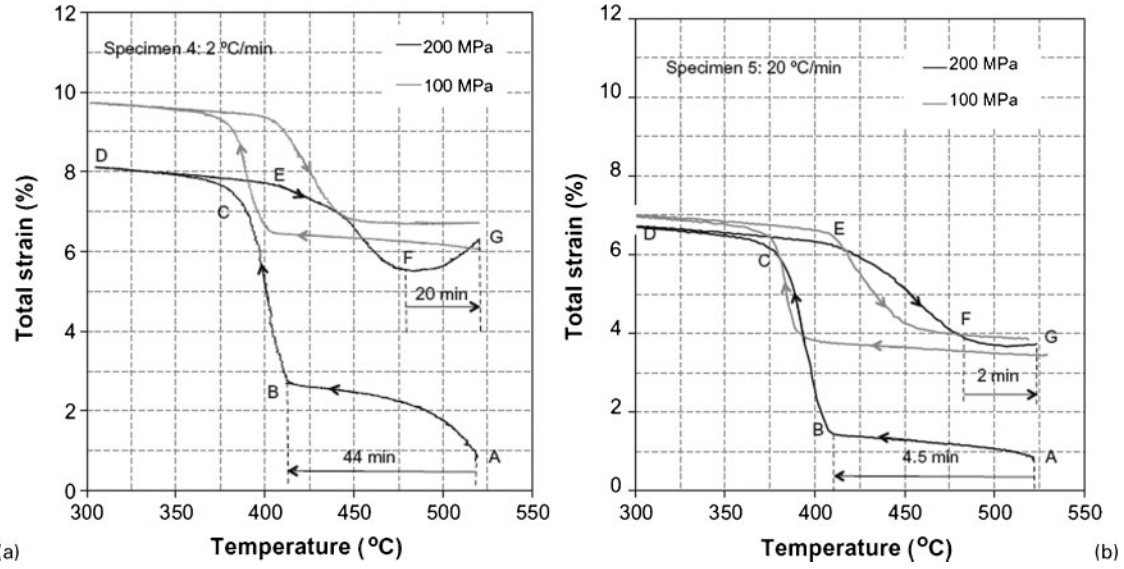

30 Creep behaviour of a $Ti_{50}Ni_{10}Pd_{40}$ HTSMA during thermal cycling under stress. Under 200 MPa, significant ε_{irr} due to creep develops. The effect of creep is greater *a* when the heating-cooling rate is slower than *b* when heating-cooling rate is faster.[99] (Reproduced with permission from Elsevier)

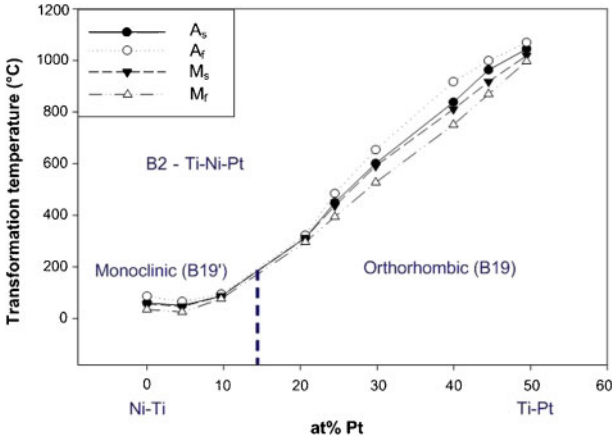

31 Pseudo binary TiNi–TiPt phase diagram for $Ti_{50}Ni_{50-x}Pt_x$ alloys.[100] (Reproduced with permission from the SPIE)

did not appear to be a function of heating cooling rate. This finding was further supported by constant temperature creep experiments under 100 and 200 MPa at 520°C. After 2·5 h, total creep strain of 1·2% was recorded for the specimen under 100 MPa, while the specimen under 200 MPa showed creep strain of 12·4%. Clearly, the combination of 200 MPa and maximum temperature of 520°C was sufficient to activate unacceptable levels of creep activity. Although the effect of creep under 100 MPa is comparatively much smaller, the net effect remains very significant. Because operating temperatures in SMA components are dictated by the transformation temperature, the $Ti_{50}Ni_{10}Pd_{40}$ HTSMA cannot be used above 100 MPa in an actuator type application.

In summary, extensive research and development of Ti–Ni–Pd alloys have produced material with reasonable stress free shape memory behaviour (i.e. one way shape memory effect), low ΔT and good work output. On the other hand, reversibility and corresponding dimensional stability still need to be further addressed and are the primary focus of several continuing research efforts. Nevertheless, current thinking is that this system is an extremely viable source of alloys for HTSMA applications in the 200–300°C range.

III.1·1.b. Ti–Ni–Pt alloys

Similar to the Ti–Ni–Pd system, replacing nickel with platinum increases the transformation temperatures, but only after a threshold value of approximately 10–15 at-%Pt is reached[70,100] (Fig. 31). At $\leqslant$10 at-%Pt, the martensite structure is B19′ (monoclinic),[101] and transformation temperatures are relatively insensitive to Pt content or decreases slightly with a minimum observed at 5–10 at-%Pt. However, at higher levels of Pt, at least 16 at-% or greater, the martensite formed is B19 (orthorhombic),[101,102] and transformation temperatures increase linearly with Pt concentration until transformation temperatures near 1000°C are reached for the binary Ti–Pt alloy (Fig. 31). Finally, in contrast to the Ti–Ni–Pd system (Fig. 25), the transformation temperatures for (Ni,Pt) rich compositions do not decline sharply with deviations from stoichiometry and a $(Ni,Pt)_3Ti_2$ precipitate phase readily occurs in alloys slow cooled from elevated temperatures.[100]

Lindquist and Wayman[70] recorded a rather small ΔT for their Ti–Ni–Pt alloys, except for the highest Pt

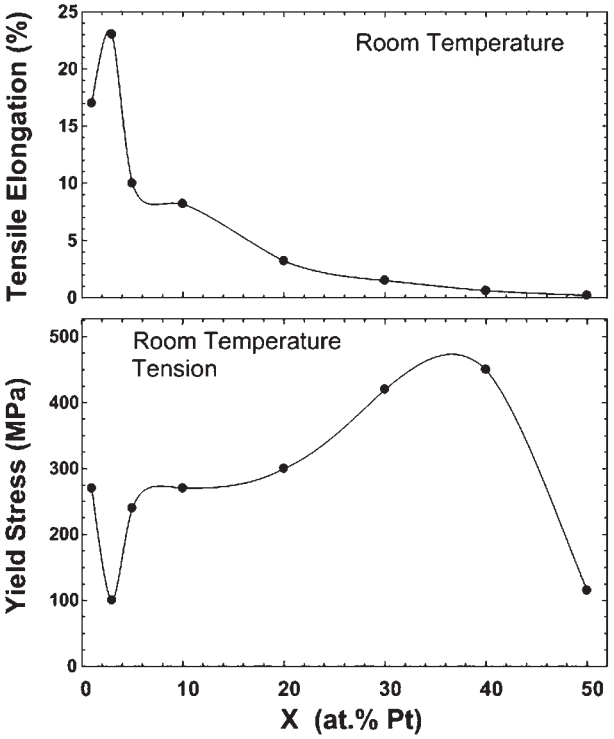

32 Room temperature tensile properties, yield strength and tensile elongation, as a function of Pt content for $Ti_{50}Ni_{50-x}Pt_x$ alloys with 0 to 50 at-%Pt (Ref. 103)

content studied at 30 at-%. This particular alloy exhibited ΔT of over 80°C, which is consistent with the later data from Rios *et al.*[100] who reported a rather wide ΔT (40–80°C) for alloys containing 30 at-% or more Pt, as shown in Fig. 31. The nature of the anomalously large ΔT at 30 at-%Pt or higher is unknown at this time, but since transformation temperatures in this composition are >500°C, the large ΔT could be caused by creep during transformation cycles, similar to that observed in the Ti–Ni–Pd HTSMAs.[99] On the other hand, ΔT is generally less than 20°C for alloys with 25 at-% or less Pt, which is desirable in any applications requiring active control of the transformation or where cycle time and frequency is critical.

Lindquist and Wayman[70] attempted to measure the recoverable shape memory strains in Ti–Ni–Pt alloys but were limited by the extremely low room temperature ductility of their alloys. Hosoda *et al.*[103] have also measured the room temperature tensile properties of an entire series of $Ti_{50}Ni_{50-x}Pt_x$ alloys from 0 to 50 at-%Pt and found that ductility generally decreased as the amount of Pt increased, but that σ_y followed a much more complicated dependence on composition, as shown in Fig. 32. Nickel actually appears to harden Ti–Pt alloys considerably, while Pt additions to Ni–Ti soften the monoclinic martensite phase, at least initially. The tensile ductility values of Hosoda *et al.*[103] are very consistent with those of Lindquist and Wayman,[70] who observed about 3·5 and 1% tensile ductility for 20 and 30 at-%Pt alloys respectively. In specimens of $Ti_{50}Ni_{20}Pt_{30}$ hot extruded at 900°C, room temperature tensile ductility of nearly 4% strain has been observed by Noebe *et al.*[104] On the other hand, when hot extrusion was carried out at 1100°C, ductility was reduced to ~1·5%. Since the extrusion texture is expected to be stronger and the grain size finer in the specimen extruded at 900°C compared to

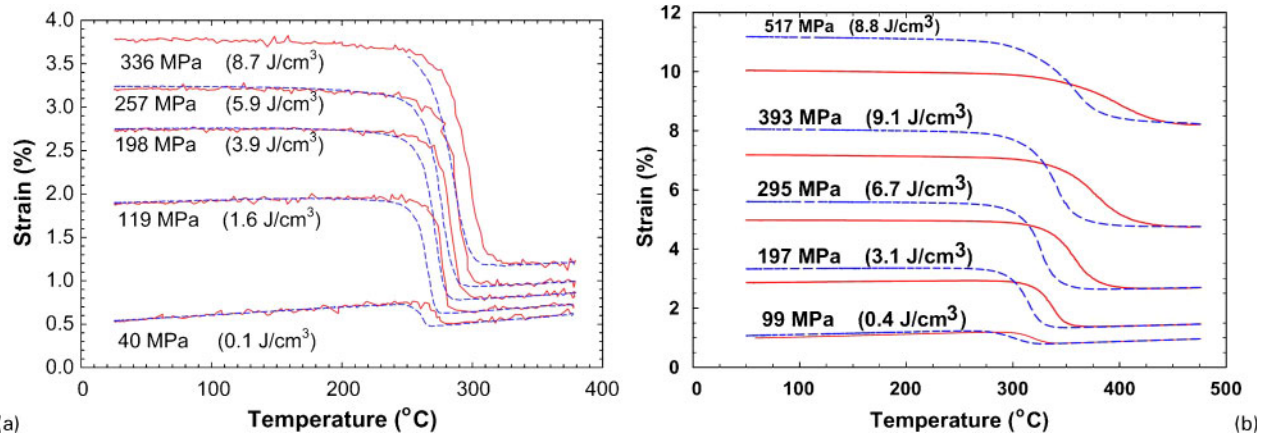

33 Constant stress thermal cycling response at different stress levels for *a* stoichiometric $Ti_{50}Ni_{30}Pt_{20}$ alloy[104] and *b* Ti rich $Ti_{50·5}Ni_{29·5}Pt_{20}$ alloy.[105] The alloys were cycled twice at each stress level and only the second cycles are shown. The stoichiometric material exhibits much better dimensional stability (Reproduced with permission from *a* the SPIE, and *b* ASM International)

one extruded at 1100°C, it is likely that extrusion temperature has an influence on tensile ductility.

Compared to the Ti–Ni–Pd alloys, the stress free shape memory response of Ti–Ni–Pt alloys has not received a similar level of attention, with the exception of the attempts by Lindquist and Wayman[70] in tension and Meisner and Sivokha for a $Ti_{50}Ni_{34}Pt_{16}$ alloy in torsion.[102] Instead, more effort has been focused toward the constant stress thermal cycling behaviour of Ti–Ni–Pt alloys including the properties of $Ti_{50}Ni_{30}Pt_{20}$ bar, fine rod and wire.[105] The effect of transformation temperature range on the work output of Ti–Ni–Pt alloys is shown in Fig. 28 and follows the same dependence as the Ti–Ni–Pd alloys and for the same reasons. Alloys with transformation temperatures up to ~300°C show reasonable work output with good reversibility for near stoichiometric compositions and Pt contents up to 20 at-%, even in the as processed, i.e. hot extruded, condition with no prior training. Ti rich alloys, however, show larger ε_{irr} at essentially all stress levels, as shown in Fig. 33. Incidentally, binary Ni–Ti alloys also show better reversibility on the Ni rich side of stoichiometry than that on the Ti rich side,[106] and this apparent dependence of stoichiometry on reversibility and dimensional stability of Ni–Ti based HTSMAs is something that is worth pursuing in greater detail in the future. Alloys with significantly higher transformation temperatures in the range of 500–600°C, such as $Ti_{50}Ni_{20}Pt_{30}$ alloys, exhibit no useful work output and significant ε_{irr} at essentially all stress levels since the reorientation stress in these alloys is significantly greater than σ_y.[98,104]

Given the potential use of these alloys in high temperature applications, the oxidation kinetics of a Ti–Ni–Pt and binary Ni–Ti alloy have been determined in detail.[107] The oxidation mechanisms were the same for both alloys, but the oxidation rate was four times greater for Ni–Ti than Ti–Ni–Pt. The presence of the large Pt atoms that reduce the overall diffusion rate in the alloy without affecting actual oxidation mechanisms is the most likely explanation. Given the rate data available, Smialek *et al.*[107] determined the expected life of various Ti–Ni–Pt wires with failure defined by a given atomic percent loss (1, 5 or 10%) of Ti in the alloy from oxide scale formation. The results for wires with a radius of 0·254 and 0·0559 mm are shown in Table 1 and indicate that for even fine wire, oxidative life is quite high as long as the temperature is 500°C or lower. But above 600°C, the oxidative life of the Ti–Ni–Pt component becomes a serious concern. At temperatures above 700°C, oxidation is problematic for any Ni–Ti based alloy.

As with the other precious metal additions to Ni–Ti, the high initial material costs will have to be offset by the increased benefits in using HTSMAs at the system level, probably limiting bulk material to high performance and demanding applications, such as those existing in the aerospace industry. While the data in most cases are still cursory, the Ti–Ni–Pt alloys with 20 at-%Pt or less show promise for such demanding applications, since they have high transformation temperatures, good work output and dimensional stability below ~350°C, low ΔT, good thermal stability and excellent oxidation resistance below ~500°C, and compares favourably to the Ti–Ni–Pd HTSMAs. Yet, the body of knowledge on the Ti–Ni–Pt system is not as thorough as that for Ti–Ni–Pd. This is not necessarily a disadvantage. On the

Table 1 Estimated oxidative life (h) for 254 μm (0·010 inch) and 559 μm (0·022 inch) radius Ti–Ni–Pt wires as function of temperature defined for several levels of Ti loss due to oxidation[107]

	R=254 μm			*R*=559 μm		
T, °C	1 at-%Ti	5 at-%Ti	10 at-%Ti	1 at-%Ti	5 at-%Ti	10 at-%Ti
500	18 927	473 177	1 892 708	91 607	2 290 177	9 160 708
600	57·6	1440	5758	279	6967	27 869
700	9·7	242	969	46·9	1172	4689
800	0·10	2·5	10	0·48	11·9	48
900	0·01	0·33	1·3	0·06	1·6	6

one hand, the maturity of Ti–Ni–Pd lends itself to immediate commercial consideration over Ti–Ni–Pt, while on the other, certain optimisation studies performed for Ti–Ni–Pd alloys has not yet been done for Ti–Ni–Pt, and it is possible that they could further improve the properties of Ti–Ni–Pt HTSMAs, which already has matched, if not outperformed that of Ti–Ni–Pd. However, the recent efforts on Ti–Ni–Pt alloys also point out some additional concerns when determining the potential upper application temperature for the so called HTSMAs.

III.1·1.c. Unconventional processing techniques for Ti–Ni–(Pd/Pt) alloys

All the alloys discussed in the previous two sections were produced by conventional ingot metallurgy processes that included thermomechanical processing of cast ingots usually followed by some form of heat treatment. Meanwhile, techniques such as physical vapour deposition and magnetron sputtering make it possible to attain unique properties in Ti–Ni–(Pd,Pt) SMA thin films. Not only is it possible to achieve grain refinement and increase σ_y using thin film fabrication techniques, but shape memory thin films are very well suited for actuator applications in miniature devices. Actuators of SMA are controlled by heating and cooling the material from an external source; therefore large sized bulk SMA actuators suffer from poor response frequencies since it takes time to cool the material, and the maximum frequency at which the actuator can operate is limited. In contrast, the small dimension of thin films allows them to be heated and cooled very quickly, and improves the response time and maximum operating frequency tremendously. Thin films enable the use of SMA actuators in micro-electromechanical devices, where the benefit of a solid state actuator stands out most conspicuously.

Grain size of as deposited amorphous films can be up to 10 to 100 times smaller than that in bulk materials after recrystallisation heat treatments[108–112] without affecting transformation temperatures significantly. Sawaguchi *et al.*[113] obtained full recoverability up to 2·9% applied strain in $Ti_{49·5}Ni_{22}Pd_{28·5}$ thin film while Grummon[5] notes full recoverability of 2·5% applied strain in Ti rich $Ti_{52·7}Ni_{18}Pd_{29}$ films. Through selective choice of substrate, it is possible to create a pseudo 'two way shape memory effect' by utilising residual stress in the film developed from differences between the thermal expansion coefficients of the film and substrate[5,114] in a similar fashion as the biasing force of an actuator. Also, with the proper choice of substrate material, large actuation stress, both tensile and compressive, can be obtained from the films, leading to more functional flexibility and higher operating transformation temperatures due to the stress assistance for the transformation.

Processing difficulties related to thin film deposition are numerous. It is challenging to obtain exact compositions due to differences among the constituent deposition and resputtering rates.[115] Titanium is often lost during the sputtering process and must be compensated by introducing sacrificial titanium.[5,115] Sluggish diffusion kinetics during deposition in the plane of the film due to its thinness often causes compositional inhomogeneity in the final product, leading to two stage transformation where one part of the film undergoes transformation before another.[5] As-sputtered films on cold substrates are generally amorphous and require a crystallisation heat treatment, but if this annealing process is done with the film attached to its substrate, severe diffusion in the normal direction to the plane of the film takes place between the substrate and film, changing composition near the film substrate interface.[115,116] Titanium's high affinity for oxygen also contributes to delamination and changes in physical properties of the film.[115,116] These issues can be mitigated somewhat through deposition onto heated substrates, which eliminates the need for crystallisation heat treatment.[115] Thin films also suffer from cyclic instabilities, such that transformation temperatures decrease and do not stabilise after 100 stress-free thermal cycles.[115] Finally, thin films are much more prone to oxidation problems due to its thinness. It was mentioned in Section III.1·1.b that a 254 μm diameter Ti–Ni–Pt wire possesses useful oxidation life of over 10 000 h at 500°C.[107] If thin film of this composition was made, the oxidation life at 500°C will be drastically reduced compared to that of the wire because of the over 100-fold reduction in critical dimension.

Severe plastic deformation processing of $Ti_{50}Ni_{30}Pd_{20}$ through equal channel angular extrusion (ECAE) yielded encouraging results.[117] Compared to the solution treated specimens, ECAE $Ti_{50}Ni_{30}Pd_{20}$ specimens processed at 400°C via route 4C resulted in a 30–40% reduction of ε_{irr} during constant stress thermal cycling experiments under 150 MPa tensile stress. Furthermore, the ECAE process eliminated early failure in the solution treated specimens during constant stress thermal cycling, which occurred at a stress level of 200 MPa. In contrast, specimens processed through ECAE route 4C at 400°C did not fail until the 350 MPa cycle. These improvements are caused by a large increase in dislocation density in the ECAE processed specimens, and also a significant reduction in grain size from ~30 μm in the solution treated specimens to ~500 nm. Although ECAE processing reduced transformation temperatures by ~7°C, the combined effect of the reduction of ε_{irr} and improved toughness allows the ECAE processed $Ti_{50}Ni_{30}Pd_{20}$ HTSMA to be used at higher stress levels without generating excessive plasticity, and therefore achieving higher work output, making it a much more useful material overall.

III.1·2. Ni–Ti–Hf and Ni–Ti–Zr

The Ni–Ti–Hf and Ni–Ti–Zr systems are possible alternatives to the much more costly precious metal containing alloys discussed above. In this case, the ternary alloying elements (Hf and Zr) are substituted at the expense of titanium. A prime motivation behind studying Ni–Ti–(Hf,Zr) alloys is the relatively low raw material cost of Hf and Zr, at least compared to Pt, Pd and Au, and their greater influence on transformation temperatures, which allows them to be used in smaller concentrations. Since the mechanical and shape memory properties of Ni–Ti–Hf and Ni–Ti–Zr alloys are very similar, they will be discussed concurrently in this section.

Figure 34 shows that additions of hafnium above 3 at-% increase the transformation temperatures of the binary Ti–Ni system.[118] This increase is only ~5°C/at-% up to 5–10 at-% hafnium, then elevates to over 20°C/at-% thereafter. Ni–Ti–Zr alloys are similar to the Ni–Ti–Pd/Pt alloys, in that any increase in

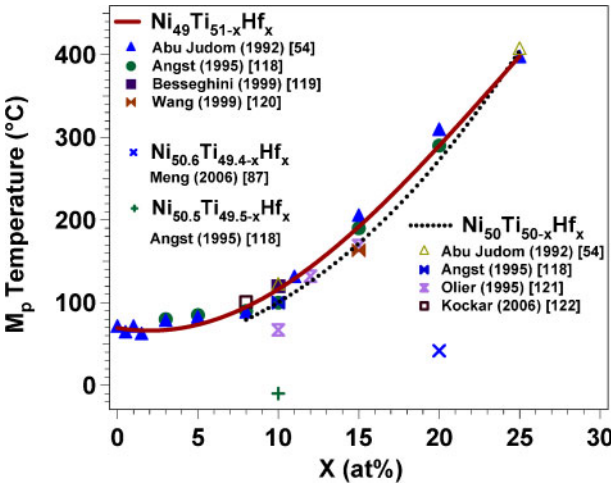

34 Composition dependence of the martensitic peak temperature, M_p, as a function of hafnium content in the Ni–Ti–Hf alloy system. Adding hafnium above 10% results in much more dramatic increase in transformation temperatures. Similar transformation temperatures are found in Ti rich and quasi-equiatomic compositions, but those in nickel rich compositions are much lower. The trendlines are the fits through all data points

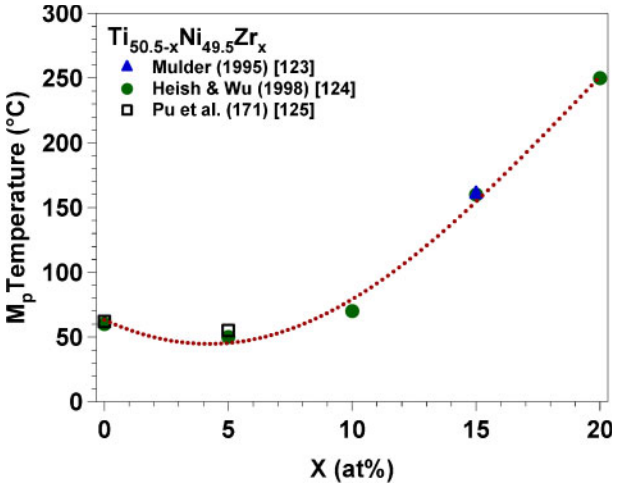

35 Composition dependence of the martensitic peak temperature as a function of Zr content in the Ni–Ti–Zr alloy system. The trendline is a fit through all data points

transformation temperature only occurs above 10 at-% zirconium (Fig. 35). At this level, further zirconium addition increases M_s at a rate of ~18°C/at-%.[123] Therefore, hafnium elevates transformation temperatures more effectively than does zirconium at identical concentrations.[118,121] In the solution treated state, the martensitic peak temperature M_p is 190°C in $Ni_{49}Ti_{36}Hf_{15}$[118] and 160°C for $Ni_{49.5}Ti_{35.5}Zr_{15}$.[124] Transformation temperatures are not notably affected by a change in nickel content in either system as long as the alloys were (Ti,Hf/Zr) rich, but dropped steeply when nickel content is increased beyond the equiatomic (50 at-%) composition,[118,123,126] consistent with the behaviour of Ni–Ti alloys in general.

Atomistic simulations showed that hafnium atoms have equal preference for titanium and nickel sites in Ni–Ti alloys,[127] which suggested that hafnium substitution for nickel instead of titanium may also change transformation temperatures. Experimentally, however, this has been disproved. Although Tong *et al.*[128] showed that replacing nickel with hafnium in the nominal composition increased transformation temperatures, there was actually no change in the composition of the transforming matrix. Instead, when nominal nickel content is reduced in favour of hafnium, the volume fraction of the $(Ti,Hf)_2Ni$ phase increased. At the same time, some of the titanium in the matrix was replaced by hafnium, causing an increase in the transformation temperatures.

Most research efforts have focused on (Ti,Hf/Zr) rich alloys with under 20 at-%Hf/Zr. In these alloys, a single stage transformation of cubic B2 parent phase to monoclinic B19′ martensite takes place,[124,125,129,130] whereas in higher Hf/Zr content compositions approximately above 20–25 at-%, orthorhombic B19 martensite appears.[125] Ti_2Ni,[131] or $Ti_4Ni_2O_x$ ($x<1$)[121] type precipitates are found in (Ti,Hf) rich Ni–Ti–Hf alloys depending on interstitial oxygen level.[119,126] The situation is more complicated in Ni–Ti–Zr alloys. In addition to Ti_2Ni type precipitates, a phase with relatively low melting point named λ_1 appears in alloys in excess of 10 at-%Zr in (Ti,Zr) rich compositions when cooled slowly from solution.[124,132] Ni–Ti–Zr appears to be physically less stable than Ni–Ti–Hf alloys with identical Ti and Ni content, and the volume fraction of the precipitates in the Ni–Ti–Zr alloys is generally higher. In both systems, precipitate volume fraction increases as alloy composition moves deeper into the (Ti, Hf/Zr) rich region of the ternary phase diagram.[124,126]

Both Ni–Ti–Hf and Ni–Ti–Zr are somewhat brittle in tension at room temperature.[120,124] For example, $Ni_{49}Ti_{36}Hf_{15}$ failed in tension at 7% strain[133] at room temperature; fortunately, ductility is improved at higher temperatures, and in the same alloy deformed at 260°C in full austenite, fracture did not occur until 30% tensile strain.[120] Ductility worsens sharply with increasing Hf and Zr concentrations.[134,135] Addition of 0·1 at-% boron did not improve the ductility of $Ni_{49}Ti_{36}Hf_{15}$,[136] but whether if it leads to grain refinement as it did for Ti–Ni–Pd alloys was not mentioned.

In solution treated $Ni_{49}Ti_{36}Hf_{15}$ alloys, full recovery of 3% applied strain, as well as a recovery rate of over 80% of 6% applied strain have been observed upon heating after either deformation at room temperature in bending,[133] or tensile deformation at 80°C,[120] both in the martensite state. On the other hand, Olier *et al.*[121] could only obtain 80% recovery rate in a $Ni_{50}Ti_{38}Hf_{12}$ alloy prepared through powder metallurgy (grain size, ~10 μm) when deformed in tension to 2·5% strain at room temperature. When they increased the deformation temperature from room temperature to 150°C (~35°C below A_s and in the fully martensitic state), σ_{DT} decreased from 535 to 390 MPa. However, the recovery rate at applied strain of 2·5% at 150°C was the same (80%) as the specimen deformed at room temperature. It is likely that martensite σ_y also decreased when the deformation temperature was increased to 150°C, nullifying the concurrent reduction in σ_{DT} and producing no improvement in recovery rate. Furthermore, it was possible to obtain full recovery of 4% applied tensile strain when the alloy is first heated to above A_f, then cooled to and deformed at 150°C (above M_s and fully in the austenite state).[121] This way, the deformation

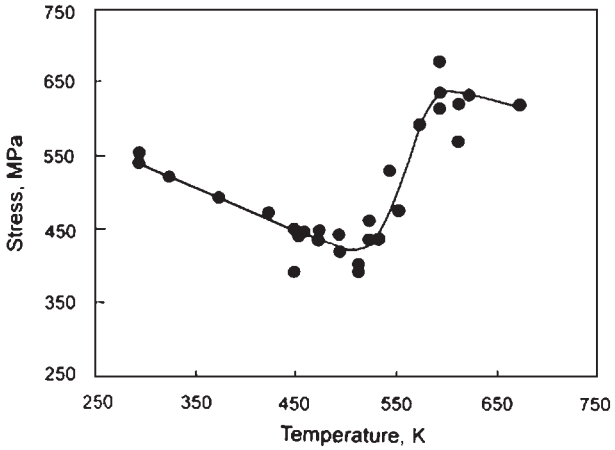

36 The temperature dependence of the stress for the onset of inelastic deformation (martensite reorientation, stress induced transformation, or plastic deformation) in $Ti_{36}Ni_{49}Hf_{15}$ alloy:[120] different regimes of temperature dependence correspond to different governing deformation mechanisms as schematically illustrated in Fig. 16

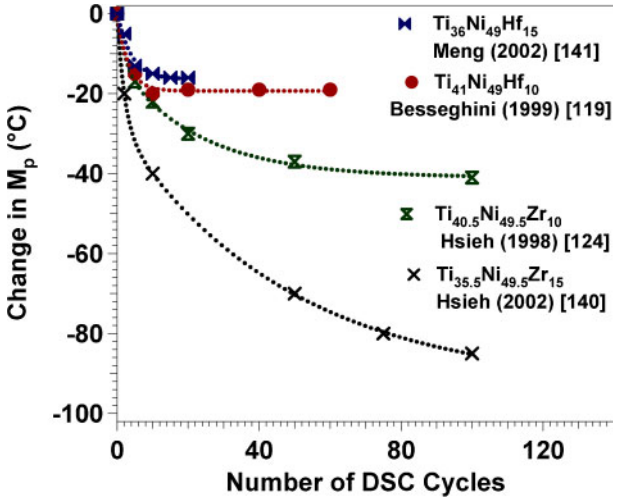

37 Decrease in the transformation temperatures of Ni–Ti–Hf/Zr alloys due to thermal cycling under stress free conditions in the DSC. The trendlines are the fits through each set of data points. Reproduced with permission from Elsevier

mechanism responsible for the shape memory behaviour changes from martensite orientation to stress induced martensitic transformation, and the better property of the latter was enabled by a lower σ_{SIM} (335 MPa) than σ_{DT} (390 MPa) at the same temperature.[121] However, unlike the temperature dependence of σ_{DT}, σ_{SIM} increases with a rise in temperature instead of decreasing, and once the alloy enters the stress induced martensite regime, increase in deformation temperature deteriorates the recovery rate very quickly.[133] Figure 36 is a summary of data by Wang *et al.*[120] showing the stress needed to activate deformation mechanisms at different temperatures, which corresponds well with Fig. 16. In addition to ordinary shape memory behaviour, two way shape memory strain of 0·25% has also been demonstrated in a $Ni_{49}Ti_{36}Hf_{15}$ alloy,[137] and could be increased up to 0·88% through 30 cycles of shape memory training.

Shape memory behaviour of Ni–Ti–Zr alloys is in general inferior to those of Ni–Ti–Hf alloys. Full recovery of up to 1·8% applied strain in bending at room temperature was possible for $Ni_{50}Ti_{35}Zr_{15}$, and up to 1·6% applied strain in bending could be fully recovered in solution treated $Ni_{50}Ti_{30}Zr_{20}$ alloys.[125] A full recovery of 1·8% applied strain in $Ni_{50}Ti_{35}Zr_{15}$ and an 85% recovery rate for 2·8% applied strain in solution treated $Ni_{49·5}Ti_{35·5}Zr_{15}$ were also observed by Mulder *et al.*[123] after room temperature deformation in compression. Overall, the maximum applied strain level at which full recovery is possible decreases with increasing zirconium content from 2·5% strain in alloys containing 5 at-%Zr to only 1·5% strain in alloys with 20 at-%Zr.[125,138] No shape memory behaviour has been reported in alloys with more than 30 at-%Zr.[130] However, it is important to note that while most studies on shape memory behaviour of Ni–Ti–Hf alloys were performed on Ti rich compositions, they were mostly carried out on quasi-equiatomic compositions in Ni–Ti–Zr. Depending on the cooling rate, some precipitates may have formed in the Ti rich compositions of Ni–Ti–Hf alloys following quenching. Their effects on shape memory behaviour were not investigated, and it is possible that they partly contribute to the better shape memory behaviour observed in Ni–Ti–Hf alloys compared to Ni–Ti–Zr alloys through precipitation strengthening.

Aging at 700°C severely lowered transformation temperatures of $Ni_{49}Ti_{36}Hf_{15}$.[131] After 20 h aging, M_s and A_s dropped by approximately 70 and 40°C respectively; these changes were accompanied by the precipitation of the $(Ti,Hf)_2Ni$ phase. An increased σ_y and ultimate tensile strength in martensite of the aged alloy provide further evidence of precipitate formation. During the course of aging, these precipitates grew in size and volume fraction, and the authors concluded that 20 h were needed for precipitates to reach the peak aged condition[131] and impart the best improvement in mechanical and shape memory properties. Further aging coarsened the precipitates, and the strengthening effect was lost. Similar precipitation kinetics was also observed in Ti–Ni–Zr thin films,[139] but no equivalent studies have been conducted for bulk Ni–Ti–Zr alloys.

Cyclic instability is a major concern for both alloy systems as shown in Fig. 37. Transformation temperatures decreased by 40°C during stress free thermal cycling of $Ni_{49}Ti_{41}Hf_{10}$,[119] stabilising after 20 cycles. Cyclic response was even worse in $Ni_{49·5}Ti_{30·5}Hf_{10}Zr_{10}$ alloys where transformation temperatures fell by 50–60°C and did not stabilise even after 100 cycles.[140] Furthermore, cyclic stability deteriorated more as composition deviated from the equiatomic toward the (Ti,Hf/Zr) rich region.[119] Stress free thermal cycling was also detrimental to TWSME obtained in $Ni_{49}Ti_{36}Hf_{15}$ alloys by shape memory training in bending, such that 50% of two way shape memory strain was lost after 10 cycles.[137]

The issue common to both alloy systems, in terms of shape memory effect, is high σ_{DT} and comparatively low σ_y in both martensite and austenite.[120,121,142,143] If one follows guidelines proposed by Otsuka *et al.* for Ti–Pd alloys,[74] shape memory properties could be improved by alloying, precipitation hardening, and thermomechanical treatments. However, while the majority of the experiments on mechanical and shape memory properties of Ni–Ti–Hf have been conducted on Ti rich or equiatomic compositions, they have done so in the

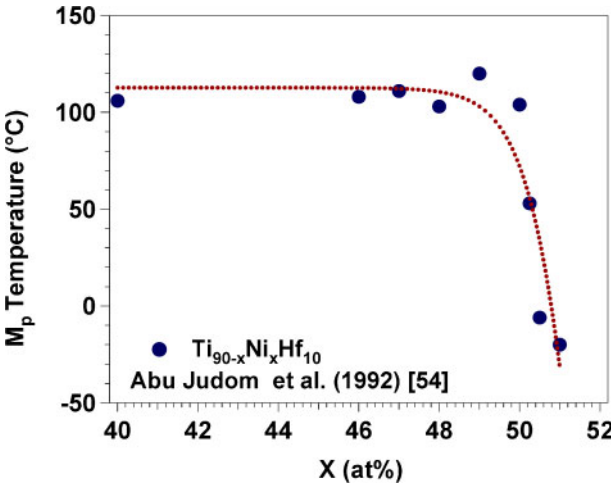

38 **Composition dependence of the martensitic peak temperature M_p of $Ni_xTi_{90-x}Hf_{10}$ alloys at compositions on either side of stoichiometric composition. Little changes exist in the (Ti,Hf) rich region, but the transformation temperatures drop off dramatically in the nickel rich region. The trendline is a fit through all data points**

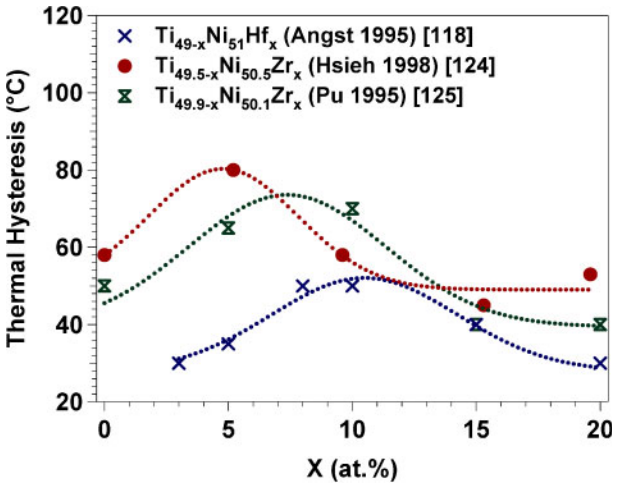

39 **Thermal hysteresis of Ni–Ti–Hf/Zr alloys as a function of composition. The trendlines are the fits through each set of data points**

solution treated instead of aged condition. Therefore, the impact of thermomechanical treatments, like those performed on the Ti–Ni–Pd/Pt alloys, on shape memory response has not been explicitly investigated. Although the feasibility of cold rolling[118] and reduction of transformation temperatures via cold rolling[124] were demonstrated, no study on the shape memory or mechanical properties of post-cold rolled and heat treated specimens is available. Meanwhile, severe plastic deformation of a $Ni_{49\cdot8}Ti_{42\cdot2}Hf_8$ alloy, through the ECAE process, has been shown to effectively strengthen the alloy by grain refinement, resulting in dramatically improved cyclic stability by reducing the plastic accommodation of the martensitic transformation.[122] However, the ECAE process also slightly reduced ε_{rec}, and the exact cause of this reduction was not revealed. Unfortunately, $Ni_{49\cdot8}Ti_{42\cdot2}Hf_8$ does not have high enough transformation temperatures to quality as an HTSMA. Nevertheless, this work has shown that improvement of the Ni–Ti–Hf/Zr alloys by thermomechanical processing can be expected.

Aging studies in Ti rich compositions of Ni–Ti–Hf alloys have shown a clear improvement in recovery rate due to precipitation hardening when the alloy is near or at the peak aged condition.[131] Although Meng *et al.*[131] noted that shape memory recovery of the material after aging was inferior to that found by Wang *et al.*,[120] the initial applied strain was larger in the former study, and improvements of recoverability of the aged specimen over an unaged one was clearly demonstrated. More recently, Meng *et al.*[87,144] successfully achieved high transformation temperatures in Ni rich Ni–Ti–Hf SMAs through aging. Untreated Ni rich $Ni_{50\cdot6}Ti_{29\cdot4}Hf_{20}$ alloy has transformation temperatures below room temperature (Fig. 38); however, the transformation temperatures increased by over 150 degrees to about 140°C after aging at 550°C for 2 h. Such enormous increase in transformation temperatures was brought about by a change in the precipitate type of the alloy. In the solution treated state, Ti_2Ni type precipitates still remained, but they were gradually replaced with Ti_3Ni_4 type precipitates during aging, which coarsened over time. Ti_3Ni_4 precipitates are rich in Ni, thus depleting the nickel content in the matrix and increasing transformation temperatures. Cyclically, only a 5–10°C decrease in transformation temperatures occurred after stress free thermal cycling in aged Ni rich alloys, a significant improvement over their Ti rich counterparts. Based on the hardness data, it also appeared that Ti_3Ni_4 precipitates achieved better strengthening of the matrix compared to Ti_2Ni precipitates; however, no mechanical or shape memory properties were reported.[87] Ni rich compositions have also been examined for Ni–Ti–Zr alloys,[145,146] and similar formation of $(Ti–Zr)_3Ni_4$ type precipitates during aging was found. However, these experiments were conducted in low Zr alloys and again no mechanical or shape memory property data were available.

One other concern with the Ni–Ti–Hf/Zr HTSMAs is that they generally have wide ΔT, an unfavourable characteristic for actuator applications (Fig. 39). Similar to binary NiTi alloys, the martensite structure of the composition range of Ni–Ti–Hf/Zr currently being studied as HTSMAs is monoclinic B19'. Applying a similar strategy that proved effective for the reduction of ΔT in binary NiTi,[147] Meng *et al.*[141,148] alloyed Ni–Ti–Hf HTSMAs with copper and sought to change the martensite structure from B19′ to B19, but found copper additions of 1 to 5 at-% to $Ni_{49}Ti_{36}Hf_{15}$ did not change the martensite structure, and actually increased ΔT instead. In addition, the 5 at-% copper addition had no effect on transformation temperatures while 3 at-% copper caused a slight decrease.[141] Although stress free thermal cycling in the alloy with 5 at-% copper produced double transformation peaks in DSC during heating, which was reported to be R phase transformation from XRD and DSC analyses,[148] there was no obvious improvement on the cyclic thermal stability in terms of the shift in transformation temperatures.[148] In other alloying efforts, Hsieh *et al.*[138,140] used equal parts of hafnium and zirconium to produce the $Ni_{49\cdot5}Ti_{30\cdot5}Hf_{10}Zr_{10}$ alloy, and found its shape memory properties, thermal and cyclic stability, and transformation temperatures to lie in between those of ternary Ni–Ti–Hf and Ni–Ti–Zr. The transformation temperatures

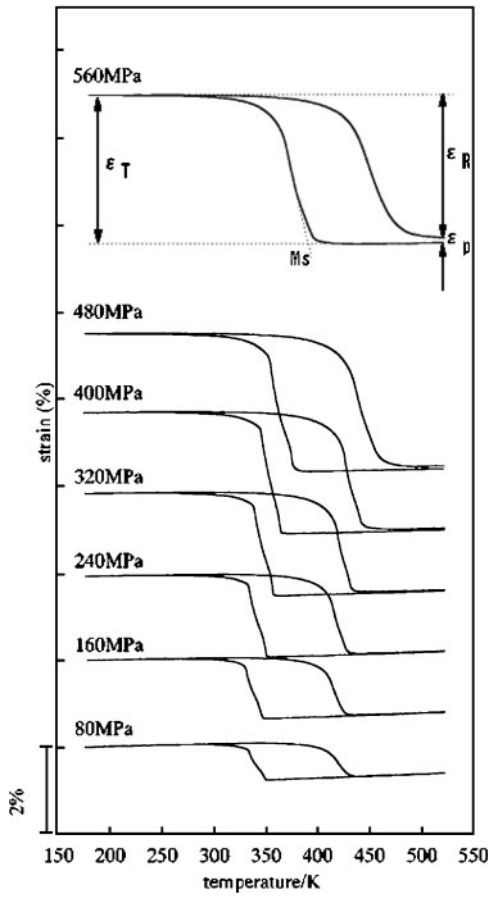

40 Strain versus temperature response of the thin film $Ni_{49·7}Ti_{35}Zr_{15·4}$ HTSMA during thermal cycling experiments under constant stress levels[139] (Reproduced with permission from Springer Science and Business Media)

and aging behaviour follow more closely those of the Ni–Ti–Hf system, and recovery rate and cyclic stability are closer in behaviour to that in the Ni–Ti–Zr system. Rhenium addition to Ni–Ti–Hf alloys was also investigated in the context of melt spun ribbons, but transformation temperatures were lowered as a result,[149] and data on shape memory properties is not available.

III.1·2.a. Unconventional processing techniques for Ni–Ti–(Hf/Zr) alloys

Multiple strengthening mechanisms can be achieved through thin film processing of the present alloy systems. For example, grain refinement is a byproduct of many thin film processing techniques and provides starting microstructures not easily achievable by conventional processing procedures. Sawaguchi *et al.*[139] produced small grains, 200 nm in size, in thin film $Ni_{49·7}Ti_{35}Zr_{15·4}$ using magnetron sputtering, and obtained over 3% recoverable strain with full recovery in thermal cycling experiments under tension (Fig. 40). This thin film also showed very high work output capacity of 16·8 J cm^{-3}, higher than bulk Ti–Ni–Pd/Pt. This fabrication method also avoided the long exposure to high temperature necessary in manufacture of bulk alloys and produced precipitate and dispersion free films that are otherwise difficult to achieve in the Ni–Ti–Zr alloys.[139] Films sputtered on unheated substrates are amorphous, and appropriate heat treatments could then be used to fine tune crystalline grains and precipitates to the desired morphology and size.[139,150] As is the case in many alloys, single target deposition methods often result in variations in composition because of different deposition rates of the individual elements. Sanjabi *et al.*[151] showed that this problem could be resolved using multiple targets, where each target holds individual elements, which received different applied deposition power to compensate for their different deposition rates.

Other techniques such as rapid solidification also successfully produced melt spun ribbons with nanometre size grains.[152] However, martensite stabilisation and difficulty in achieving homogeneous distribution of alloying elements continue to pose tough challenges in rapidly solidified ribbons.[153] A very important outcome of the thin film studies on these alloy systems is that with a desirable microstructure, it is possible to obtain good shape memory behaviour in Ni–Ti–(Hf,Zr) HTSMAs. This further highlights the need for a set of systematic studies on the thermomechanical treatments and their effects on shape memory properties of Ni–Ti–(Hf,Zr) SMAs, similar to what was done for the Ti–Ni–Pd system.

As evident in many thin film studies, hafnium imparts better glass-forming abilities onto binary Ni–Ti.[150,151] Metallic glass fabrication techniques have been explored for Ni–Ti–(Hf,Zr) alloys to circumvent their poor cold formability by utilising the ease of forming offered in the supercooled liquid region of metallic glasses.[154,155] In respect to the binary Ni–Ti system, zirconium was identified to be a better glass-former than hafnium, while copper is thermal cycling appreciably better in this aspect than either Hf or Zr.[156] However, copper reduces transformation temperatures significantly, and hafnium is more effective in increasing transformation temperatures than zirconium.[156] As such, it appears that the criteria for good glass forming ability are at odds for the formation of alloys with high martensitic transformation temperatures.[154] In other words, compositions showing desirable martensitic transformation temperatures are poor glass formers.

Powder metallurgy is another useful tool in producing fine grained alloys with high σ_y, but there are a number of drawbacks to the fabrication of Ni–Ti–(Hf,Zr) HTSMAs through traditional cold compaction and reactive sintering of elemental powders. Sintering is usually performed at 900–1000°C in an inert atmosphere.[157,158] At these temperatures, the chemical properties and reactivity of the elements create many problems in terms of the quality of the specimens produced. Relatively large volume fraction of precipitates form during the sintering process,[157] and the high temperature required to achieve chemical homogeneity causes the formation of oxides due to the high oxygen affinity of titanium, hafnium and zirconium.[157,158] Porosity is also a problem, often exceeding 15 vol.-% because of mechanisms such as vacancy formation from differential diffusion rates of elements (Kirkendall effects), pressure from CO_2, CO, H_2O and H_2 gas formation, highly exothermic nature of Ni–Ti formation, and the capillary actions of liquid phases formed during the sintering process.[158] A powder metallurgy process involving the use of calcium vapour as a reducing agent during the sintering process was devised to alleviate many of these problems.[159,160] The vapour

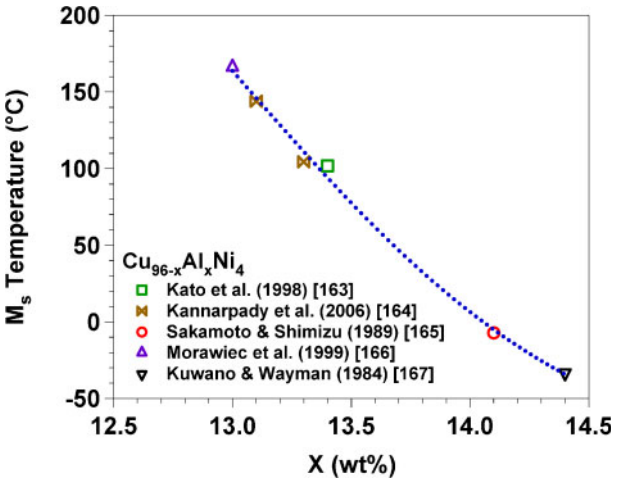

41 Composition dependence of the martensitic start temperature, M_s, on aluminium content in Cu–Al–Ni alloys. As shown in the figure, an increase in the aluminium content leads to a dramatic drop in M_s. The trendline is a fit through all data points

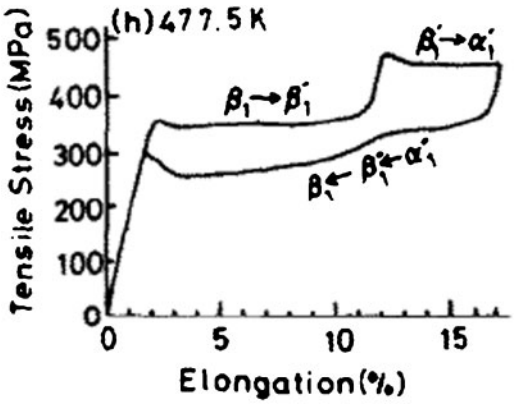

42 Tensile deformation behaviour of a [001] single crystal $Cu_{81·8}Al_{14}Ni_{4·2}$ (wt-%) SMA deformed at 204·5°C in the fully austenitic state. Perfect superelasticity up to 17% is observed; the alloy undergoes a two stage transformation.[169] Reproduced with permission from Elsevier

phase calciothermic reduction process utilises the high oxygen affinity of calcium to reduce oxide formation and the overall oxygen content of the Ni–Ti–Zr specimen.[160] Since oxides act as a barrier to diffusion, their elimination also improves the chemical homogeneity of the matrix.[159] Mechanical or shape memory behaviour of the samples produced through powder metallurgy processes have not been reported.

Overall, reversibility of the martensitic transformation in Ni–Ti–Zr alloys appears inferior to that in Ni–Ti–Hf alloys, but neither system exhibits comparable shape memory properties to those found in the Ti–Ni–Pd system. Yet, the extremely high work output capability in the $Ni_{49·7}Ti_{35}Zr_{15·4}$ thin film[139] suggests that the inferior shape memory properties in bulk alloys may be an issue of inadequate processing and unoptimised microstructure rather than an inherent material problem. However, ΔT is in general larger in Ni–Ti–Hf and Ni–Ti–Zr alloys, and cyclic and aging stability of both are inferior to Ti–Ni–Pd and Ti–Ni–Pt alloys. Nevertheless, vast possibility for the improvement of shape memory behaviour remains since systematic thermomechanical optimisation of the microstructure and chemical optimisation of these alloys are almost absent. Data are also lacking especially for higher transformation temperature alloys with Hf/Zr contents greater than 15–20% where the martensite structure changes from B19′ to B19 and ΔT decreases. If these limitations can be overcome, the inherently lower cost of Ni–Ti–(Hf,Zr) alloys will ensure their competitiveness as a possible commercial HTSMA system.

III.1·3. Cu based SMAs

Beside Ni–Ti alloys, copper based SMAs are currently the most widely commercialised SMAs. Although their shape memory and mechanical properties are inferior to those of Ni–Ti alloys in polycrystalline form, the lower cost allows copper SMAs to be competitive in some applications. There are two main Cu based binary alloy systems: Cu–Zn and Cu–Al. Of the two, Cu–Al is identified as a more likely candidate for high temperature shape memory applications, not only because of the higher transformation temperatures, but also for its superior microstructural stability over its Cu–Zn counterpart. Perhaps because of their commercial prevalence, studies on most copper based SMAs have described compositions in weight (or mass) percent instead of atomic percent; this convention will be adopted in this subsection and all compositions will be listed in weight per cent. It should be noted that in all other sections of this review, alloy compositions are presented in atomic percent.

In the binary Cu–Al system, the high temperature β phase can be quenched to form a metastable bcc austenite with $L2_1$ order near the eutectoid composition of 11·8 wt-%Al upon quenching.[2] When Al content is less than 11 wt-%, the austenite transforms to a 9R (α') orthorhombic martensite; when Al content is 11–13 wt-%, the austenite transforms to an 18R orthorhombic martensite; and when it is above 13 wt-%, the austenite transforms to a 2H (γ') tetragonal martensite.[161,162] In compositions exhibiting shape memory behaviour with transformation temperatures above 100°C, the Al content is generally around 12–13 wt-%, and the martensite structure is composed of the dominant 18R martensite with small volume fraction of γ' martensite.[162] At the eutectoid composition of 11·8 wt-%Al, M_s is ~400°C,[2] but increasing aluminium content leads to its rapid decline as shown in Fig. 41. However, when the Al content is close to the eutectoid aluminium concentration, the parent phase is highly unstable and readily decomposes to equilibrium α and γ phases. Consequently, nickel is added to stabilise the parent phase.[162] While nickel also lowers the transformation temperatures, it does so by only ~20 °C/wt-%, which is much less influential than the effect of aluminium (160 °C/wt-% change in transformation temperatures).[168] ΔT in the Cu–Al alloys is generally around 30°C, comparable to those in Ti–Ni–Pd alloys.

Shape memory and superelastic properties of single crystalline Cu–Al–Ni alloys are astounding. In $Cu_{81·8}Al_{14}Ni_{4·2}$ (wt-%) [001] single crystals, complete superelastic recovery of up to 17% applied strain is possible at 205°C, as shown in Fig. 42, due to a unique two step stress induced martensitic transformation.[163,169] In other single crystal compositions, perfect superelastic and shape memory behaviours of over 8% strain are common at deformation temperatures over

100°C.[164,170] Unfortunately, shape memory and mechanical properties of polycrystalline Cu–Al–Ni alloys bear little resemblance to their single crystal counterparts. The main problems with polycrystalline Cu–Al–Ni are lack of ductility due to transgranular fracture caused by large grains around 1 mm in size, large elastic anisotropy of the alloy, and precipitation of brittle γ phase at grain boundaries.[162]

For potential use as HTSMAs, both Cu based single crystals and polycrystals face several different types of problems. Prolonged exposure at high temperatures activates several time dependent processes in Cu–Al–Ni SMAs, which produce instabilities in the transformation behaviour. These processes can be classified into two groups: those based on ordering changes and others based on equilibrium phase precipitation.

Together, these two groups of mechanisms create a conflicting situation for in Cu–Al–Ni SMAs. To avoid formation of equilibrium phases, the alloys are quenched after solution treatment following casting.[171] However, quenching also creates a large concentration of vacancies and causes disorder in the alloy. Transformation temperatures of Cu–Al–Ni alloys are very sensitive to the degree of order in the material, and can vary up to 100°C between ordered, partially ordered, and disordered states.[2,171] In compositions with higher transformation temperatures, around 200°C, reheating above A_f during shape memory cycles is enough to activate the reordering process, and since transformation temperatures are higher in the ordered state, this effect is manifested in an increase in transformation temperatures with shape memory cycles.[165,172–176] In fact, this effect completely overshadows the usual reduction of the transformation temperatures due to defect generation during cycling.[175] The most effective solution to this problem is to age the alloy near 200–300°C to allow the restoration of full order before use,[176] but unfortunately, this aging temperature is sufficient to activate the decomposition process where equilibrium γ phase precipitates out of solution.[175–177] In fact, transformation temperatures of these Cu based SMAs are usually high enough to activate a slow decomposition process, which creates a 'lifetime' window for the operation of the alloy in both single crystalline[178] and polycrystalline Cu–Al–Ni alloys[2] where macroscopic behaviours are minimally impacted for up to several months before seriously affected by the decomposition of equilibrium γ phase.

Intense efforts have produced several possible solutions to both the problems of phase instability and brittleness. To tackle the lack of ductility, titanium,[174,179] boron,[175,180] vanadium[176] and zirconium[2] have been introduced in small amounts, bringing about 10-fold or greater reduction in grain size and associated improvement in ductility. Alloying with titanium is particularly effective, allowing for a 100-fold reduction in grain size since titanium suppresses diffusion of the constituent elements.[179] Precipitation of brittle γ phase can be suppressed by increasing nickel content, but overabundance of nickel causes an inherent reduction in ductility as well. Instead, using manganese in place of nickel[180] is effective both in improving ductility and in suppressing γ precipitation. Thermomechanical treatments through warm rolling and annealing[181] further improve ductility by reducing grain size to few micrometres, and increase elongation to failure to up to 10% in tension at room temperature.[162,181] However, alloying has so far been the only effective solution to the decomposition problem. By decreasing aluminium and increasing nickel equivalent amount,[162] the β phase can be stabilised against γ precipitation; however, this method is limited by transformation temperature requirements.

In solution treated bulk Cu–Ni–Al alloys, shape memory recovery rate is poor when deformed at room temperature, but improves steadily as deformation temperature is increased. For example, Eucken *et al.*[182] observed 2·4% recoverable strain with 0·6% ε_{irr} after deformation just below M_s of 150°C in tension in solution treated $Cu_{80\cdot1}Al_{11\cdot9}Ni_5Mn_2Ti_1$ alloy (wt-%), but could not attain full shape memory recovery at any applied strain level. By increasing the deformation temperature to above A_f (193°C), perfect shape memory recovery of up to 1·2% strain could be obtained from the recovery of stress induced martensites after heating without superelastic behaviour in the same alloy. Although the exact cause was not specified in the study, this is most likely because σ_{DT} below A_s is higher than σ_{SIM} immediately above A_f. Therefore, deformation by stress induced martensite right above A_f caused less plastic deformation than deformation by martensitic orientation below A_s, similar to the behaviour observed in Ni–Ti–Hf SMAs.[121]

Some Cu–Ni–Al alloys also showed superelasticity when deformed above A_f. Morris[180] found full tensile superelastic recovery up to 2% applied strain in a solution treated $Cu_{80\cdot96}Al_{12}Ni_4Mn_3B_{0\cdot04}$ alloy at 150°C and a maximum of 4·5% recoverable strain for a $Cu_{79\cdot96}Al_{12}Ni_4Mn_4B_{0\cdot04}$ alloy deformed to 5% total strain at 150°C. Two way shape memory behaviour has been achieved in both single and polycrystalline samples[163,164,182,183] by constant stress thermal cyclic training,[163,164,183] superelastic training,[182] and through martensite stabilisation.[183] Up to 0·9% two way shape memory strain has been observed in $Cu_{83}Al_{13}Ni_4$ single crystals after 10 training cycles.[163]

It is important to note that crystallographic texture plays an important role in the superelastic behaviour of polycrystalline Cu–Al–Mn–Ni alloys.[184] It was experimentally demonstrated in a low temperature polycrystalline Cu–Al–Mn–Ni SMA that tensile superelasticity is the best in samples cut 45° (MD) from the cold rolling direction (RD) (Fig. 43*a*), in agreement with theoretical predictions seen in Fig. 43*b*, which show that recoverable strains are expected to be larger in the samples with tensile directions 45° from the RD. Texture appears to have an even greater effect on ductility. Specimens cut parallel to the transverse direction fracture at 5% applied strain at room temperature, but ones cut 45° to the RD did not fail even at strains up to 11%. It is expected that texture will also affect shape memory behaviour, and is relevant not only for the Cu–Al–Mn–Ni SMAs, but all SMAs in general. Unfortunately, no such studies have been performed on alloys with high transformation temperatures. Given that the high temperature compositions suffer from ductility problems, texture effects on these alloys should be carefully investigated.

Recently, niobium[185–188] and silver[189–192] have been added to binary Cu–Al alloys as a replacement for nickel in an effort to improve ductility and phase stability.

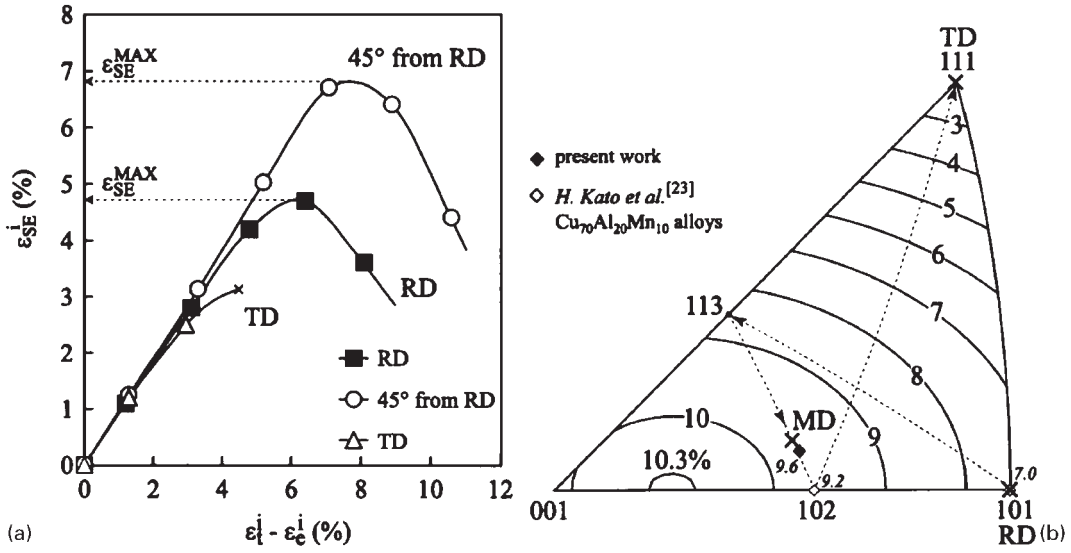

43 Texture dependence of superelastic strain and ductility: *a* experimental results showing the difference in superelastic behaviour and *b* theoretical predictions of transformation strains for orientations in a standard stereographic triangle; RD=rolling direction, TD=transverse direction, MD=45° from rolling direction; $\varepsilon_t^i - \varepsilon_e^i$ is the applied strain.[184] (Reproduced with permission from Springer Science and Business Media)

Ductility is improved significantly in Cu–Al–Nb alloys by way of grain sise reduction,[185] reaching 12·5% in tension at room temperature in $Cu_{84\cdot44}Al_{13}Nb_{2\cdot56}$ alloy with M_s of 305°C.[188] However, silver worsens ductility, and only less than 1% elongation to failure was possible in $Cu_{83\cdot6}Al_{10\cdot6}Ag_{5\cdot8}$ alloys, which can be increased to 1·17% with 0·1 wt-% addition of rare earth cerium.[191] Addition of either Nb or Ag retards the decomposition process, and also increases transformation temperatures.[188,190,191] M_s temperature as high as 313°C can be reached in $Cu_{86\cdot23}Al_{13\cdot5}Nb_{0\cdot27}$ (Ref. 188), and 376°C in $Cu_{87\cdot5}Al_{9\cdot8}Ag_{2\cdot7}$.[190] Although the increase in transformation temperatures may seem appealing at first glance, it is important to note that the temperature for the activation of decomposition processes is only slightly increased. For higher transformation temperature Cu–Al–Ag alloys, the martensitic transformation vanishes after the alloys have been heated to above their A_f temperature (over 400°C), due to phase decomposition in this temperature range.[191,192] Cyclic stability also suffered as a result, so that transformation temperatures shifted by 25°C after five DSC cycles in Cu–Al–Nb alloys.[185] It is very difficult to suppress decomposition processes at such high temperatures and the useful lifetime and stability of these alloys are very limited. The shape memory behaviour of these alloys are also unknown; while it was mentioned that the $Cu_{86\cdot23}Al_{13\cdot5}Nb_{0\cdot27}$ alloy is capable of 98% recovery rate after bending at room temperature, the applied strain level was not mentioned.[188]

Further alloying the Cu–Al–Nb system with nickel, chromium and cobalt can lower transformation temperatures to levels where decomposition occurs more slowly, as well as increase the intrinsic stability of the austenite and martensite.[186,187] While the ductility of these quaternary alloys are worse than ternary Cu–Al–Nb alloys, tensile elongation to failure in all compositions is still around 6–8% at room temperature and remains superior to identically processed Cu–Al–Ni alloys.[187] Transformation temperatures remain stable in nickel containing quaternary compositions with A_f of 179°C after 30 thermal cycles, and decomposition did not affect the behaviour until after 1000 min aging at 300°C.[186] Quaternary additions have little effect on shape memory behaviour, with the exception of chromium, which decreases the maximum recoverable strain.[187] Shape memory behaviour has not been studied in the Cu–Al–Ag alloys. Other potential Cu Based SMAs include Cu–Al–Co and Cu–Al–Zr with M_p around 250°C and thermal hysteresis of nearly 100°C.[192] Both show poor cyclic and thermal stability and will not be discussed further.

Several unconventional processing techniques could benefit Cu based SMAs since they aim at producing ultra fine grains and would alleviate the lack of ductility in polycrystalline Cu–Al based HTSMAs. Melt spinning of Cu–Al–Ni alloys produces ribbons with fine grains around 10 μm in thickness[166] and improved tensile strength over the solution treated alloy, but transformation temperatures dropped by ~30°C and ΔT increased by 5°C. The authors explained the decrease in transformation temperatures to be caused by higher defect concentration from the fast quenching. A maximum of 4% applied strain with full recovery was possible during thermal cycling under 20 MPa in a melt spun $Cu_{83}Al_{13}Ni_4$ alloy annealed for 30 min at 900°C.[166] The melt spun ribbons showed a ⟨100⟩ fibre-like texture with components of sheet texture.[166] Although not explicitly mentioned in the aforementioned work, it is believed that this texture is responsible for the high recoverable strain exhibited by these ribbons.

Powder metallurgy of Cu–Al–Ni alloys has been particularly successful in the improvement of both ductility and shape memory behaviour. By using hot isostatic pressing, essentially pore free specimens could be produced.[193] Additional hot working and annealing of a $Cu_{s1}Al_{12}Ni_5Mn_2$ alloy enables complete superelastic recovery of 4% applied strain both in bending and tension at 120°C.[194] The chemical homogeneity and compositional accuracy could be further improved by mechanically alloying the elemental powders in a ball mill[194–196] before powder consolidation through hot

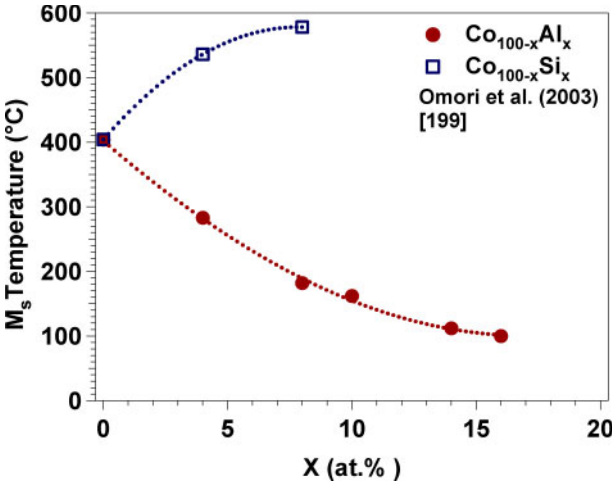

44 Dependence of martensitic start temperature, M_s, on the addition of aluminium or silicon to cobalt. The trendlines are the fits through each set of data points

pressing. Alloys produced through powder metallurgy also possess excellent cyclic stability with 100 thermal cycles producing almost no discernable changes in shape memory recovery rate.[194]

Overall, the copper based HTSMAs face some daunting roadblocks: ductility improvements are still needed and no real effective solution for combating instabilities from both quenched-in disordering and γ precipitation has been found. As a result, the prospects for Cu based HTMSAs designed to operate at temperature above 200°C appear bleak. On the other hand, at temperatures in the 100–200°C range, the material shows some promise as useful amounts of shape memory and superelastic strain have been observed. The low material cost, the possibilities for more microstructural optimisation like those performed for the Ti–Ni–Pd alloys, and amazing single crystal properties warrant continued interest in Cu based HTSMAs. Achieving smaller grain sizes and ⟨100⟩ texture should offer the most immediate improvements for the shape memory behaviours of these alloys.

III.1·4. Co based non-thermoelastic HTSMAs

Pure cobalt reversibly transforms from fcc parent phase (γ) to HCP martensite (ε) non-thermoelastically at ~400°C.[4] This transformation temperature depends heavily on purity, grain size and heating or cooling rate.[4] Initial reversibility of the transformation is very poor, providing only 10–20% recovery rate in the first cycle to an applied strain of ~1%, but is improved with increasing number of cycles to 60% after seven deformation reheating cycles.[4] Although thermal hysteresis (~100°C) of this transformation is small compared to other non-thermoelastic transformations such as iron based SMAs, it is still much larger than those in thermoelastic martensitic transformations.[4]

Binary alloying to pure cobalt imparts profound changes to transformation temperatures and can be classified into three categories based on their overall effects.[4,197–199] Zirconium or molybdenum additions significantly reduce transformation temperatures,[4] while aluminium or nickel lowers transformation temperatures only slightly.[4,199] Germanium or silicon increases transformation temperatures,[4,197] and thus will be discussed separately in Section IV.2·2 where HTSMAs with characteristic transformation temperatures between 400 and 700°C are introduced. The opposing effects of aluminium and silicon on the transformation temperature of Co are presented in Fig. 44.

Most of these alloying additions to Co do little to improve shape memory properties such as recoverable strain level or reversibility. Zirconium and molybdenum increase the ΔT and reduce reversibility,[4] while nickel fails to affect the reversibility at all.[4] The major exception is aluminium; in fact, extensive work by Omori *et al.*[197–200] discovered large improvements in shape memory behaviour and in particular the recovery rate of Co–Al alloys over that of pure cobalt.

Ordered parent phase is usually correlated with better shape memory behaviour in SMAs. By adding aluminium to cobalt, Omori *et al.* sought to promote ordering and thereby improve the reversibility of the transformation.[199] Indeed, under a bending deformation of 1·2% at room temperature, shape memory recovery rate was improved from 40% in pure cobalt to above 80% in a solution treated $Co_{86}Al_{14}$ (at-%) alloy. Aging at 900°C for 30 min improved shape memory properties compared to the solution treated case, providing over a 90% recovery rate after 2% applied bending deformation at room temperature in $Co_{86}Al_{14}$.[200] This is believed to be caused by precipitation of an ordered B2 (β) phase. Since the β phase is the austenite phase for the thermoelastic Co–Ni–Al SMAs, this would suggest aluminium addition to cobalt creates a tendency for long range order, making the transformation more thermoelastic in nature.

Ternary alloying to Co–Al alloys can be divided into several categories based on their effects on the transformation temperatures.[201] Belonging to the first category are titanium, vanadium, iron, niobium, molybdenum, tantalum and tungsten, and their presence leads to a large decrease in transformation temperatures.[201] Nickel and manganese suppress transformation temperatures only mildly as compared to the first group. The third group comprised of chromium and silicon has little effect on transformation temperatures. Most ternary additions impair shape memory reversibility, but improve tensile ductility.[201] A notable exception is the addition of nickel, which strongly enhances the reversibility while lowering the transformation temperature. The Co–Ni–Al system will be discussed separately in Section III.1·5.

Aside from transformation temperatures and recovery rate, very little information exists on Co based non-thermoelastic SMAs. Training cycling is known to improve the reversibility,[4] but full recovery has not been reported in any compositions under any degree of deformation. The non-thermoelastic nature of the transformation mainly stems from excessive defect generation during transformation, but it is also known that perfect recovery has been observed in non-thermoelastic Fe–Mn–Si single crystal SMAs.[202] It is expected, however, that the exact transformation mode and the nature and the storage of transformation defects should be different in Co and Fe based SMAs, and therefore it is questionable whether similar full reversibility could ever be obtained in non-thermoelastic Co based alloys. However, if this were possible, the superb ductility of Co based HTSMAs would justify future research efforts on

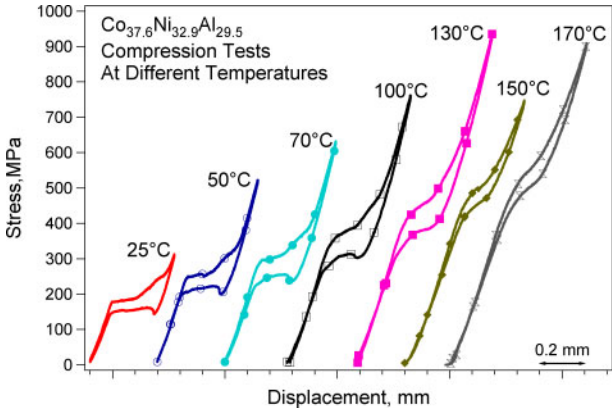

45 Superelastic response of solution treated polycrystalline $Co_{37.6}Ni_{32.9}Al_{29.5}$ (with subscripts) under compression at various temperatures.[206] (Reproduced with permission from Elsevier)

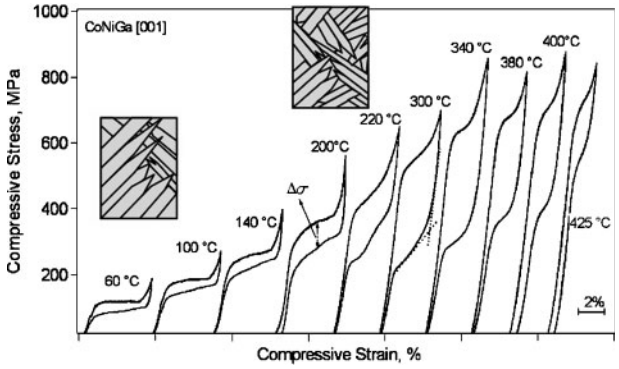

46 Superelastic responses of $Co_{49}Ni_{21}Ga_{30}$ single crystals oriented along the [001] direction under compression at various temperatures. The schematics illustrate the martensite morphology. Note that internal twinning of variants is not shown.[209] (Reproduced with permission from Elsevier)

this system in applications such as joining and coupling. The inherently large ΔT and small ε_{rec} exclude these alloys from actuator applications.

III.1·5. Co–Ni–Al/Ga SMAs

The Co–Ni–(Al,Ga) SMAs cannot be classified with Co based non-thermoelastic SMAs for a very important reason: the increased Ni and Al/Ga content in Co–Ni–(Al,Ga) alloys creates a fully ordered parent structure, capable of undergoing a thermoelastic martensitic transformation. Co–Ni–(Al,Ga) alloys transform reversibly from B2 (β) austenite to $L1_0$ non-modulated tetragonal martensite. These alloys have been heavily studied due to their potential for magnetic shape memory properties, which are considered only at low temperatures below their Curie temperatures of 100 to 250°C. On the other hand, it is known that transformation temperatures of Co–Ni–(Al,Ga) alloys can be increased to over 200°C by reducing Co or Al/Ga content,[203,204] or through aging.[205] For example, the $Co_{45}Ni_{25}Ga_{30}$ alloy shows M_s of 128°C, while M_s of $Co_{50}Ni_{20}Ga_{30}$ and $Co_{43}Ni_{25}Ga_{32}$ alloys are −35 and 22°C, respectively.[204] However, other than transformation temperatures, shape memory related properties in high transformation temperature compositions have not been reported. Nevertheless, in compositions with transformation temperatures at or below room temperature, very appealing superelastic properties have been found which are still operational even at very high temperatures.

Karaca *et al.*,[206] found a large 'superelastic window' under compression in solution treated polycrystalline $Co_{37·6}Ni_{32·9}Al_{29·5}$ alloy with A_f of −26°C. Perfect superelastic behaviour spanned from room temperature to 170°C, where greater than 5% applied strain was fully recovered (Fig. 45). This alloy possesses a very high austenite σ_y of greater than 1100 MPa at room temperature. Perfect superelastic recovery of 6% was also found in $Co_{40}Ni_{33}Al_{27}$ single crystalline tensile samples up to 100°C, but no information was provided at higher temperatures.[207] However, polycrystalline samples of this composition are very brittle in tension.[208] The intrinsically poor tensile ductility in these alloys could be related to the cubic⇌tetragonal martensite transformation. Since there are only three tetragonal martensite variants to a cubic austenite, it is not enough to satisfy the five independent deformation systems required by the Taylor's Criteria for general deformation,[37] therefore, the inability to satisfy geometric compatibility creates high stresses at grain boundaries, and leads to premature fracture.

In single crystalline Co–Ni–Ga alloys, the superelastic window can reach over 400°C. Dadda *et al.*[210,211] observed up to 2·6% full superelastic recovery at 380°C in the [100] single crystals of $Co_{49}Ni_{21}Ga_{30}$ under compression with an A_f of 17°C (Fig. 46). The [100] single crystals should result in the best transformation reversibility and recovery rate in these alloys since dislocation slip is extremely difficult in the [100] orientation due to the lack of available slip systems in most ordered B2 alloys along this orientation under uniaxial loading. Indeed, Chernenko *et al.*[211] validated the excellent high temperature superelasticity by observing full recovery of 2–4% strain in non-[100] oriented single crystals, although at lower temperatures than that of Dadda *et al.*[210,211] observed. In $Co_{49}Ni_{21}Ga_{30}$ single crystals oriented along the [001] direction, fully recoverable superelastic strain of 8% was obtained in tension at 40°C, and fully recoverable superelastic strain of 6% remained even at a deformation temperature of 300°C.[212] Shape memory behaviour of this composition was not evaluated in the polycrystalline state, but due to their brittle nature, it is likely that without special crystallographic texture, the polycrystalline form would fracture before appreciable superelasticity can occur.

The studies on Co–Ni–(Al,Ga) alloys consist mainly of the experiments performed on single crystals. For this reason, there is a good understanding on how crystallographic orientation affects the various properties relevant to superelasticity. Figure 47 shows the dependence of theoretical transformation strain on orientation in Co–Ni–Al single crystals near the $Co_{40}Ni_{33}Al_{27}$ composition,[207,213] which was calculated using the energy minimisation theory.[23] It is clear that in tension, highest theoretical transformation strain is available along the [001] orientation and polycrystals with fibre textures near [100] would be expected to have high recoverable strain as well. In many other alloy systems, such fundamental studies would accelerate the alloy design process and should be actively pursued. High σ_y and relatively low σ_{SIM} in Co–Ni–Al SMAs are largely responsible for their superb superelastic behaviour at high temperatures.[208,210] Although σ_{SIM} and transformation stress hysteresis both increased with

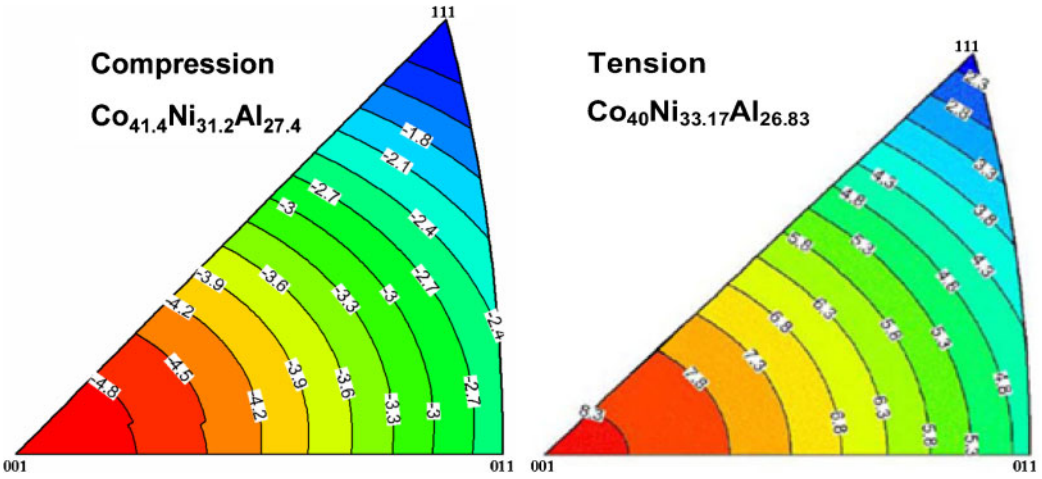

47 Theoretical transformation strains of $Co_{40}Ni_{33}Al_{27}$ single crystals at all orientations of a standard stereographic triangle under compression[213] and tension.[207] (Reproduced with permission from Elsevier)

temperature, there was still sufficient difference between σ_y and σ_{SIM} to enable superelastic behaviour even at high temperatures.

As mentioned before, tensile ductility of Co–Ni–Al/Ga polycrystals is very poor. Although ductility can be improved by inducing ductile fcc γ precipitates, these come at a cost of shape memory reversibility since the γ phase does not transform and is prone to deformation by dislocation slip.[207] Similarly, phase stability and decomposition issues as in the case of Cu based HTSMAs should also be studied in Co–Ni–(Al,Ga) alloys to evaluate their long term reliability both in superelastic recovery and shape memory behaviour at high temperatures. For ductility improvements in polycrystalline materials, similar strategies to those applied to Cu based alloys can be followed. Overall, brittleness in tension of polycrystalline materials currently poses a problem for Co–Ni–(Al,Ga) alloys. The potential for high temperature shape memory behaviour also exists in alloy compositions with higher transformation temperatures, but these properties currently remain unexplored. If high temperature superelasticity is desired, polycrystalline Co–Ni–Al may be a good choice provided that ductility in tension can be improved, which may not be at all an easy task.

III.1·6. Ni based HTSMAs

Ni based HTSMAs have a long history, for they are among the first SMAs to be extensively studied with transformation temperatures above 100°C. The two main systems are Ni–Al and Ni–Mn, and both have been thoroughly investigated for over 35 years since the discovery of shape memory effects in them. Relatively low cost and a fairly thorough knowledge of related structural materials such as Ni based superalloys and nickel aluminide ordered intermetallics have provided a firm basis for the study of Ni based HTSMAs. It is, however, unfortunate that their shape memory behaviour leaves much to be desired.

III.1·6.a. Ni–Al system

Martensitic transformation occurs in Ni–Al alloys near the Ni_2Al stoichiometric composition. In 1971, Enami and Nenno first identified both shape memory and superelastic behaviour in $Ni_{63·2}Al_{36·8}$ (at-%).[214] Au and Wayman showed in 1972 that ΔT was only 10°C, and that transformation was thermoelastic.[55] As shown in Fig. 48, M_s of Ni–Al increases with decreasing Al concentration by ~130°C/at-%Al and reaches 100°C at $Ni_{64}Al_{36}$,[55] and 370°C in $Ni_{66}Al_{34}$.[56] The parent phase is an ordered B2 structure that transforms to 3R body centred tetragonal (β') martensite with $L1_0$ order.[216] However, an intermediate 7R martensitic phase appears in Ni–Al alloys with Al content over 37%.[215] Ternary alloying in small amounts up to 5–10 at-% with V, Cr, Mn, Fe, Zr, Mo, Ta or W decreases transformation temperatures moderately, alloying with Nb, Ti or Si decrease them significantly,[217] while Co, Cu or Ag additions have no effect on or slightly increase transformation temperatures.[215,217] Maximum ε_{rec} in binary solution treated $Ni_{63·1}Al_{36·9}$ was reported to be 3–4% by Au and Wayman,[55] but no other studies have been able to reproduce ε_{rec} higher than 1·5% in alloys of

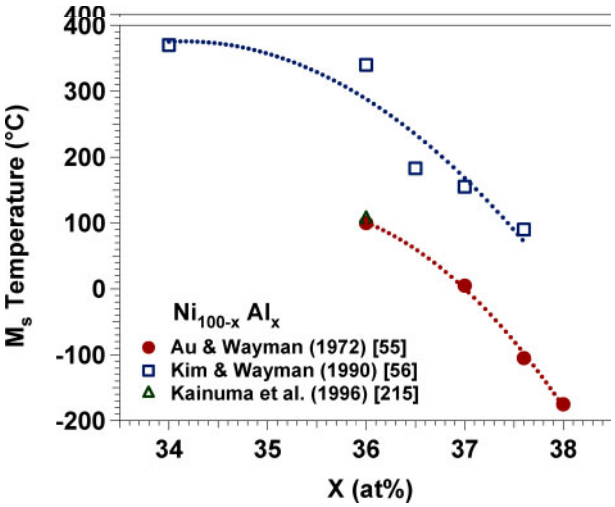

48 Martensite start temperature, M_s, dependence of Ni–Al alloys on aluminium content. M_s is highly sensitive to aluminium content, decreasing significantly as aluminium content increases. The large difference in reported transformation temperatures between the sets of studies is likely caused by small differences between the actual and reported composition. This further highlights the importance of composition control in Ni–Al. The trendlines are the fits through each set of data points

similar compositions in any loading mode. When aluminium is removed to increase transformation temperatures above room temperature, the shape memory properties become very poor in binary Ni–Al alloys. No more than 0·5% ε_{rec} was possible in solution treated $Ni_{63·8}Al_{36·2}$ prepared by powder metallurgy.[218] Even in this small strain range, recovery rate is commonly less than 50%.

The lack of satisfactory shape memory behaviour in Ni–Al HTSMAs has several roots: poor tensile ductility, phase decomposition processes, and texture. While Jee *et al.*[218] reported 9·5% strain to failure in solution treated $Ni_{63·8}Al_{36·2}$ in compression, Kim *et al.*[56] was only able to achieve 0·5% strain to fracture in bending for solution treated $Ni_{63·5}Al_{36·5}$, which failed by transgranular fracture in the elastic range. Two reasons exist for this poor ductility: easy intergranular fracture due to large grain sizes and inherently poor fracture toughness, and transgranular fracture, due to the insufficient number of slip systems in the β' martensite to accommodate polycrystalline deformation at room temperature.[216] Ternary additions of Fe and Co are highly effective in increasing ductility,[216,219] mainly as a consequence of the precipitation of ductile γ fcc phase. Although boron addition suppresses intergranular failure, it does not improve ductility by itself because the alloy will fail instead by transgranular fracture.[216] A combination of boron and Fe or Co addition is most effective in increasing ductility since both intergranular and transgranular failure modes are suppressed. Grain refinement processes, such as rapid solidification, are effective in further improving ductility in Ni–Al alloys containing Fe or Co, and will be discussed further at the end of this section.

Texture should be an important factor for the shape memory behaviour of Ni–Al alloys, but in hot extruded samples, Jee *et al.*[218] found no differences in recoverable strain levels between hot extruded samples cut along the extrusion direction and that cut along the transverse direction. However, no actual texture measurements were provided, and it is known that hot extrusion texture is relatively weak. No other studies have been published on the effect of texture on the shape memory properties of high temperature Ni–Al SMAs.

Similar to Cu based HTSMAs, phase instabilities and decomposition cause significant problems in Ni–Al SMAs. Two types of microstructural decomposition processes are relevant. In alloys with high Al or high Fe/Co content, γ phase appears after quenching or aging. Although the γ phase improves ductility as mentioned previously, it does not undergo martensitic transformation and is therefore detrimental to reversibility of the shape memory behaviour.[220] The appearance of the γ phase can be avoided by appropriate composition selection, and training can overcome some of the deleterious effects of the γ phase in dual phase alloys. For example, Ni–Al–Fe alloys with $\gamma+\beta$ dual phases have shown complete recovery of 0·6% applied tensile strain in a $Ni_{58}Al_{26}Fe_{16}$ alloy.[220] George *et al.*[216] also was able to obtain full recovery of 0·7% applied strain after constant tensile stress thermal cycling of $Ni_{58·5}Al_{25·5}Fe_{16}$ for at least 20 cycles.

The second type of decomposition process, however, poses a far greater threat to the potential of Ni–Al alloys as HTSMAs. It was observed in many binary Ni–Al compositions that after forward transformation by cooling from austenite, the reverse transformation disappears upon reheating. Instead, an exothermic peak is observed in the DSC profile,[221,222] which was identified as a decomposition process directly from the $L1_0$ martensite into the equilibrium Ni_5Al_3 phase[221] that itself does not undergo a martensitic transformation. Several studies[222–224] on this transformation to the Ni_5Al_3 phase reveal that it is an irreversible process, and although the transformation is diffusion driven,[222] the kinetics are very rapid near the transformation temperatures of the Ni–Al SMAs.[222,225] From these studies, it is apparent that decomposition to Ni_5Al_3 proceeds more favourably from martensite than from austenite,[225] and the temperature at which the decomposition to Ni_5Al_3 occurs is mostly a function of the ratio between nickel and aluminium, such that decreasing aluminium content lowers the temperature at which the decomposition starts.[225] In $Ni_{65}Al_{35}$, the decomposition temperature is 300°C,[225] for instance. Since transformation temperatures also increase with decreasing aluminium content, decomposition will occur before A_s is reached during heating and shape memory behaviour will not exist in Al poor alloys such as $Ni_{66}Al_{34}$.[225] The decomposition process is inherent in the Ni–Al system and cannot be suppressed without changing the composition of the alloy,[222] therefore making it impractical if not impossible to produce functional HTSMAs from the binary Ni–Al system.

The decomposition temperature can be increased through alloying to either stabilise the martensite phase or suppress the diffusion kinetics leading to Ni_5Al_3 formation.[226] By replacing nickel with cobalt, the decomposition temperature can be increased slightly, and transformation temperatures are lowered so that complete transformation is observed in $Ni_{56}Al_{34}Co_{10}$ alloy.[225] Addition of 2 at-% rhenium at the expense of aluminium increased the decomposition temperature by 150°C in a melt spun ribbon,[226] though whether similar effect on bulk material occurs is not known. This increase was concluded to be a consequence of the stabilisation of martensite phase by rhenium with respect to Ni_5Al_3 instead of a retardation of diffusion because in the rhenium doped alloy, Ni_5Al_3 formation did not occur when the specimen was aged at a temperature where decomposition normally took place in the alloy without Re addition.[226] Compared to the $Ni_{64}Al_{36}$ alloy, transformation temperatures of $Ni_{64}Al_{34}Re_2$ were $\sim$100°C higher. In addition to alteration of alloy composition, if the austenite phase is stable with respect to Ni_5Al_3 decomposition at A_f or higher, heat treatment above A_f could be used to introduce Ni_2Al precipitates in a controlled manner to take advantage of precipitation hardening.[225] This would further stabilise the alloy against decomposition in the martensitic state by increasing aluminium content in the matrix relative to nickel. Alloys treated in this manner were cyclically stable so that no changes in transformation temperatures were detected during 20 thermal cycles.[225] Certain processing techniques, such as splat cooling,[227] have also been shown to increase decomposition temperature and will be discussed in Section III.1·6.c.

Other authors have also shown dual phase ($\gamma+\beta$) $Ni_{58·36}Al_{25·5}Fe_{16}B_{0·14}$ SMAs with M_s of 155°C to be cyclically stable with no change in transformation

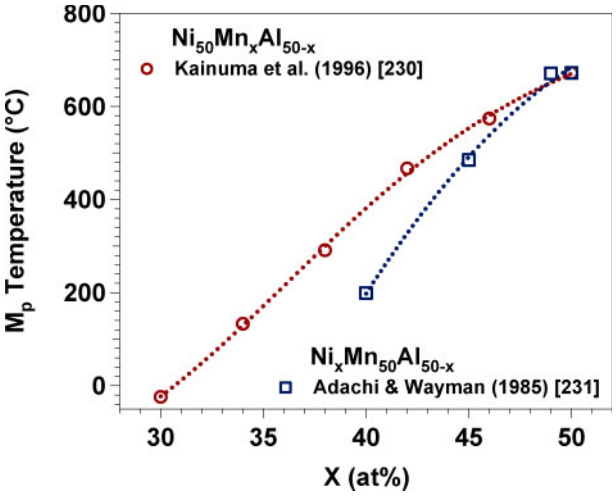

49 Martensitic peak temperatures, M_p, of the Ni–Mn–Al alloy system as a function of either Ni or Mn concentrations. Replacement of manganese with aluminium resulted in lower transformation temperatures than those resulting from the replacement of Ni with Al. The trendlines are the fits through each set of data points

temperatures for up to 1760 stress free thermal cycles, but ductility and shape memory reversibility were slightly reduced after cycling.[228] Aging at 100°C of the same dual phase alloy produced no changes in the microstructure, although a slight reduction in ductility was observed. On the other hand, aging at 300°C or above caused significant reduction in ductility within 10 h; this loss was attributed to the formation of the Ni_5Al_3 phase.[228] Oikawa *et al.*[229] reported a 5°C decrease in transformation temperatures in $Ni_{56·5}Al_{25}Fe_{18·5}$ dual phase alloy after 1 h aging at 200°C, and an 80°C decrease in transformation temperatures after 1 h aging at 300°C in the same alloy. The large reduction in transformation temperature during aging at 300°C was attributed to the formation of an iron rich bcc phase.[229]

III.1·6.b. Ni–Mn system

The Ni–Mn alloy system is similar to the Ni–Al system in many aspects. This system is based on equiatomic binary Ni–Mn with M_s of 674°C.[230] Transformation is observed only for equiatomic Ni–Mn and Mn rich compositions, proceeding from B2 austenite to $L1_0$ tetragonal martensite (θ phase).[231] Increasing Mn content in Mn rich compositions decreases transformation temperatures slightly.[230,232] Although the thermal hysteresis in this system is very large (75–150°C), the martensitic transformation was still determined to be thermoelastic in nature based on microstructural studies of the resulting martensite structure.[231] In addition, binary Ni–Mn alloys are extremely brittle, particularly in Mn rich compositions such as $Ni_{45}Mn_{55}$, where cracks were found in a specimen right after quenching.[231]

Ternary alloying imparts profound changes to both phase transformation and mechanical properties of binary Ni–Mn alloys, and most are based on the Ni–Mn–Al system, where a wide range of transformation temperatures can be obtained (see Fig. 49). Although Adachi and Wayman[231] concluded that Ti, Al, Cu or B additions did not improve ductility, results from later studies contradicted this finding. Instead, Potapov *et al.*[233] reported that elongation to failure in compression at room temperature increased from less than 2% strain in $Ni_{50·2}Mn_{49·8}$ to above 10% for a $Ni_{40·3}Mn_{50·1}Ti_{9·6}$ (at-%) alloy and over 15% strain in $Ni_{39·7}Mn_{50·3}Al_{10}$. Ductility in bending was worse than in compression in all cases, but up to 10% strain in bending was still possible without cracking in $Ni_{39·7}Mn_{50·3}Al_{10}$.[233] The improvements due to Ti addition were argued to be caused by a decrease in grain size, and improvements from Al addition to be a result of the formation of the ductile γ phase. Replacement of Ni by Al, Ti, Cu or Fe reduces transformation temperatures more than replacement of Ni by Mn in identical amounts.[230,231,234] These ternary additions up to 10 at-% also lowered ΔT to 25°C.[218] Addition of titanium or aluminium also led to changes in the martensite structure. Kainuma *et al.*[230] indicated that in the Ni–Mn–Al system with more than 30 at-%Mn, an additional monoclinic 7R martensite can be found. Jee *et al.*[218] reported that 10 at-%Ti addition caused a complex 4R orthorhombic martensite to form in the Ni–Mn–Ti system.

Shape memory properties of Ni–Mn based alloys are far superior to those of the Ni–Al system. Specimens deformed in compression to 3% total strain yielded ε_{rec} of 2·8%, and 5% ε_{rec} was obtained from 8% total applied strain in $Ni_{45·1}Mn_{44·9}Ti_{10}$.[218] In bending thermal cycling experiments under constant stress of 290 MPa, 3·5% ε_{rec} (88% recovery rate) of ~4% applied strain was also found in $Ni_{42·5}Mn_{50}Ti_{7·5}$.[234] Shape memory reversibility is inferior in Ni–Mn–Al alloys compared to Ni–Mn–Ti because of non-transforming and soft γ phase precipitates. Maximum of 0·6% ε_{rec} with complete recovery is possible in bending thermal cycling experiments of $Ni_{39·7}Mn_{50·3}Al_{10}$, and ε_{rec} of 1·5% is possible in the same alloy with 75% recovery rate.[235] Yang and Mikkola[236] investigated the shape memory recovery rate of several Ni–Mn based ternary and quaternary alloys in the solution treated conditions under room temperature compression. While none of these alloys were capable of full recovery, both Ni–Mn–Ti and Ni–Mn–Al alloys showed reasonable recovery rates of around 70% up to very high applied strain levels shown in Fig. 50. Improvements in shape memory behaviour in the Ni–Mn–Ti system with titanium concentrations near 10 at-% is most likely related to the change in the martensite structure from tetragonal to the 4R orthorhombic in these alloys.[218] This reduction in the structural symmetry of martensite increases the number of independent deformation systems for the shape memory behaviour from three to six.[37] This increase allows a non-textured polycrystalline alloy to accommodate strain by only the martensitic reorientation mechanism and reduces irrecoverable strain levels. Please refer to Section II.2·2 for further discussion.

Similar to Ni–Al alloys, diffusion based decomposition processes also occur in Ni–Mn alloys. γ phase precipitates readily in compositions where the Ni content is less than 50 at-% for binary Ni–Mn,[231] ternary Ni–Mn–Fe and Ni–Mn–Al, and quaternary Ni–Mn–Al–Fe alloys.[233,235,237] Decomposition of γ phase during aging in $Ni_{60}Mn_{16}Al_{19}Fe_5$ caused large shifts in the transformation temperatures. Transformation temperatures in this alloy are also argued to be affected by quenching rate from solution,

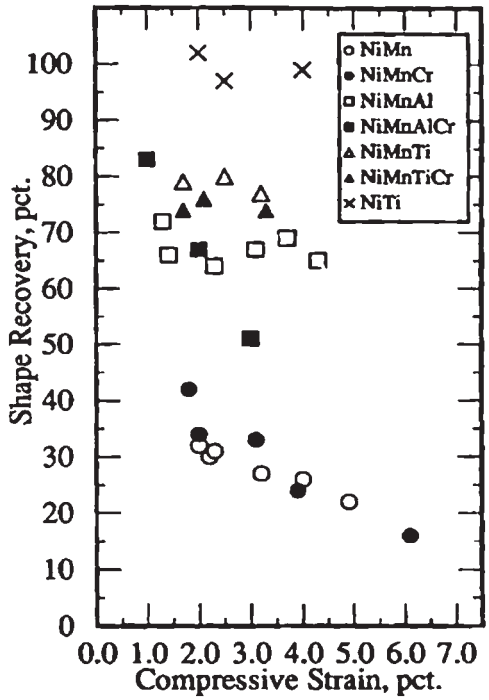

50 Summary of shape recovery rates of several Ni–Mn based HTSMAs under compression.[236] (Reproduced with permission from the Materials Research Society)

which is most likely related to the formation of γ phase during quenching.[238] Although phase decomposition mechanisms similar to Ni_5Al_3 formation does not take place in binary Ni–Mn alloys, a 'tempering' of martensite occurs where the reverse transformation is suppressed by the disappearance of martensite twins[231] due to recovery and recrystallisation effects. A similar effect has also been observed in high transformation temperature compositions of Ti–Ni–Pd alloys and was discussed in detail in Section III.1·1. Fortunately, this process is limited to temperatures above 400°C and does not appear to interfere with the phase transformation behaviour of quenched alloys with transformation temperatures near 200°C. However, alloys with excessive nickel and aluminium content, such as $Ni_{60}Mn_{15}Al_{25}$, continue to experience Ni_5Al_3 formation near 300°C and suffer from the same issues as the Ni–Al alloys.[215]

III.1·6.c. Unconventional processing techniques for Ni–Al and Ni–Mn HTSMAs

To address some of the concerns with Ni–Mn and Ni–Al based HTSMAs, unconventional processing techniques have been extensively studied. One early problem with Ni–Al alloys was the sensitivity of transformation temperatures to changes in composition, so powder metallurgy was used to produce alloys with more uniform composition and enable better composition control.[56] The lack of ductility in the Ni–Al and Ni–Mn alloys makes improvements in shape memory behaviour through traditional thermomechanical treatments difficult, so several unconventional techniques can be used to achieve grain refinement in order to improve both shape memory behaviour and ductility. Grain sizes can be reduced from 100–500 μm in solution treated Ni–Al or Ni–Mn alloys to less than 5 μm with rapid solidification methods such as melt spinning[226,239] and splat cooling.[227] In general, rapid solidification causes a decrease in transformation temperatures,[225] and was argued to be most likely due to a minor composition shift coupled with the extremely steep dependence of transformation temperatures on the Al content, but could also be caused by the reduction in grain size or the excess vacancy concentration caused by rapid solidification. On the other hand, splat cooled Ni–Al samples with higher transformation temperatures and higher Ni_5Al_3 decomposition temperatures than bulk alloys of the same composition have been made, with both effects believed to be caused by the internal stress field due to small grain size (1–5 μm) and quenched-in dislocations created in the alloy during fast cooling.[227] For example, in a splat cooled $Ni_{65}Al_{35}$ alloy, the Ni_5Al_3 formation temperature was raised ~200°C over that of the bulk alloys.[227] Since composition control is not as precise in melt spun or splat cooled samples as in powder metallurgy, the discrepancy in these results can again be attributed to small composition variations. The cyclic and thermal stability of these samples are unknown and mechanical and shape memory properties were not determined.

Overall, the Ni–Al and Ni–Mn based SMAs suffer from similar problems as in the Cu based systems. Decomposition and poor ductility are serious issues that must be overcome. While shape memory properties in the Ni–Al system are very poor and unsuitable for application, those of Ni–Mn based alloys in bending and compression are satisfactory and compare favourably to polycrystalline Cu–Ni–Al. However, no shape memory data are available at all in tension because of limited tensile ductility. Although microstructural evolution and phase transformation characteristics appear to be well understood, studies on improvement and optimisation of shape memory behaviour are inadequate. While there are doubts to whether Ni–Mn based alloys will ever acquire properties necessary to be fit for commercial use, the fundamental problems which prevent this are well understood. Given the low cost, existing metallurgical knowledge, and the absence of detailed characterisation of shape memory properties in these alloys, some further scientific exploration is at least warranted even though the alloy will not be ready commercially in the immediate future.

III.1·7. Ni–Mn–Ga SMAs

Near stoichiometric Ni_2MnGa Heusler type alloys have been thoroughly studied for their magnetic shape memory behaviour.[240–243] In these alloys, transformation temperatures shift sharply when compositions are displaced from stoichiometry, with increasing nickel content leading to an increase in transformation temperatures.[244] Jiang *et al.*[245] discovered that the increase in transformation temperatures is greater by replacing gallium with nickel than replacing manganese with nickel as summarised in Fig. 51. Quaternary elements can also be used to control transformation temperatures, and adding cobalt up to ~10 at-% at the expense of manganese increases transformation temperatures while addition of cobalt or iron up to ~5 at-% at the expense of nickel decreases them.[246] Replacement of manganese with copper up to 2 at-% increases transformation temperatures by roughly 30°C/at-%.[252] This trend is correlated with the valence electron to atom (e/a) ratio.[38,244,245,253] Higher e/a ratio corresponds to higher transformation temperatures, therefore replacing low valence elements such as gallium and

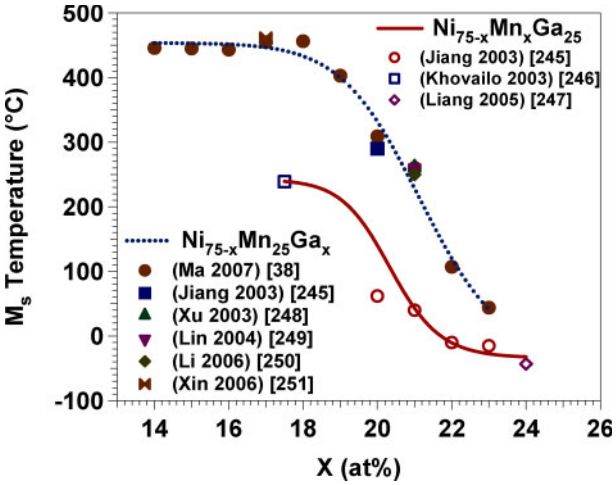

51 Composition dependence of the martensitic start temperatures, M_s, of Ni–Mn–Ga alloys. Replacement of gallium by nickel is much more effective in increasing M_s than the replacement of manganese by nickel in the same amounts. Above 44 at-% of Mn+Ga, M_s drops significantly with further increase in Mn+Ga content. The trendlines are the fits through each set of data points

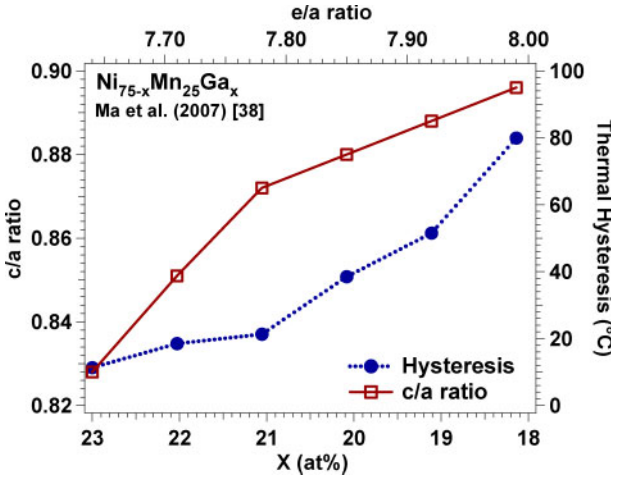

52 The dependence of ΔT and c/a tetragonality ratio on the valence electron to atom (e/a) ratio and corresponding composition in a series of $Ni_{75-x}Mn_{25}Ga_x$ alloys: in the range considered, both c/a ratio and ΔT increased as gallium content decreased. Transformation temperatures also increase with a higher e/a ratio, as seen in Fig. 51. The trendlines are the fits through each set of data points

manganese with high valence nickel is very effective in raising transformation temperatures. For example, in a $Ni_{58}Mn_{25\cdot3}Ga_{16\cdot3}$ alloy, M_s is as high as 466°C.[253] The e/a ratio also controlled other aspects of the transformation, such as ΔT (Fig. 52). However, since the addition of many such quaternary elements, such as iron, cobalt and copper introduces precipitation of second phases with compositions different than the matrix, the nominal alloy composition can be far from the composition of the transforming matrix. For example, addition of Fe or Co above 5 at-%, or Cu above 2 at-% no longer has any effect on the transformation temperatures of the matrix because their solubility in the matrix was reached, and the extra atoms simply go into the second phase. Therefore, e/a ratios should not be computed from the nominal composition, but from the measured matrix composition instead.

It is known that several types of martensite can form in the Ni–Mn–Ga system, leading to multistage complex transformation sequences at different temperature ranges.[254,255] In compositions with transformation temperatures above 100°C, however, there is an agreement that the $L2_1$ parent phase transforms to the 2M (non-modulated tetragonal) martensite in polycrystalline samples.[253,256]

Since tensile ductility is very limited, all studies on the mechanical and shape memory properties of Ni–Mn–Ga alloys have been conducted in compression. Very good compressive ductility (20·5%) and complete shape memory recovery of 6·1% applied strain have been found in single crystalline $Ni_{54}Mn_{25}Ga_{21}$ alloys[248] deformed at room temperature. Furthermore, excellent superelasticity with up to 6% fully recoverable strain has been demonstrated in compression in both [001] and [110] oriented single crystals of $Ni_{53\cdot1}Mn_{26\cdot6}Ga_{20\cdot3}$ deformed between 120 and 150°C and for $Ni_{51\cdot2}Mn_{31\cdot1}Ga_{17\cdot7}$ deformed between 160 and 200°C.[257]

Unfortunately, like many other alloy systems, the performance of Ni–Mn–Ga single crystals does not extend to polycrystalline forms. Coarse grained alloys suffer from poor ductility, cracking at as little as 4% strain in compression.[249] Lin *et al.*[249] improved ductility to 16% strain (10% without cracks) through grain refinement by fast quenching. In the fine grained polycrystalline $Ni_{54}Mn_{25}Ga_{21}$ alloy, shape memory recovery rate of 70% was attained from 10% applied compressive strain at room temperature.[249] Additions of rare earth elements, such as Nd, are also effective in increasing compressive ductility, but have been studied only in compositions near stoichiometric Ni_2MnGa,[258] which do not have high transformation temperatures. Increasing the deformation temperature deteriorated shape memory properties in a $Ni_{54}Mn_{25}Ga_{21}$ alloy. Deformation to 8% applied strain in compression at 250°C (below M_f) yielded a recovery rate of only 50% (4% total strain recovered),[250] and samples deformed at 360°C (above A_s) show no superelasticity.[250]

Several authors studied the effect of composition on the mechanical and shape memory properties in both single and polycrystals. Ma *et al.*[38] reported shape memory behaviour in single crystals with nickel concentrations up to 61 at-% at a constant manganese concentration of 25 at-%, but recovery deteriorated in compositions with a higher nickel content. Nickel additions increase σ_{DT}, and thus reduce the difference between σ_y and σ_{DT}, and also increase the c/a ratio of the alloy. The latter effect takes the c/a ratio closer to one, and thus brings the parent phase closer shape to the martensite and decreases theoretical transformation strain.[38] Increasing Ni content beyond 57 at-%, which the authors concluded to be the solubility limit, no longer increases the transformation temperatures because nickel rich γ phase readily precipitates out of solution.[38]

Since the Ni rich fcc γ phase is ductile, several researchers[252,259–262] intentionally induced its appearance by either increasing nickel content or introducing iron,[260,262] cobalt[259,260] or copper[252,261,263] as a quaternary

addition to improve the ductility of polycrystalline Ni–Mn–Ga alloys. For example, the ductility was indeed improved from 12·8% strain to failure in $Ni_{54}Mn_{25}Ga_{21}$ alloy to 15·8% in $Ni_{58}Mn_{25}Ga_{17}$ and 28·8% in a $Ni_{50}Fe_8Mn_{25}Ga_{17}$ alloy containing 8 at-% iron at the expense of nickel.[262] Improvement in ductility in both alloys corresponded to increasing volume fractions of γ phase. This improvement in ductility comes at a cost in shape memory properties, and in an Fe containing alloy, only 36% recovery rate was possible from 7% applied strain at room temperature.[262] Similar degradation in shape memory properties were observed in cobalt[260] and copper[252] containing alloys with γ precipitates. The γ phase, which does not undergo a martensitic transformation and plastically deforms readily, was responsible for the decline in recoverability.[262]

In compositions with M_s near 200°C, both single and polycrystalline Ni–Mn–Ga alloys are stable cyclically. Ma *et al.*[256] observed no change in transformation temperatures measured by DSC in $Ni_{54}Mn_{25}Ga_{21}$ after 1000 stress free thermal cycles between room temperature and 350°C. Xu *et al.*[248] observed minimal differences in both recovery rate and recoverable strain in a $Ni_{54}Mn_{25}Ga_{21}$ single crystal alloy in experiments before and after 1000 similar thermal cycles. However, transformation temperatures increased by 4–8°C after isothermal aging in martensite, and this change is magnified to 16–45°C when alloys were aged in austenite for 100 h.[251,264,265]

Thin films of $Ni_{53·97}Mn_{25·67}Ga_{20·36}$ alloy were fabricated successfully by Liu *et al.*[266] using magnetron sputtering methods. Transformation temperatures were ~100°C lower in the thin film than the bulk alloys of similar composition, and 14M martensite was found instead of non-modulated 2M seen in the bulk material. The extreme brittleness of Ni–Mn–Ga polycrystals does not even allow hot working techniques to be used without special modifications to the process. One such modification was used by Besseghini *et al.*[267] to successfully hot roll polycrystalline $Ni_{53}Mn_{23·5}Ga_{23·5}$ alloys up to 82% reduction in thickness at 1000°C. This was accomplished by wrapping the Ni–Mn–Ga alloy in thin niobium foil and putting it into an iron can. Such thermomechanical processing is needed for these alloys, and other similar HTSMAs, in order to better homogenise as cast structures and refine their grain sizes, which will also help with the brittleness problem. In addition, if a desired texture can be imposed, it would be beneficial for achievable transformation strain and recoverable strain levels, as discussed in Section II.2·3.

Existing research on Ni–Mn–Ga alloys indicate that their potential as a polycrystalline HTSMA is limited. Lack of ductility and deterioration of shape memory properties in the polycrystalline state and at increasing temperatures restrict their ability to be used in most applications and makes thermomechanical processing into useful forms problematic. However, it must be noted that research efforts in improving tensile ductility is still in a very early stage compared to other alloy systems such as Ni–Al.

III.1·8. Zr based intermetallic HTSMAs

There are a number of zirconium based intermetallics with B2 ordered structures and few of these undergo a reversible martensitic reaction, namely, Zr–Rh,[268] and Zr–Cu.[269] Zr based alloys transform from B2 austenite into monoclinic B19′ martensite[268,269] in a similar fashion to binary Ti–Ni alloys. However, in Zr–Cu alloys, transformation to another monoclinic martensite with space group C_m was also possible.[270] The M_s in equatomic binary Zr–Cu is 140°C,[269] and M_s of equiatomic Zr–Rh is 450°C.[268]

In quasi-equiatomic compositions of $Zr_{50}(Cu,Co,Ni)_{50}$, shape memory behaviour is decidedly poor. Perfect shape recovery has been found only after room temperature deformation in bending up to 0·4% applied strain in equiatomic Zr–Cu, and after 0·5–1·3% deformation, the recovery rate dropped to 85–90%.[271] A similar limited shape recovery of less than 0·5% strain was observed in equiatomic Zr–Rh alloys.[268,272] Equiatomic Zr–Cu and Zr–Rh have very large ΔT of 190 and 200°C, respectively. Such a large hysteresis is a sign of a non-thermoelastic transformation, which was indeed confirmed by Koval *et al.*[271] and Firstov *et al.*[273] Waterstrat *et al.*[272] did not share the same opinion regarding Zr–Rh alloys by concluding that Zr–Rh does transform thermoelastically from studies on the martensite structure; though no explanation for the large ΔT was offered. The ductility of Zr–Rh alloys was poor,[272] and no further studies of shape memory behaviour have been conducted on this system. Instead, further studies have focused on the Zr–Cu based alloys.

To improve shape memory behaviour, the Zr–Cu system has been modified with ternary and quaternary additions.[271,274] Replacing copper with nickel up to 20 at-% increased transformation temperatures by ~20°C/at-%, but reversibility suffered, while replacing zirconium with titanium had the opposite effect: decreasing transformation temperatures while improving reversibility. Finally, replacing copper with cobalt decreased transformation temperatures slightly, but improved recoverability.[270,247,275] During the course of these studies, an interesting behaviour was discovered in the Zr–Cu system: by changing the alloying elements, both martensite structure and the thermoelastic nature of transformation could be changed.[271] By replacing copper with cobalt, the transformation became thermoelastic as it was evident from a decreasing thermal hysteresis to ~60°C in the $Zr_{50}Cu_{25}Co_{25}$ alloy from 190°C in the $Zr_{50·1}Cu_{49·9}$ alloy.[269,271] On the other hand, when nickel was added instead of cobalt, martensite changed to a C_m monoclinic structure[270] and the transformation became non-thermoelastic. This means that cobalt and nickel have opposite effects on the Zr–Cu alloy: cobalt decreases transformation temperatures while improving thermoelasticity, while nickel increases transformation temperature but makes transformation non-thermoelastic. The result suggests some type of compromise where both cobalt and nickel are added to the base Zr–Cu to optimise both transformation temperatures and reversibility. The composition dependence of transformation temperatures in the Zr–Cu–Co–Ni system is shown in Fig. 53.

Further optimisation of composition generated a $Zr_{49·6}Cu_{28·2}Co_{15·4}Ni_{6·8}$ alloy with M_s of 247°C, capable of achieving ε_{rec} of 2·5% from 8% applied strain in compression at 247°C, and a $Zr_{42·3}Cu_{29·9}Ni_{11}Co_{10·2}Ti_{6·6}$ alloy with M_s of 177°C, achieving ε_{rec} of 3·5% from 8% applied strain in compression at 177°C.[276,277] Both alloys showed better reversibility when deformed near M_s rather than at room temperature, and the Ti

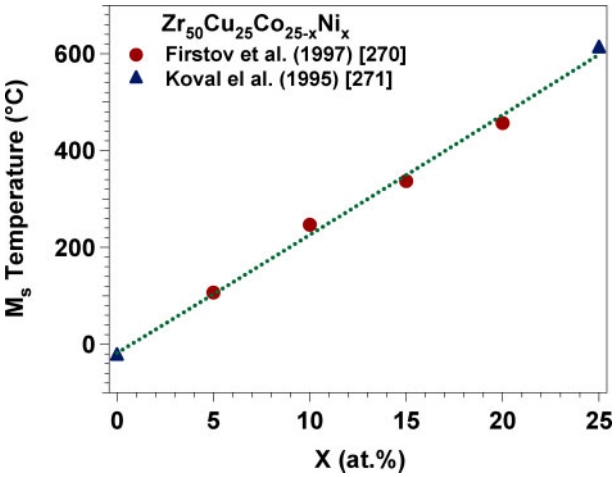

53 Increase in martensitic start temperatures, M_s, with increasing nickel content (at the expense of Co) in the $Zr_{50}Cu_{25}Co_{25-x}Ni_x$ system. The trendline is a fit through all data points.

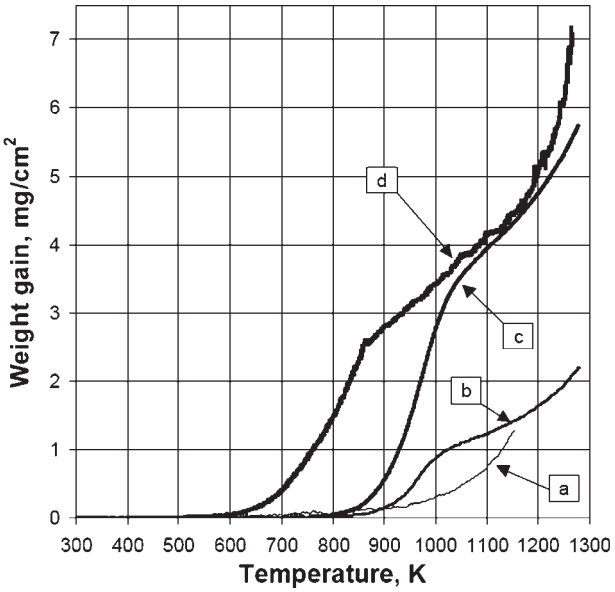

54 Oxidation measured by weight gain of *a* $Ti_{50}Ni_{50}$, *b* $Ti_{35\cdot95}Ni_{49\cdot42}Hf_{14\cdot63}$, *c* $Ti_{33\cdot01}Ni_{48\cdot78}Zr_{18\cdot21}$ and *d* $Zr_{42\cdot3}Cu_{29\cdot9}Ni_{11}Co_{10\cdot2}Ti_{6\cdot6}$ alloys[277]

containing Zr–Cu–Ni–Co alloy displayed similar recoverable strain as Ni–Ti–Hf and Ni–Ti–Zr alloys at 8% applied strain.[276,277] However, it should be noted that while perfect shape memory recovery could be obtained for Ni–Ti–Hf and Ni–Ti–Zr alloys when the applied strain is less than 3%,[276,277] this was not possible in any of the zirconium based alloys. Additionally, even though B19′ is the martensite structure in both sets of alloys, ΔT of Ni–Ti–Hf/Zr alloys are only half of that of Zr–Cu–Ni–Co–Ti.[276,277]

Although data are limited, the cyclic transformation temperature stability of zirconium based alloys appears to be satisfactory. Semenova *et al.*[268] found no changes in transformation temperatures of equatomic Zr–Rh after several heating and cooling cycles. Firstov *et al.*[270] found that although 40 DSC cycles were needed to stabilise the transformation temperatures in the $Zr_{42\cdot3}Cu_{29\cdot9}Ni_{11}Co_{10\cdot2}Ti_{6\cdot6}$ alloy, there were no shift in the reverse transformation temperatures. Instead, there was an increase of 30°C in the forward transformation temperatures, resulting in an overall reduction in ΔT.

Generally, the Zr based SMAs suffer from significant plasticity during transformation and thus notable ε_{irr}. A possible solution would be to increase the strength of matrix against dislocation slip by such processes as grain refinement, work hardening, solid solution strengthening, and precipitate hardening. For example, in thin film $Zr_{50\cdot59}Cu_{29\cdot56}Ni_{19\cdot85}$, produced by rapid solidification methods,[278] grains of 30–50 nm in size could be obtained using appropriate crystallisation heat treatments. No mechanical or shape memory properties were determined on these films.

The oxidation resistance measured by weight gain in air of the $Zr_{42\cdot3}Cu_{29\cdot9}Ni_{11}Co_{10\cdot2}Ti_{6\cdot6}$ was worse than the $Ti_{35\cdot95}Ni_{49\cdot42}Hf_{14\cdot63}$ alloy and binary Ni–Ti over all temperature ranges,[277] as shown in Fig. 54. For example at 800°C, the rate of weight gain is about three times higher in the $Zr_{42\cdot3}Cu_{29\cdot9}Ni_{11}Co_{10\cdot2}Ti_{6\cdot6}$ alloy than $Ti_{35\cdot95}Ni_{49\cdot42}Hf_{14\cdot63}$. At temperature above 700°C, the oxidation resistance of both $Ti_{33\cdot01}Ni_{48\cdot78}Zr_{18\cdot21}$ and $Zr_{42\cdot3}Cu_{29\cdot9}Ni_{11}Co_{10\cdot2}Ti_{6\cdot6}$ are similar, and both much worse than that of $Ti_{35\cdot95}Ni_{49\cdot42}Hf_{14\cdot63}$.[277] Compared to the Ti–Ni–Zr alloy though, oxidation begins to be a concern for the $Zr_{42\cdot3}Cu_{29\cdot9}Ni_{11}Co_{10\cdot2}Ti_{6\cdot6}$ at much lower temperatures of around 400°C, whereas $Ti_{33\cdot01}Ni_{48\cdot78}Zr_{18\cdot21}$ does not appear to experience an oxidation problem until 550°C.[277]

While the ductility of the Zr based Intermetallics is better than those of Ni based systems, the reversibility of shape memory behaviour is poor. For these alloys to be usable in applications, additional work must be performed to determine whether perfect shape memory behaviour can be obtained at any level of applied strain. Compared to other alloy systems like Ti–Ni–Pd, the Zr based HTSMAs are very far away from being considered for applications.

III.1·9. Other alloy systems

III.1·9.a. β-Ti HTSMAs

Shape memory behaviour has been observed in certain β-Ti alloys based on the Ti–Mo,[279,280] Ti–Nb,[281,282] and Ti–Ta[283,284] systems. In these alloys, the high temperature disordered bcc (β) phase can be retained at room temperature when the specimen is water quenched from a high temperature. The shape memory behaviour occurs as a martensitic transformation from the β phase to a disordered orthorhombic α'' phase.[285] Major impetus for research into β-Ti SMAs, particularly the Ti–Nb based SMAs, include their excellent ductility (easily cold rolled to 99% reduction in thickness at room temperature), and biocompatibility for applications in the biomedical industry. Through combinations of work hardening and precipitation hardening treatments, stable and fully recoverable shape memory and superelastic behaviour have both been obtained at room temperature.[281,282]

By reducing the amount of beta stabilising elements such as Nb and Ta, the transformation temperature can be raised to over 200°C.[281,284] For example in the Ti–Nb system, transformation temperatures increase linearly by ~43°C from each 1 at-% decrease in Nb, such that M_s of the $Ti_{74}Nb_{26}$ alloy is ~0°C,[281] while M_s of $Ti_{80}Nb_{20}$ is ~205°C.[286] However, the HTSMA prospect of β-Ti SMAs are dampened by phase instability of the β

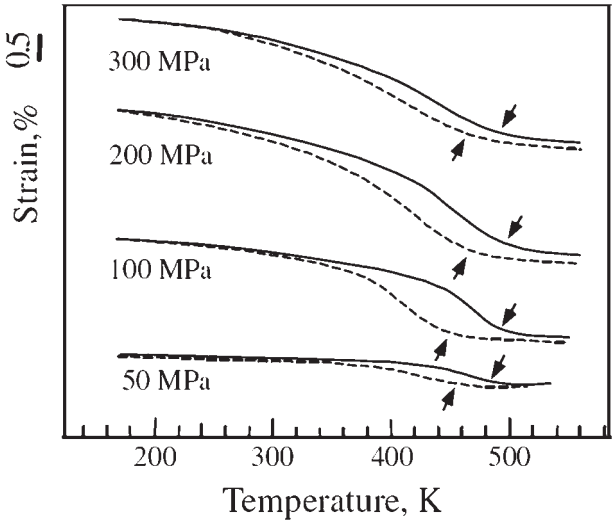

55 Shape memory behaviour during thermal cycling of a $Ti_{68}Ta_{32}$ SMA.[284] Arrows indicate the M_s and A_f temperatures. (Reproduced with permission from Elsevier)

austenite. Above ~150°C,[285] hexagonal ω phase begins to precipitate from the matrix. These precipitates do not transform, and cause compositional changes in the matrix as they are titanium rich. Controlling and suppressing ω precipitation is the greatest challenge in using these alloys as HTSMAs.

Compared to other β-Ti SMA systems, the Ti–Ta alloys appear to be the most stable against ω precipitation.[284,287,288] In a $Ti_{68}Ta_{32}$ alloy cold rolled to 98% reduction in thickness, then solution treated at 900°C for 30 min (M_s of ~170°C), Buenconsejo *et al.*[284] demonstrated ε_{rec} up to 2% from thermal cycling experiments under constant tensile stress of 200 MPa, as shown in Fig. 55. Additionally, after five heating cooling cycles under 50 MPa with a maximum temperature of 240°C, M_s of the alloy decreased by ~10°C.[284] However, if the maximum temperature during heating cooling cycles was increased to 300°C, the decrease in M_s after five thermal cycles under the same stress level was over 60°C. Alternatively, M_s also decreased by 60°C when the specimen was held at 300°C under 50 MPa for 1 h (Fig. 56). The decrease in transformation temperature is caused by isothermal ω precipitation; as ω is titanium rich, its appearance causes an increase in the tantalum content in the matrix.[284]

Buenconsejo *et al.*[288] attempted to further improve precipitation resistance of Ti–Ta SMAs through ternary addition of V, Cr, Fe, Zr, Hf, Mo, Sn and Al up to 3 at-%, replacing titanium, in a base alloy of $Ti_{70}Ta_{30}$. Transformation temperatures decreased in all cases compared to the base alloy after aging at 300°C for 1 h. Compared to $Ti_{70}Ta_3$, which experienced a 100°C decrease in transformation temperature after aging, alloying additions of Al and Sn improved stability, reducing the transformation temperature drop to 66 and 54°C, respectively. These values are comparable to the decrease in transformation temperature in the $Ti_{68}Ta_{32}$ alloy mentioned previously.[288] Since M_s of $Ti_{69}Ta_{20}Al_1$ and $Ti_{69}Ta_{20}Sn_1$ are about 20–40°C lower than M_s of $Ti_{68}Ta_{32}$, these ternary additions did not improve the stability of the Ti–Ta alloy for compositions with the same transformation temperature.

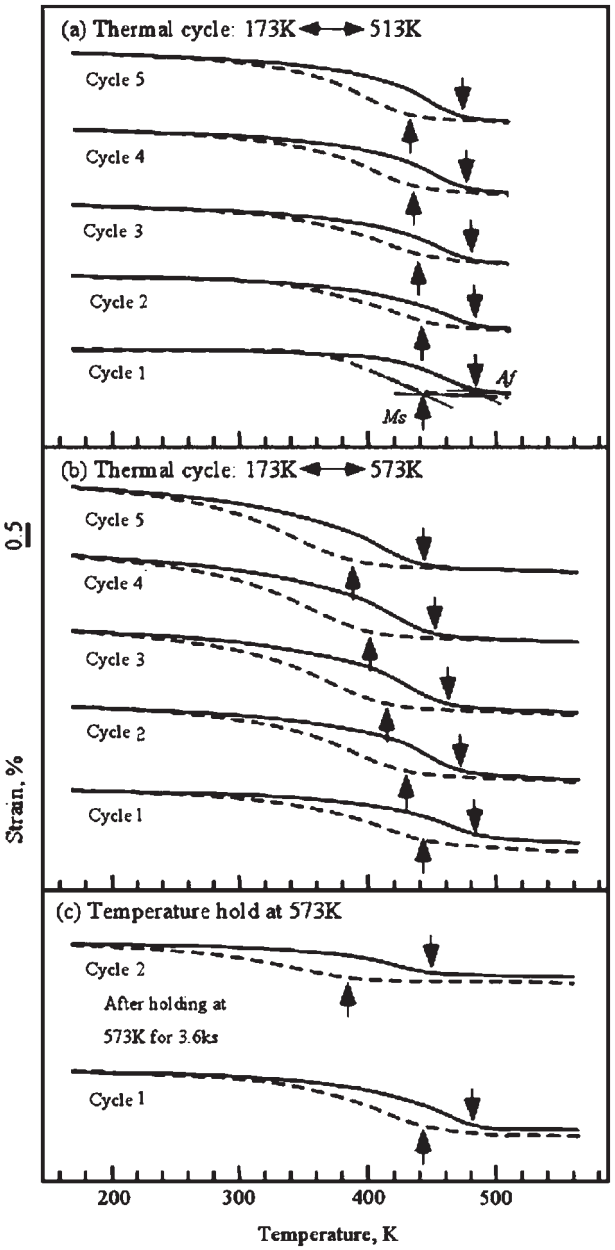

56 Cyclic and aging instabilities in the $Ti_{68}Ta_{32}$ HTSMA due to the precipitation of ω phase: *a* transformation shifts only minimally when the maximum heating cooling temperature is 260°C, but *b* when maximum cycle temperature is increased to 300°C, transformation temperatures drop disastrously as a function of the number of cycles. Similarly, when the specimen is aged *c* at 300°C, a large drop in transformation temperatures is also observed.[284] (Reproduced with permission from Elsevier)

Ping *et al.*[289,290] evaluated the shape memory behaviour of a $Ti_{79\cdot94}Nb_{18\cdot45}Pd_{1\cdot61}$ alloy with M_s of 288°C, and was able to obtain a recovery ratio of 90% from applied tensile strain of 3% at room temperature. When applied strain was increased to 4·4%, the recovery ratio dropped to 70%. The high temperature shape memory stability of the alloy was not directly studied, though the authors noted that ω precipitation was observed at 140°C.[289] Although the impact of Pd on the stability of the Ti–Nb alloy is not known, the poor high temperature stability of Ti–Nb SMAs[284] suggest that the $Ti_{79\cdot94}Nb_{18\cdot45}Pd_{1\cdot61}$ alloy is not a

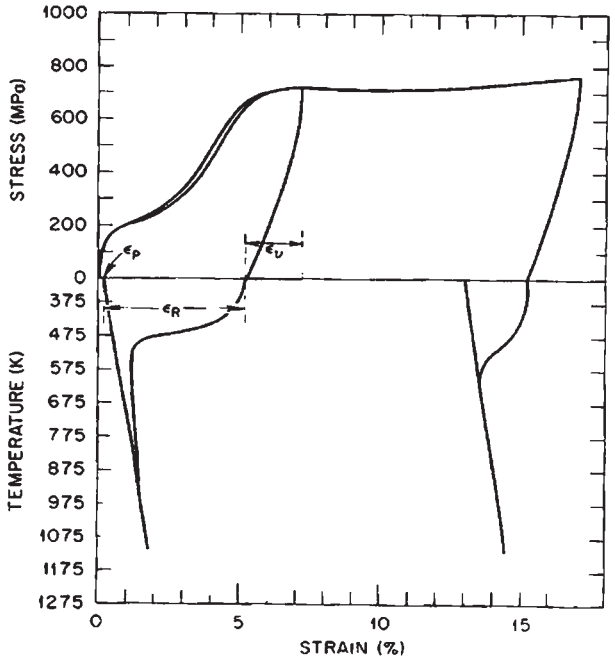

57 Shape memory behaviour of the $U_{86}Nb_{14}$ HTSMA loaded in tension at room temperature.[291] (Reproduced with permission from Springer Science and Business Media)

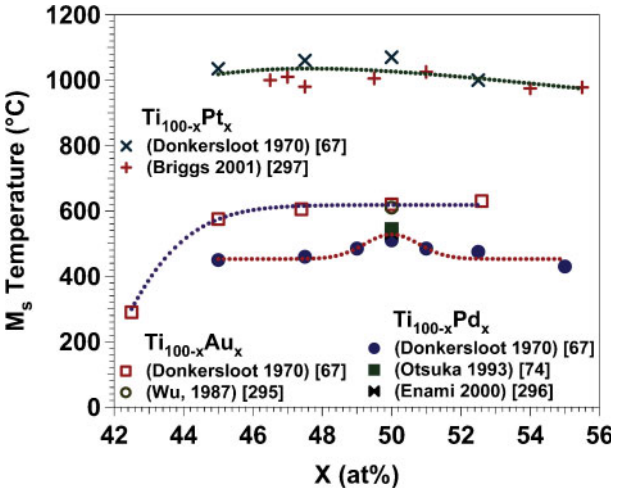

58 Effect of stoichiometry on the martensitic start temperature M_s for Ti–X binary systems where X=Pd, Au and Pt. While, Ti–Pd and Ti–Pt both exhibit maximum transformation temperarures at the equiatomic composition and Ti–Au exhibits a steep decline below 46 at-%Au, all three systems are relatively insensitive to stoichiometry over a fairly broad range in composition. The trendlines are the fits through all data points

viable HTSMA due to the low niobium content and high transformation temperatures near 300°C.

III.1·9.b. U–Nb HTSMAs

Despite the limited number of studies performed on the shape memory response of U–Nb alloys, they have been found to possess some very interesting properties and may have specialised use. The bcc high temperature phase (γ) transforms to either a tetragonal martensite (γ^0) if the niobium content exceeds 15·4 at-%, or a monoclinic martensite (α'') with less than 15·4 at-% niobium.[291]

In the $U_{86}Nb_{14}$ alloy, M_s corresponding to the γ to α'' transformation is 177°C with a thermal hysteresis of 35°C.[292] Good shape memory properties are obtained in the $U_{86}Nb_{14}$ composition where 6·8% strain could be recovered upon heating above A_f from a tensile strain of 7% applied at room temperature, as shown in Figure 57.[291,292] Theoretical transformation strain levels are very large for both compression and tension at 7·6 and 6·5% respectively.[291] Room temperature ductility is also very good with 17–18% tensile elongation in $U_{85·4}Nb_{14·6}$. However, increasing the niobium content beyond 14 at-% reduces the transformation strain and recovery rate in these alloys, leading to deterioration in shape memory behaviour.[293] This is a consequence of both composition effects and a change in martensite structure from α'' to γ^0. Finally, while the initial properties are encouraging, as with most of the other systems reviewed, the constant stress strain temperature response of this alloy has not been reported so there is no clear indication as to the potential work characteristics of the alloy, and the fact that the alloy is uranium based precludes any common use of these materials.

III.2. Alloys with characteristic temperatures between 400 and 700°C

The temperature range of 400–700°C is particularly important in aerospace applications involving components with high proximity to engines or fuel systems but poses an interesting challenge for SMAs. Although some alloy systems are capable of attaining transformation temperatures within this range, diffusion based mechanisms such as phase decomposition, creep, or recovery and recrystallisation are very active at such high temperatures. Since many of the HTSMAs that have been identified are based on metastable phases, they cannot tolerate long term exposure above ~400°C, while those HTSMAs based on equilibrium phases generally have transformation temperatures above 700°C and are discussed in a subsequent section. This is the main reason for the lack of potential SMA systems specifically identified for this temperature range.

III.2·1. Ti–Pd and Ti–Au HTSMAs

Several binary Ti–X B2 alloys possess the ability to transform martensitically between 400 and 700°C,[67,294] and of these, Ti–Pd and Ti–Au alloys show shape memory behaviour.[69,295] The cubic B2 austenite to orthorhombic B19 martensite transformation in these alloys is thermoelastic and is accompanied by a moderate thermal hysteresis around 40°C.[69,295] The majority of studies have focused on Ti–Pd alloys with large ternary nickel additions and lower transformation temperatures. These ternary alloys have already been discussed in Section III.1·1, and the focus here is on the higher transformation temperature binary and near binary alloys.

Transformation temperatures of the Ti–Pd and Ti–Au binary systems were first studied systematically by Donskerloot and Van Vucht.[67] They found maximum M_s of 510 and 630°C for $Ti_{50}Pd_{50}$ and $Ti_{47·4}Au_{52·6}$ respectively. In the Ti–Pd system, maximum transformation temperatures occur at the equiatomic composition and decrease initially by 10–25°C/at-% on either side of stoichiometry before leveling off, as shown in Fig. 58. Transformation temperatures remain fairly constant on the gold rich side of Ti–Au alloys, but drop off considerably in Ti rich compositions when Ti

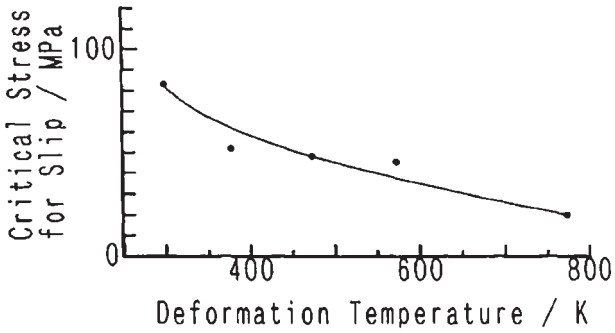

59 Dependence of σ_y on deformation temperature in equiatomic Ti–Pd HTSMA. σ_y is determined by finding ε_{irr} at several stress levels for a given deformation temperature and extrapolating linearly to the stress where ε_{irr} is zero at that particular temperature.[74] (Reproduced with permission from Elsevier)

concentration exceeds 55 at-%.[67] Ternary additions up to ~3 at-%, such as Fe, Co, Ni, Cu, Ru, Rh, Pd, Ag, Ir and Pt lowers transformation temperatures of the equiatomic $Ti_{50}Au_{50}$ alloy,[298] although it is not known how transformation temperature will be affected by ternary additions greater than 3 at-%. As for the $Ti_{50}Pd_{50}$ alloy, ternary additions of 14 at-%Fe,[299] up to 10 at-%V,[296] and up to 9 at-%Cr,[300] decreases transformation temperatures.

The temperature and stress at which deformation takes place has enormous impact in the reversibility of shape memory behaviour in Ti–Au and Ti–Pd alloys. Complete shape memory recovery of 3% applied strain at room temperature occurs in both $Ti_{50}Au_{50}$ and $Ti_{50}Au_{40}Ni_{10}$ alloys in tension.[295] Although a ε_{rec} of 8·7% was measured from 10% applied tensile strain in $Ti_{50}Pd_{50}$,[74] the validity of this result is very questionable since the martensite elastic modulus measured from the stress–strain curves was only ~15 GPa, and the specimen deformed at room temperature showed elastic strain up to 4%. Disregarding the quantitative aspect of this study, the results show that as deformation temperature is increased, the shape memory behaviour, especially ε_{irr}, deteriorates significantly. No shape memory behaviour is observed at deformation temperatures as low as 440°C (below M_s) in $Ti_{50}Pd_{50}$,[74] and superelasticity is also completely absent at higher temperatures.

Otsuka *et al.*[74] noted that the deterioration in reversibility of shape memory behaviour of Ti–Pd alloys was caused by a rapid decrease in σ_y (Fig. 59), which meant that significant plastic deformation would take place before stress induced transformation (in the case of superelasticity) or detwinning (in the case of shape memory behaviour) could be completed. Their suggestion that alloying, thermomechanical treatment, and precipitation hardening could be used to increase σ_y, and thus, improve the performance of SMAs has been demonstrated successfully in the Ti–Ni–Pd alloys,[71,75,81] and serves as the basis for most current HTSMA development efforts.

The reason why it is quite difficult to develop an SMA with transformation temperatures above 400°C is that in addition to low σ_y, thermal stability becomes problematic within the operational temperature range of these alloys. Studies on the diffusion based behaviour of Ti–Pd revealed that 500–550°C is enough to activate recrystallisation in equiatomic Ti–Pd and recovery would be expected at even lower temperatures.[301,302] Indirectly, recovery and recrystallisation can be identified by an increase in reverse transformation temperatures with increasing aging time. At an aging temperature of 560°C in martensite (A_s, ~575°C), A_s and A_f in equatomic Ti–Pd increased by 2–4°C within 115 h, and did not stabilise with further aging.[303] This behaviour was rationalised based on the microstructural observation that internal twins in martensite disappeared during aging.[303] The loss of internal twins results in a loss of stored elastic energy created by the martensitic transformation. Stored elastic energy assists the reverse transformation process since it is released when the alloy returns to the austenitic state, and their loss will result in greater energy requirements (in the form of overheating) for the reverse transformation and raising A_s.[303] In Ti rich compositions, an initial increase in transformation temperature with aging is followed by a subsequent decrease as the Ti_2Pd phase is precipitated from the matrix.[304]

The cyclic stability of shape memory behaviour is unknown in these alloys, but problems of cycling associated with poor ductility have rendered attempts to induce two way shape memory behaviour in both $Ti_{50}Au_{40}Ni_{10}$ and $Ti_{50}Au_{50}$ unsuccessful.[295] The $Ti_{50}Au_{40}Ni_{10}$ sample failed within 20 training cycles and no two way behaviour was observed during that interval,[295] and the binary Ti–Au alloy failed in even fewer cycles than the nickel containing alloy.

To date, optimisation techniques used in Ti–Ni–Pd alloys, such as work and precipitation hardening, have not been successfully applied to higher temperature compositions of the Ti–Pd and Ti–Au alloys. It is clear that the added challenge of having to stay below the recovery and recrystallisation temperatures of an alloy will limit the usefulness of most systems at higher temperatures. Specifically, in the case of Ti–Pd and Ti–Au alloys, this challenge places a practical upper limit of ~400°C. Furthermore, few alternative systems are available with transformation temperatures in this temperature range and success with low temperature compositions may not translate to equal success for higher temperature alloys.

III.2·2. Other potential HTSMAs for range of 400–700°C

III.2·2.a. Co–Si non-thermoelastic HTSMAs

Figure 44 in Section III.1·4 showed that the addition of silicon to cobalt increases the transformation temperatures of the non-thermoelastic martensitic transformation in Co, with the highest M_s of 588°C occurring at 14 at-%Si.[197,201] The shape memory properties and alloy structures of Co–Si are very similar to those of the Co–Al SMAs. However, unlike aluminium additions, silicon does not improve shape memory recoverability of cobalt and maximum recovery rate is only 40% in bending at room temperature for $Co_{96}Si_4$.[197] Very little work has been done otherwise on these materials. Similar to the Co–Al alloys, it is suspected that shape memory properties may be improved through ternary additions, perhaps through nickel; though it is likely that transformation temperature would also decrease in that case. It is questionable whether useful shape memory properties can be obtained at compositions with transformation temperatures greater than 400°C.

III.3. High temperature SMAs with characteristic temperatures above 700°C

Ultra HTSMAs with operational temperature above 700°C are rare, since diffusion controlled mechanisms are extensive and low σ_y make plastic deformation exceedingly difficult to avoid. Moreover, many techniques used for lower temperature HTSMAs to improve shape memory behaviour, such as work and precipitate hardening, are no longer effective at very high temperatures. Nevertheless, certain alloy systems are still able to demonstrate some shape memory behaviour at temperatures even above 1000°C. Unlike for lower temperature HTSMAs, shape memory behaviour in many alloys in this temperature range is based on equilibrium phases. This actually means that the stability of such alloys is excellent. In fact, the main challenge for HTSMAs in this temperature range is simplified to essentially suppressing plastic deformation. Of course, other metallurgical problems associated with high temperatures such as creep and oxidation are highly amplified. Coupled with the difficulty of experimentation at such high temperatures, development of these ultra high temperature SMAs presents a unique challenge.

III.3·1. Pt based HTSMAs

Donkersloot[67] first reported martensitic transformation in binary equiatomic Ti–Pt alloys occurring at ~1070°C. Since then, many other alloy systems with high transition temperatures have been studied for shape memory effect, including Ti–Au and Ti–Pd. However, similar work on Ti–Pt was not conducted until the late 1990s, when the search for potential HTSMAs resumed with studies on the shape memory behaviour of Pt based alloys.

Like many other Ti–X binary B2 alloys, transformation temperatures in the Ti–Pt system are the greatest at the equiatomic composition (Fig. 58),[67,305] but do not decline noticeably on either side of stoichiometry.[67,305,306] The M_s was reported to be 990°C (Ref. 307) and 1018°C (Ref. 100) in the equiatomic Ti–Pt composition by thermal analysis techniques, which are slightly lower than the value reported by Donkersloot *et al.*[67] who used X-ray techniques, which tend to naturally overestimate transformation temperatures. High temperature B2 austenite transforms to orthorhombic B19 martensite thermoelastically with thermal hysteresis near 40°C, but no shape memory behaviour exists due to relatively low σ_y (~130 MPa at A_s) in the binary alloy.[308] The binary composition shows good ductility at room temperature and can be cold rolled to 50% reduction in thickness[297] without surface cracking.

Improvement in the σ_y is possible through alloying. Nickel additions at the expense of platinum have produced good shape memory behaviour, but lowered the transformation temperatures significantly.[306] A detailed discussion of the Ti–Ni–Pt system can be found in Section III.1·1.b. The addition of iridium increases both σ_y and transformation temperatures;[307] by replacing 37·5 at-%Pt with Ir, σ_y at temperatures just above A_s was increased from 130 to 280 MPa while M_s increased from 990 to 1184°C. Shape memory behaviour also improves with the addition of Ir. In $Ti_{50}Pt_{37·5}Ir_{12·5}$, 2% ε_{rec} appeared upon heating above A_f after 22% applied compressive strain at room temperature. The recovery rate doubled in the $Ti_{50}Pt_{25}Ir_{25}$ alloy, but no shape memory behaviour was found in $Ti_{50}Pt_{12·5}Ir_{37·5}$. Although not exhibiting shape memory behaviour, the higher Ir containing alloys actually displayed better superelastic response than alloys with lower iridium content, such that 4% strain was recovered superelastically in $Ti_{50}Pt_{12·5}Ir_{37·5}$ deformed to 10% applied strain in compression at temperatures above A_f.[308] However, it is not quite clear why shape memory behaviour cannot be observed in $Ti_{50}Pt_{12·5}Ir_{37·5}$. According to the authors,[308] σ_y of martensite in this composition reaches 700 MPa at ~1000°C, at which point σ_{DT} is only ~400 MPa. For shape memory experiments in that study, the specimen was deformed at nearly 1180°C (below M_s), at which point the difference between σ_{DT} and σ_y is much smaller. Therefore, it might be expected that shape memory properties might improve if the deformation temperature is lowered.

Most of other binary Pt–X systems do not exhibit a thermoelastic martensitic transformation, such as Pt–Cu and Pt–Mn, or are very brittle, such as Pt–Cr and Pt–V.[305] The Pt–Ga and Pt–Al systems show high temperature martensitic transformations around the Pt_3X composition at 1000 and 320°C respectively.[305] Further alloying of the Pt–Al system with ruthenium or nickel both suppress transformation temperatures. No shape memory or work related properties were determined in any of these alloy systems.

Development of Ti–Pt, and Pt based SMAs, with the exception of Ti–Ni–Pt, is very immature, and the lack of thermomechanical processing possibilities makes it very doubtful that an alloy with sufficiently low ε_{irr} can be developed in the polycrystalline form. Theoretically, it may be possible to reduce ε_{irr} through texturing in such a way that the slip and deformation twinning systems have smaller Schmid factors than that of martensitic transformation or detwinning. But it is not clear how texture can be retained due to recrystallisation. For critical applications, it may be possible to use single crystals, if they can be made. Nevertheless, the potential high temperature capabilities of these alloys will certainly be revisited if the demand for very high temperature SMAs continues to grow, since there are very few alternative systems with such high transformation temperatures. Realistically, unless SMAs with very high transformation temperature can achieve breakthrough improvements in high demand applications, the high cost of these alloys will certainly hinder their development.

III.3·2. Ta–Ru and Nb–Ru HTSMAs

The Ta–Ru and Nb–Ru systems possess remarkably high transformation temperatures: over 1000°C for Ta–Ru and 900°C for Nb–Ru alloys. At the equiatomic composition of either alloy, the B2 ordered parent phase (β) experiences a tetragonal distortion, and transforms thermoelastically into tetragonal β' martensite.[309] A second martensitic transformation takes place at a slightly lower temperature between tetragonal β' and monoclinic β'' martensites.[310] The reversible β to β' transformation is believed to be responsible for the shape memory behaviour in these systems[310] with small hysteresis of 10–20°C.[310,311] Increasing Ta or Nb at the expense of Ru in the binary alloys lowers transformation temperatures,[311,312] as shown in Fig. 60. Only single stage transformations

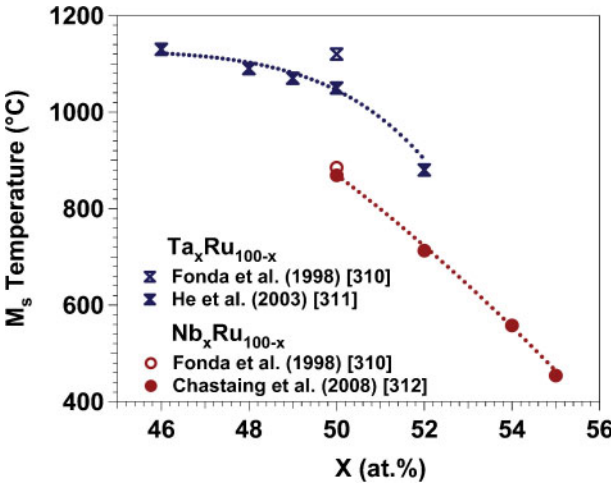

60 The martensitic start temperature, M_s, of both Ta–Ru and Nb–Ru systems increase with increasing ruthenium content. The Ta–Ru system has overall higher transformation temperatures than the Nb–Ru system. The trendlines are the fits through each set of data points

were reported in a Ta poor $Ta_{49}Ru_{51}$ alloy[313] and a Nb rich $Nb_{55}Ru_{45}$ composition.[312]

Shape memory properties of Ta–Ru and Nb–Ru alloys were first investigated in equiatomic compositions by Fonda *et al.*[310,314] through high temperature three point bending and compression experiments on polycrystalline samples. In bending at 900°C, total deformation of 8% strain in the outermost fibre produced shape memory recovery of 5% strain after reheating. However, in compression at identical temperature, only 2% strain recovery was possible from 4% applied strain. Recovery rate improves when the deformation temperature is lowered, and Gao *et al.*[315] successfully achieved complete recovery of 2% applied compressive strain in $Ta_{50}Ru_{50}$ at room temperature. It was noted in TEM observations that samples deformed to 1·5% strain show martensitic reorientation only while dislocations were widely visible in samples deformed to 3%.

Three point bending experiments in equiatomic Nb–Ru alloys produce total recoverable strain of 3·7% upon heating from 4·2% applied strain at 800°C.[310] Further investigation by Chastaing *et al.*[312] reveals up to 3% recoverable strain with 90% recovery in bending at 840°C. The only full recovery observed at any test temperature occurred in bending at 500°C in the $Ru_{50}Nb_{50}$ alloy, and consisted of 1·3% shape memory strain.[312] After deforming the $Ru_{45}Nb_{55}$ alloy in bending at 500°C, where the microstructure consists of a mixture between austenite and martensite, and heated up to 1200°C, the specimen demonstrated two shape memory behaviour when again cooled into the martensite region. No explanation or possible mechanisms for the TWSME was offered. Because of the high temperature, it is not clear if this TWSME was caused by dislocations generated during bending since recovery quickly occurs at 1200°C. The SC-SRO point defect mechanism cannot satisfactorily explain this TWSME either since 1200°C is about $0{\cdot}7T_m$; point defects should easily adapt to the austenite symmetry configuration at this temperature.

At room temperature, ductility of Ta–Ru alloys is very poor. Fracture under compression occurred at 5% strain,[315] and cracks were observed in bending at 8% equivalent strain on the tensile surface.[310] Nb–Ru alloys are only slightly better in ductility than Ta–Ru alloys.[310,314] Large grain size, averaging 1 mm, and deformation twinning in martensite were blamed for the poor ductility.[310,316] Addition of iron to Nb–Ru alloys reduced grain size while slightly lowering transformation temperatures.[317] It is not known if and how iron addition affects the shape memory behaviour.

A unique characteristic of Ta–Ru and Nb–Ru alloys is that the transformation phases are based completely on equilibrium phases. Thus these alloys are expected to be stable and less susceptible to aging and cyclic effects, which trouble lower temperature HTSMAs based on metastable phases. This is indeed the case for Ta–Ru alloys, and is assumed to be the case for Nb–Ru alloys although no relevant data is available for the latter system. Both equiatomic Ta–Ru and $Ta_{51}Ru_{49}$ were found to be unaffected by 24 h aging at 500°C.[313,317] In addition, the thermal cyclic response of the equiatomic Ru–Ta alloy was quite stable; transformation temperatures from DSC cycles between 650 and 1250°C completely stabilised after only one cycle.[313]

Ta–Ru and Nb–Ru alloys are at the frontier of HTSMAs with some of the highest known transformation temperatures. While preliminary data reveal extremely promising shape memory properties, numerous obstacles exist to their utilisation: poor environmental resistance, low ductility, and poor workability being among these. In fact, characterisation and use of these alloys is only possible in vacuum and yet they may be promising for certain niche applications.

III.4. Summary

A quick glance through Section III confirms the expected: the higher the temperature, the fewer available HTSMA systems. At temperatures in the 100–300°C range, several alloy systems show useful shape memory behaviour, such as Ti–Ni–Pd, Ti–Ni–Pt, Ni–Ti–Hf, Ni–Ti–Zr and Cu–Al–Mn–Ni. Other alloy systems face one or more significant problems that require further work. Some alloys also show high temperature superelasticity, such as in the Cu–Al–Mn–Ni and Co–Ni–Ga/Al, but these are much rarer compared to the number of alloys showing high temperature shape memory effect. Temperatures No prospective HTSMAs with transformation temperatures greater than 300°C have yet shown satisfactory load-biased shape memory behaviour or superelasticity.

A summary of transformation temperatures, crystal structures, and other remarks on HTSMA systems is provided in Table 2. Table 3 is a collection of individual alloys that show either high temperature shape memory effect or superelasticity, and include transformation temperatures, shape memory or superelastic properties, work output, tensile ductility, thermal hysteresis, maximum operational temperature due to creep, oxidation, or phase decomposition, and the processing condition of the alloy described. Perhaps one of the most informative pieces of information provided by Table 3 is what it does not provide; many fields for many alloys are empty as no thermomechanical experiments have been conducted to determine these properties. This highlights the need for experimental data on HTSMAs in general.

Figure 61 graphically summarizes the transformation temperatures and shape memory properties of the various alloy systems. On the left side of the figure,

Table 2 Potential HTSMA alloy systems and their characteristics

System	Transformation temperature range, °C	Transformation phases	Comments
Ti–Ni–Pd	100–530	B2 (bcc)–B19 (orthorhombic) >10%Pd	High work output, large recoverable shape memory strain, most commercial ready
		B2 (bcc)–B19' (monoclinic) <10%Pd	High materials cost, irrecoverable strain difficult to eliminate in load bias tests
Ti–Ni–Pt	100–1100	B2 (bcc) – B19 (orthorhombic) >10%Pt	High work output, full recovery possible in load bias tests, good environmental resistance
		B2 (bcc)–B19' (monoclinic) <10%Pt	Very high materials cost
Ni–Ti–Hf	100–400+	B2 (bcc) — B19' (monoclinic) <15%Hf	Reasonable shape memory behaviour, relatively low materials cost
		B2 (bcc)–B19 (orthorhombic) >20%Hf	Large hysteresis, formability difficulty
Ni–Ti–Zr	100–250+	B2 (bcc)–B19' (monoclinic) <15%Zr	Relatively low materials cost
		B2 (bcc)–B19 (orthorhombic) >20%Zr	Stable phase precipitation, large change in transformation temperatures during cycling
Cu–Al–Ni	100–400	β (bcc-$L2_1$)–α' (9R orthorhombic) <11%Al	Low cost, reasonable shape memory and pseudoelastic behaviour
		β (bcc-$L2_1$)–18R orthorhombic 11–13%Al	Brittle in tension
		β (bcc-$L2_1$)–γ' (2H tetragonal) >13%Al	Stable phase precipitation near 200°C, reordering causes shift in transformation temperature in quenched specimen
Cu–Al–Nb/Ag	100–400	β (bcc-$L2_1$)–α' (9R orthorhombic) <11%Al	Good workability
		β (bcc-$L2_1$)–18R orthorhombic 11–13%Al	Poor shape memory response
		β (bcc-$L2_1$)–γ' (2H tetragonal) >13%Al	
Co–Al	100–400	γ (fcc)–ε (hcp)	Good workability
			Non-thermoelastic, large hysteresis
Co–Ni–Al/Ga		B2 (bcc)–γ ($L1_0$ non-modulated)	High temperature pseudoelasticity, very high yield strength
			Poor tensile ductility
Ni–Al	100–300	B2 (bcc)–β' (3R L10 bct) <37%Al	Low materials cost, low hysteresis
		B2 (bcc)–7R (L10 bct) >37%Al	Very poor ductility and shape memory response, stable phase precipitation from martensite near 250C
Ni–Mn	100–670	B2 (bcc)–θ ($L1_0$ tetragonal)	Ternary alloy allows for low hysteresis and improved shape memory response
			Poor tensile ductility, loss of shape memory effect above 400°C
Ni–Mn–Ga	100–400	$L2_1$–2M (tetragonal)	Very poor tensile ductility
Zr–Cu	100–600	B2 (bcc)–B19 (orthorhombic)	Good ductility
		B2 (bcc)–Cm (orthorhombic)	Poor shape memory response, large hysteresis
Ti–Nb	100–200	β (bcc)–α'' (orthorhombic)	Excellent ductility and workability
			Precipitation of omega at 300°C
U–Nb	100–200	γ (bcc)–γ0 (tetragonal) >15·4%Nb	Good ductility, good shape memory response, large transformation strain
		γ (bcc)–α'' (tetragonal) <15·4%Nb	Suspect to oxidation, contains uranium
Ti–Au	100–630	B2 (bcc)–B19 (orthorhombic)	High materials cost
Ti–Pd	100–510	B2 (bcc)–B19 (orthorhombic)	Good ductility
			Recovery occurs at transformation temperature, high materials cost
Ti–Pt–Ir	990–1184	B2 (bcc)–B19 (orthorhombic)	Very high yield strength
Ta–Ru	900–1150	β (bcc)–β'' (monoclinic)	Small hysteresis, stable microstructurally
			Poor oxidation resistance
Nb–Ru	425–900	β (bcc)–β'' (monoclinic)	Small hysteresis, stable microstructurally
			Poor oxidation resistance

Table 3 Individual HTSMAs and their properties.

Alloy, at-%	Transformation temperature range, °C	Shape memory characteristics	Pseudoelastic characteristics	Max known work output, J cm^{-3}	Tensile ductility	Thermal hysteresis, °C	Maximum operational temperature, °C	Best known processing condition
$Ti_{50}Ni_{20}Pd_{30}$ (Refs. 71, 75 and 81)	215–269	(Tension, 170°C) 5·4% strain 100% recovery	(Tension, 262°C) 4% strain 90% recovery	8–11	(170°C) 6%+	25·7	550	Cold work+heat treat 400°C 1 h+training
$Ti_{50}Ni_{30}Pd_{20}$ (Refs. 73, 147 and 340)	232–297	(Tension, thermal cycle 10–380°C) 2·6% strain 100% recovery		9	(220°C) 3·4%	20	500	Cold work+heat treat 440°C 1 h
$Ti_{36}Ni_{49}Hf_{15}$ (Refs. 118, 120, 121, 133 and 137)	148–231	(Tension, 80°C or bending, 100°C) 3% strain 100% recovery			(25°C) 7%	60		Aging 20 h at 700°C
$Ti_{34·9}Ni_{49·8}Zr_{15·3}$ (Refs. 123, 125, 138 and 139)	139–222	(Bending, 25°C) 1·8% strain at external fibre 100% recovery		16·8 (thin film)	5–7%	54		Solution treated
$Cu_{80}Al_{11·9}Ni_5Mn_2Ti_1$ (wt-%) (Ref. 182)	133–193	(Tension, 155°C) 3% strain 80% recovery			(25°C) 4%	21·5	200	Solution treated
$Cu_{70·96}Al_{12}Ni_4Mn_4B_{0·04}$ (wt-%) (Ref. 180)	41–96		(Tension, 200°C) 5% strain 90% recovery		(150°C) 5·5%			Aged 300°C 30 min
$Co_{86}Al_{14}$ (Ref. 200)	134–283	(Bending, 25°C) 2% strain at external fibre 90% recovery			High	121		Cold work+heat treatment 600°C 1 h
$Co_{37·6}Ni_{32·9}Al_{29·5}$ (Ref. 206)	–57–(–26)		(Compression, 170°C) 5% strain 100% recovery		Poor	15·5		Solution treated
$Ni_{42·5}Mn_{50}Ti_{7·5}$ (Ref. 234)	200–240	(Torsion bending, thermal cycle 160–280°C) 3·9% strain 90% recovery			Poor	20	400	Solution treated
$Ni_{54}Mn_{25}Ga_{21}$ (Refs. 248, 249, 250 and 262)	231–335	(Compression, 25°C) 10% strain 70% recovery			Very poor	85		Solution treated
$Ti_{68}Ta_{32}$ (Ref. 284)	Room temperature–205	(Tension, thermal cycle –100–260°C) 2% strain 95% recovery		~4	Excellent	40	260	98% cold roll+heat treatment 900°C 30 min
$Zr_{42·3}Cu_{29·9}Ni_{11}Co_{10·2}Ti_{6·6}$ (Refs. 276 and 277)	67–247	(Compression, 177°C) 8% strain 44% recovery				70	400	Solution treated
$U_{86}Nb_{14}$ (Refs. 290 and 291)	77–212	(Tension, 25°C) 7% strain 97% recovery			(25°C) 17%	35		Solution treated
$Ti_{50}Pd_{50}$ (Ref. 74)	539–591	(Tension, 25°C) 10% strain 88% recovery			Good	40	500	Solution treated
$Ti_{50}Au_{50}$ (Ref. 295)	575–650	(Tension, 25°C) 3% strain 100% recovery				35		Solution treated
$Ti_{50}Pt_{25}Ir_{25}$ (Refs. 307 and 308)	1068–1190		(Compression, 1200°C) 10% strain 40% recovery			66·5		Solution treated
$Ru_{50}Ta_{50}$ (Ref. 315)	1040–1070	(Compression, 900°C) 4% strain 50% recovery			Poor	20		Solution treated
$Ru_{50}Nb_{50}$ (Refs. 310 and 312)	869–919	(Bending, 800°C) 4·2% strain 88% recovery			Poor	20		Solution treated

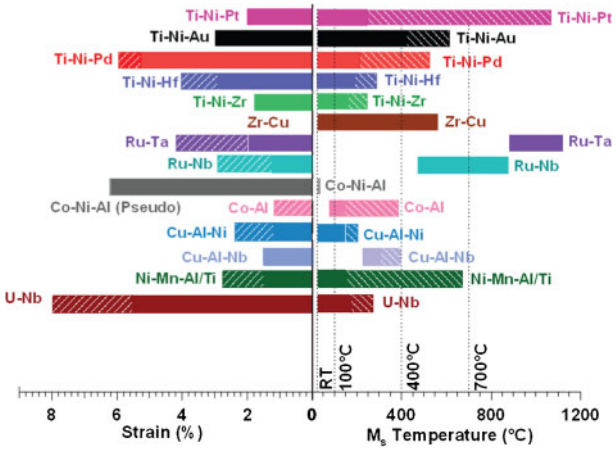

61 A comparison of transformation temperatures, and shape memory strains for all reported HTSMAs. See text for details

solid bars indicate the highest level of ε_{rec} possible in the alloy system while still achieving recovery rate of 100%. Moreover, the slashed bar extends to the ε_{rec} level where at least a recovery rate of 85% can be obtained. On the right side, solid bars extend to M_s of the composition showing the best shape memory properties, while the slashed bars extend to the maximum possible M_s for the alloy system.

IV. Potential applications of HTSMAs

There are a large number of applications that involve the use of SMAs outside of the biomedical field.[318,319] Many of these applications and devices, which currently use commercial Ni–Ti and Cu based SMAs, can be retrofitted with a HTSMA to deliver similar results but in a different temperature regime. However, the focus of this section is on the many unique applications that depend on the successful commercialisation of HTSMAs.

Most of the prospective high temperature applications are based on the use of SMAs as solid state actuators. Because SMAs can respond to a temperature change (stimulus) with a mechanical strain (response), it is easy to envision how shape memory materials can be viewed as a solid state motor or actuator. In fact as shown in Fig. 62, SMA elements have a higher energy density than pneumatic actuators or DC motors and are equivalent in performance to hydraulic actuators while weighing significantly less and maintaining a much more compact footprint.[320,321] Actuators of SMA also produce a large stroke in relation to their weight compared to other systems such as thermostat metals (bimetallics), magnetic solenoids and wax actuators.[322] Another advantage of SMA solid state actuators compared to hydraulic, pneumatic, and motor driven systems is the reduction in total part count, ease of inspection, and overall reduction in inspection requirements. Shape memory actuators also are frictionless, quiet, and result in a clean smooth motion. These advantages all equate to lower aftermarket costs for equipment inspection and maintenance. Finally, the compact nature and reduced weight of SMA actuators compared to non-solid state systems is a major benefit and often the enabling factor in many applications, especially aerospace related.

In general, one way shape memory effect is used for SMA actuators with a bias, or restoring force to provide

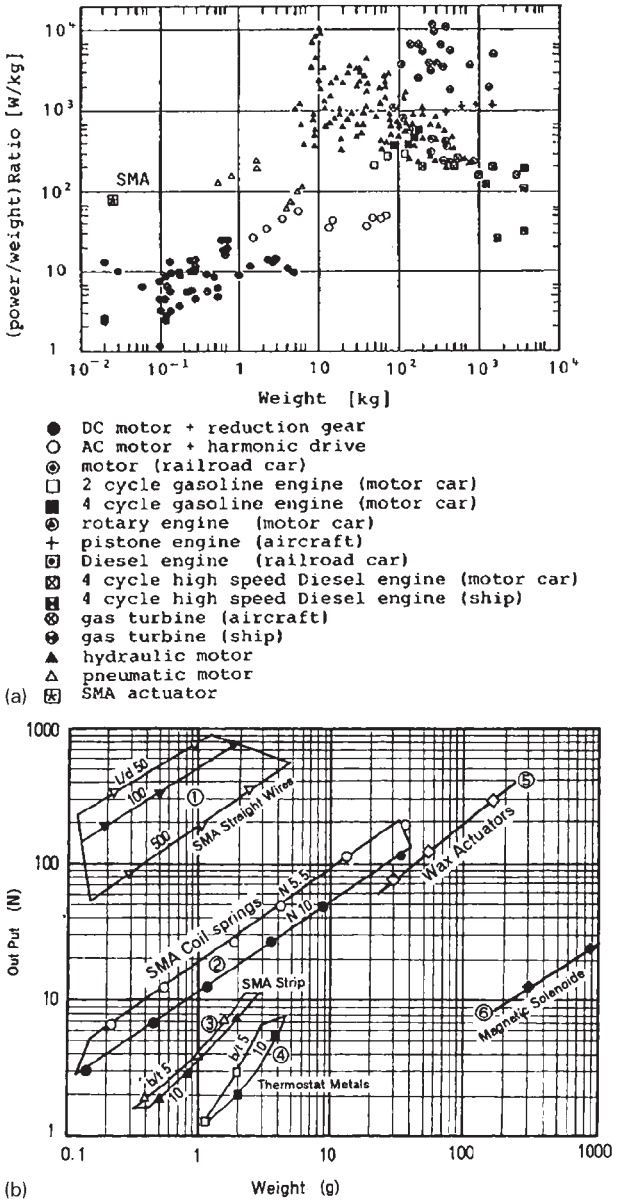

62 Actuation properties of SMAs as compared to *a* conventional actuation systems[320] and *b* other solid state actuator materials. For wires, *L*/*d* refers to the ratio between length and diameter. For spring coils, *N* is the number of active windings in the coil, and for strips, *b*/*t* is the ratio between width and thickness.[322] Reproduced with permission from *a* the Robotics Society of Japan, and *b* Cambridge University Press

the alloy with a pseudo two way effect. The restoring force can manifest itself in several forms such as bias springs, constraining substrates in thin films, pressure differentials, the use of opposing actuators, and often times the system itself. One of the most important criteria for actuator applications is work output. Noebe *et al.*,[84,104] and Kohl *et al.*[323] have found that work output of many Ti–Ni–Pd and Ti–Ni–Pt HTSMAs are comparable to that of binary Ni–Ti, which has among the highest work output to weight ratios of all available actuator materials.[319,321] A small thermal hysteresis is also critical to many actuator applications, especially where actuator response time and frequency are important, since materials with large thermal hysteresis require longer reheat and response times.[84,324]

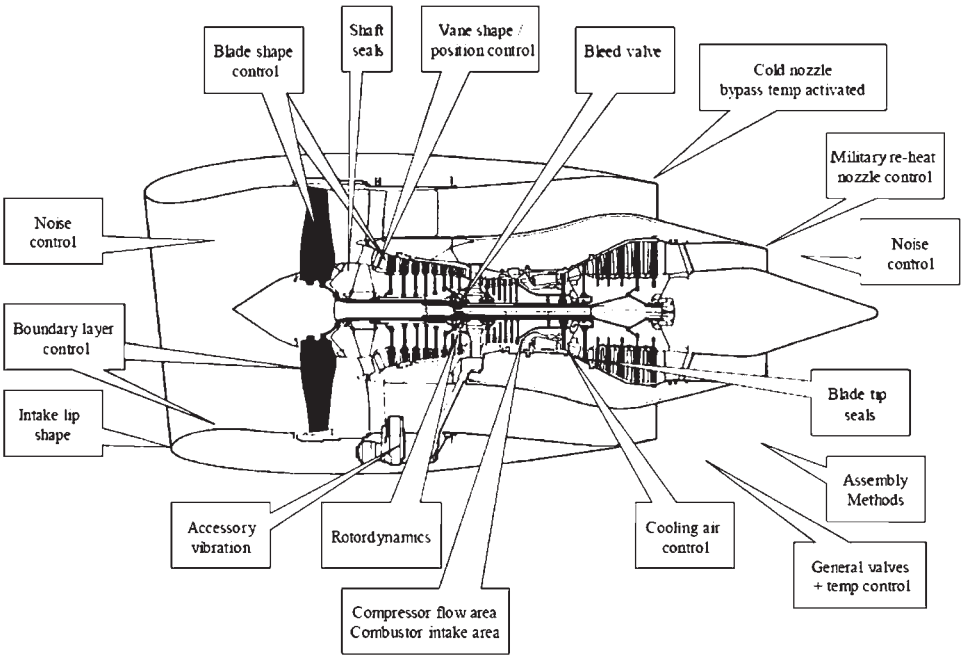

63 Identified opportunities for HTSMA use in a gas turbine.[325] Reproduced with permission from the SPIE

The resurgence in commercial HTSMA activity has been driven primarily by the needs of the aerospace industry. In fact, the development of commercial HTSMAs would represent an enabling technology, allowing designers to meet future aircraft efficiency, emissions, and noise goals through the development of adaptive structures. Figure 63 shows potential components of an aircraft gas turbine engine that may benefit from SMA actuators.[325] For example, noise reduction during aircraft takeoff has become a major focus of new engine technologies to meet strict noise ordinances within communities. To this end, chevrons have been shown to be quite effective in reducing noise during takeoff by causing mixing of the free, fan and primary exhaust streams, thereby reducing the acoustic energy at the back of the engine. While this is beneficial for noise reduction during take off, the effect of the chevron nozzle in the exhaust stream is detrimental to fuel efficiency during cruise.[326] Therefore, a variable geometry or adaptive chevron is needed for maximum benefit during each phase of the flight envelope. The Boeing Company has recently flight tested a variable geometry fan chevron on a 777-300ER with GE-115B engines, demonstrating the utility of binary NiTi alloys to provide in flight aerostructure morphing capability[327,328] (Fig. 64). While the temperature requirements of this particular fan chevron application permits the use of commercial Ni–Ti, low bypass engines would benefit more by having chevrons attached to the core exhaust, where temperatures reach several hundred degrees centigrade, requiring the use of HTSMAs. While HTSMA technology is not as nearly mature as binary NiTi alloys, a Ti–Ni–20Pt alloy with transformation temperatures near 300°C was successfully used to actuate a core exhaust chevron in a coaxial fan/core flow test rig with a core temperature of 100°C,[329] demonstrating the capability of high temperature Ti–Ni–Pt alloys to act as solid state actuators.

High temperature SMAs would also have an enabling impact on the development of variable area or variable geometry inlets and other adaptive aerostructures for supersonic business jets or military aircraft. Ideally, adaptive inlets would be capable of transforming from a geometry optimised for low speed flight to another that optimises performance during supersonic cruise. Hydraulic systems, while effective in performing the needed shape changes, are generally too bulky and heavy for such an application, especially in smaller aircraft. Furthermore, new high temperature materials are needed for this application since aerodynamic heating would increase the temperature of the inlet beyond the capability of conventional SMAs. Inlet designs incorporating HTSMAs are currently being developed and an initial demonstration of a NiTi–20Pt actuated ramp in a supersonic wind tunnel up to speeds of Mach 1·0 was successfully completed, again demonstrating the viability of Ti–Ni–Pt HTSMAs.[330]

Development of a novel Ti–Ni–Pd–Pt HTSMA with operating temperature capability of 250°C and its processing into wire form has allowed investigators at NASA to demonstrate the ability of such alloys to be used as the motive force in compact, lightweight, high force actuation systems.[95] Bench top testing indicated that a Ti–Ni–Pd–Pt based actuator system was more than capable of meeting the force requirements and actuation time needed for use in a surge control mechanism while being the only type of actuator capable of meeting the temperature and space requirements for use in the centrifugal compressor of current T-700 helicopter engines.[95] Additional research on Ti–Ni–Pd–Pt springs indicated that a further reduction in actuator size could be achieved while still meeting minimum operating requirements for this particular application when the wire actuator was replaced by an HTSMA spring of the same material.[331]

In several other specific applications, the use of HTSMAs has not been specifically demonstrated, but significant effort has been spent developing and understanding SMA activated structures. For example, SMAs are also being considered in designs for a variable area fan nozzle due to the benefits in thrust specific fuel

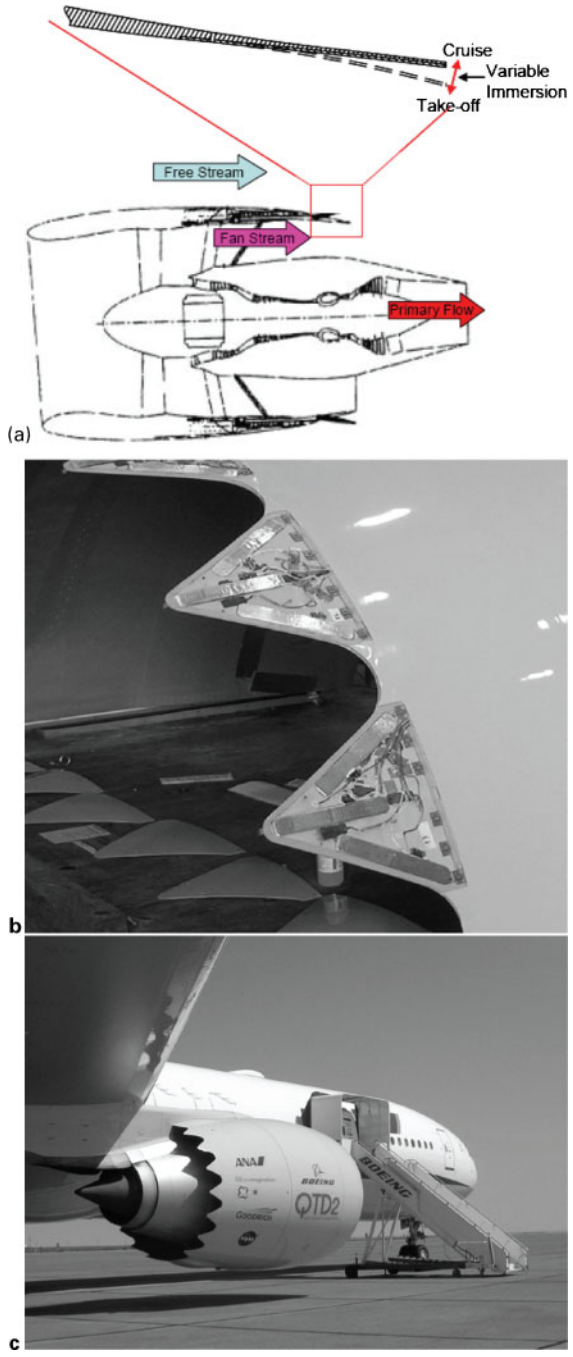

64 **Boeing's SMA actuated variable geometry chevron for active or passive noise reduction. *a* Illustrates the desired configurations of the chevron exhaust nozzle, *b* SMA bending actuators control the deflection of the chevron and *c* flight testing of the variable geometry chevron nozzle.[328] Reproduced with permission from the SPIE**

consumption[332] (Fig. 65) and potential benefits in noise reduction during takeoff.[333] Again the advantages of using SMA technology are the light weight and low complexity compared to conventional actuator systems making SMA an enabling technology, though conventional alloys can probably be used for fan nozzle applications. However, HTSMAs are being considered for related applications such as variable area and variable geometry exhaust nozzles, where the temperature requirements are much more severe. The application of

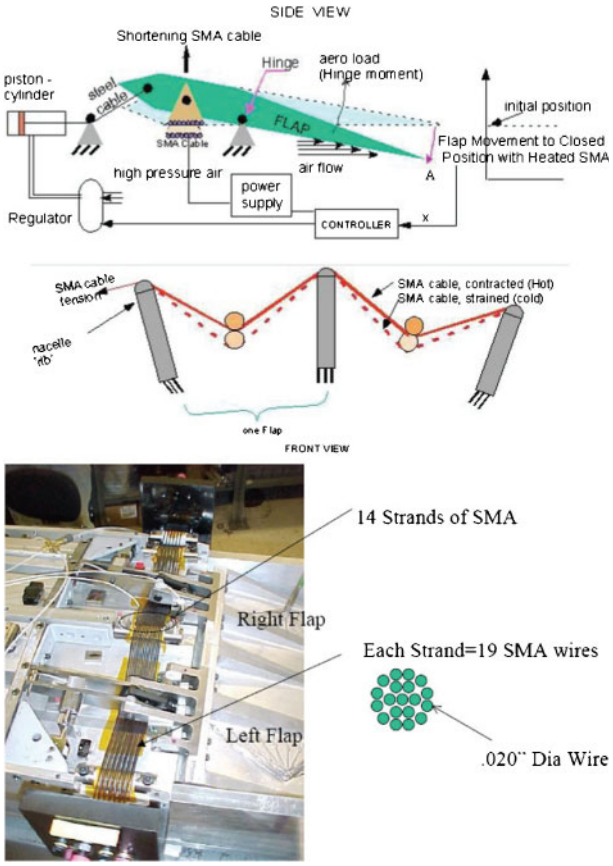

65 **Variable geometry nozzle flap design. A system of SMA wires are used to control the configuration of the flap.[332] Reproduced with permission from the SPIE**

HTSMAs is also being considered for use in clearance control in the compressor and turbine sections of aircraft engines as shown in Fig. 66. During engine start-up, the blades elongate due to centrifugal force and the casing must allow for proper clearance to avoid contact, otherwise the blade tips will wear away. Then as the case warms up, thermal expansion of the materials causes radial expansion of the case and tip clearance increases, decreasing the efficiency of the engine. Development of

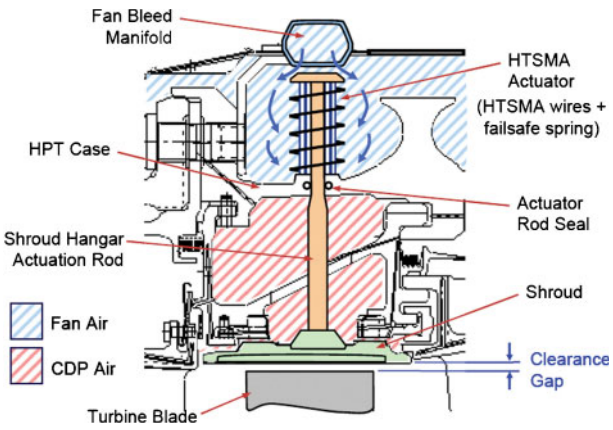

66 **High temperature SMA active clearance control concept for the high pressure turbine section of aircraft engines. The HTSMA linear actuators work against a bias spring to control the clearance gap.[334] Reproduced with permission from the SPIE**

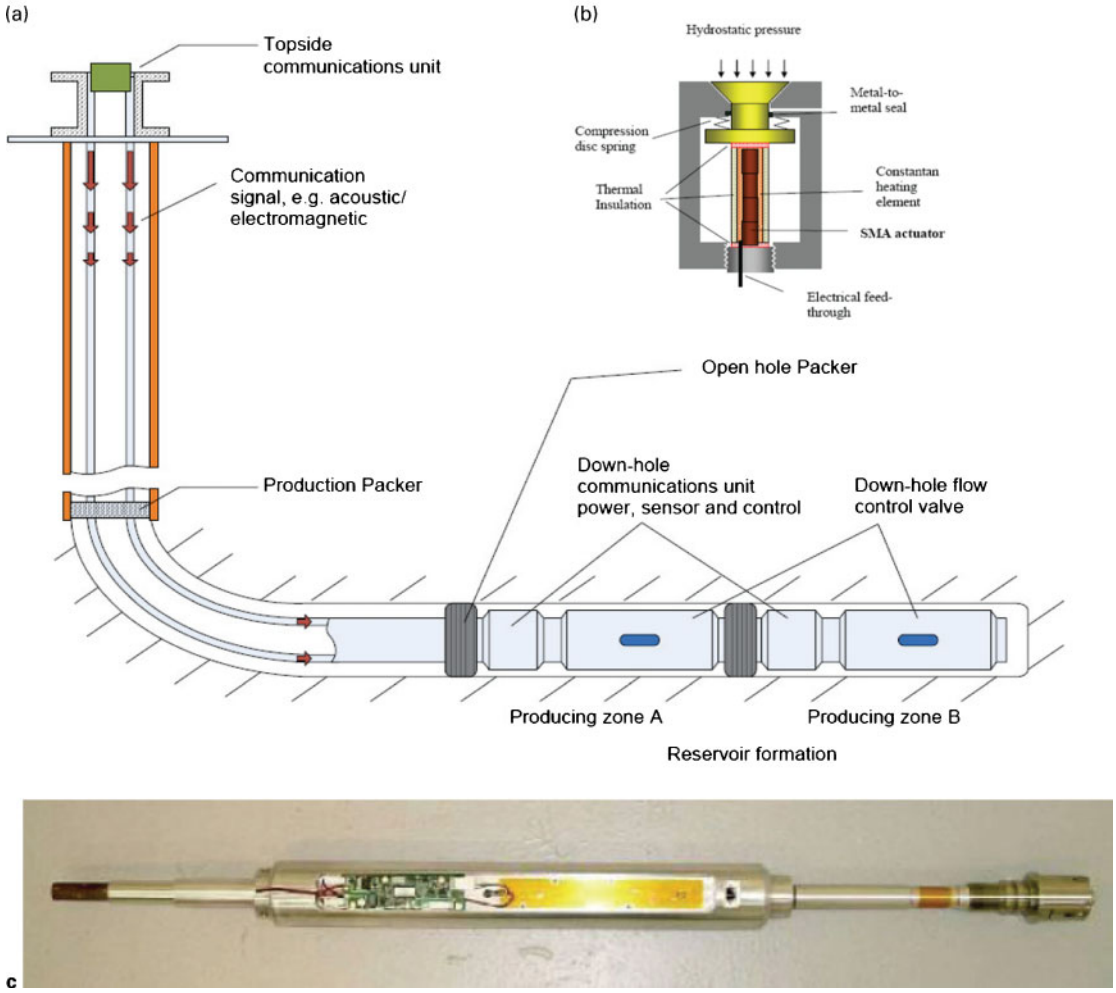

67 Shape memory actuators for down well petroleum exploration applications. *a* SMA actuators are used as a part of the 'Smart Well' system that uses various remotely controlled actuators to achieve control of flow rates in various down well production zones. SMA is advantageous over traditional hydraulic systems because it can be easily controlled remotely and require less power. *b* Illustrates an SMA based trigger valve for flow control and *c* the complete SMA valve assembly including electronics, power, and communications.[339] Reproduced with permission from the SPIE

numerical models describing the behaviour of Ti–Ni–Pt HTSMAs[334] and their incorporation into system level trade studies[335] indicate that these HTSMAs are viable candidates for actuation of systems that would allow for radial contraction of the case upon engine warming, thus increasing engine efficiency.

Other aviation and space applications have been proposed for HTSMAs such as actuators for deployment of space structures in satellites, deployable shields and screens to protect space structures from debris, washer type seals for booster ring segments of rockets, and release mechanisms during rocket launch,[336] all of which require high transformation temperatures. Many potential uses for HTSMAs have also been proposed for under the hood applications in automobiles for fuel management and engine control purposes.[337] A more recent but growing area of interest for HTSMAs is in energy exploration for down hole oil and gas applications such as flow control valves,[338,339] safety valves and other compact actuators (Fig. 67). The advantage of HTSMAs in energy exploration is the simplicity and durability of SMAs and their ability to work in harsh corrosive environments that include high temperatures and pressures.

In MEMS applications, strict dimensional limits often make SMA actuation one of the very few viable options in a device. For example, Liu *et al.*[340] used a magnetron sputtered Ti–Ni–Pd thin films with M_s of 150°C in a micro valve, as seen in Fig. 68. The valve was actuated by resistance heating and was capable of operating at temperatures up to 120°C. The shape memory valve could supply up to 75 μN of actuation force, and was able to stop the flow of 70 kPa gas pressure with less than 0·1% leakage. Also, due to the high cooling rates through the thin film, a minimum response time of 22 μs or maximum actuation frequency of 30 Hz was obtained. Compared to binary Ni–Ti microvalves of the same design, a greater amount of power was required for operation, but faster response time was possible with Ti–Ni–Pd valves.[340]

A unique application that takes advantage of the superelastic properties of HTSMA thin films is a strain gage for a pressure transducer, recently developed by Orbital Research, Inc.[341] This pressure transducer was developed for diesel and jet turbine engine applications and uses a Ti–Ni–Pd or Ti–Ni–Pt thin film strain gauge deposited on a silicon substrate to measure pressure pulses at high temperatures. These HTSMA based

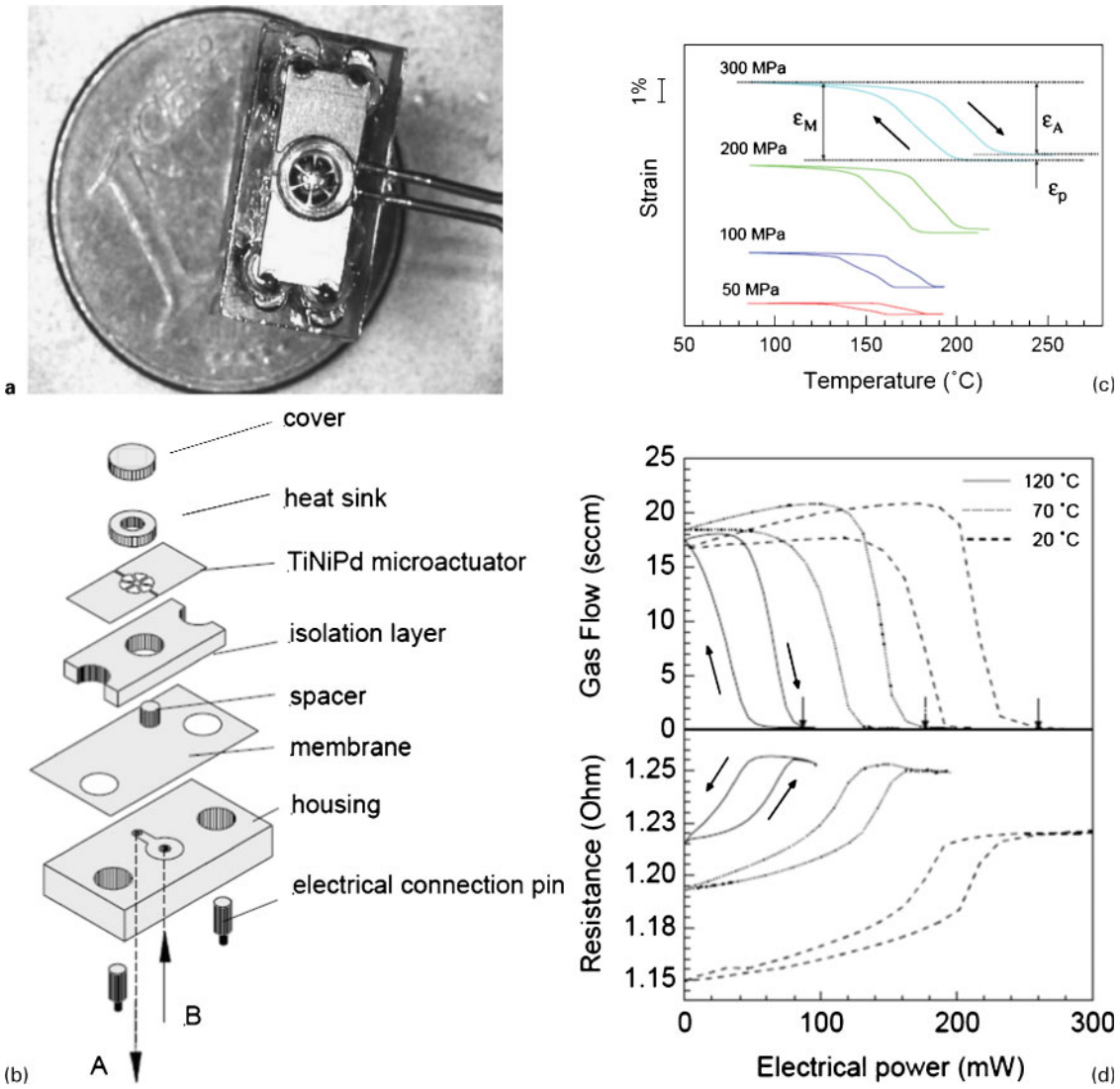

68 Illustration of a $Ti_{50}Ni_{30}Pd_{20}$ thin film microvalve. *a* Size of the completed assembly, *b* exploded view of the microvalve, *c* shape memory response of the thin film under constant stress heating cooling experiments, maximum ε_{rec} of ~3·2% can be achieved under 200–300 MPa and *d* performance of the actuator for gas flow at a fixed pressure difference of 70 kPa (Ref. 340). Reproduced with permission from Elsevier

pressure transducers have a 6 to 10 times sensitivity improvement over standard metal thin film gages, coupled with high frequency response (60–80 kHz) and high operating temperature. The reason for the high frequency response is that the operation of the sensor is not based on the thermal transformation of martensite to austenite (as in actuators) but is based instead on the resistance change in the material when the austenite is transformed to martensite through a stress induced transformation. In other words, the sensor is relying on the superelastic properties of the material in order to achieve both good resolution and fast response time as a sensor. Consequently, the sensor employs a heating unit to keep the alloy within the A_f to M_d (temperature above which stress induced martensitic transformation is no longer possible) temperature range, enabling the pressure variations to induce martensite. Since the martensite phase has significantly different electrical properties than austenite, variances between the two can be calibrated back to the external pressure. These sensors can be used in diesel engines replacing existing in cylinder pressure transducers and next generation transducers are being developed for aeroturbine engines to control combustion to increase fuel efficiency, and reduce emissions and screech.

Finally, bulk HTSMAs have found use in non-shape memory functions. For example, titanium metal matrix composites have been reinforced with Ti–Ni–Pd–W 'fibres' to produce multifunctional material with high yield stress at high temperatures (>200°C).[342] Shape memory alloys also exhibit good damping capabilities due to the energy absorption of the twinned martensitic structure, which is attributed to the high mobility of the martensite interfaces including twin variant interfaces and twin planes.[343] This leads to several other potential aerospace applications including the use of SMAs in:

(i) acoustic liners to dampen acoustic energy from the aircraft engine
(ii) self-damping components or connectors in mechanical systems, such as fuel line clamps, to help reduce fatigue damage
(iii) flutter control or damping of fan blades.[344]

These are just a few of the more extensively investigated applications for HTSMAs. The potential applications for

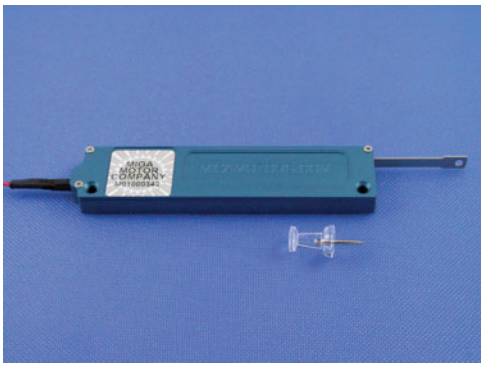

69 Example of a prototype linear HTSMA based actuator developed by MIGA Motors, capable of up to 22·2 N force and 6·35 mm deflection using TiNi–30Pd wire so it can operate safely in environments up 200°C (Ref. 345)

these systems exceed the current realm of conventional actuation to include such areas as vibration control, coupling, and sensors. The limiting factor restricting the application of HTSMAs at the moment is commercial availability of the alloys in any form but particularly in forms that are appropriate for various applications such as wire. Otherwise commercial HTSMA based actuators would be fairly common place as several manufacturers have already developed the capability to package HTSMAs in compact actuator systems and sell them in limited quantities as wire becomes available (Fig. 69).[345]

V. Summary: remaining challenges of HTSMAs

As seen in this review, the transformation temperatures for most common SMA systems are relatively well known along with the basic mechanisms for manipulating the transformation temperatures through compositional control, heat treatment, and thermomechanical processing. Of course, the functional capability of HTSMAs clearly depends on much more than simply a high transformation temperature. In addition to the intricate microstructural and thermomechanical issues associated with shape memory and superelastic behaviours, HTSMAs face similar challenges to those of traditional high temperature structural alloys. The abundance of thermal energy at higher temperatures promotes many rate dependent processes that are otherwise inactive at room temperature, and creates a series of tough challenges related to thermal and microstructural stability, deformation and creep resistance, recovery and recrystallisation, and environmental resistance.

The ease of dislocation motion brought about by the reduction in σ_y for both austenite and martensite at high temperatures is a significant issue. For materials with transformation temperatures in the range of 150–200°C such as Ti–Ni–Pd, the decline in σ_y with rising temperature is not notably large enough to cause catastrophic deterioration of shape memory properties. However, at temperatures above ~350°C, σ_y of austenite can decrease to values below that required for σ_{SIM} in most alloys, severely impacting superelastic behaviour and the isobaric strain temperature response of the material negatively, limiting its work capability and usefulness as a solid state actuator.[98] At intermediate temperatures, deformation near M_s produces better shape memory behaviour in some alloys than when the same material is deformed at room temperature due to a minimum in the σ_{DT} at M_s.[71,75,120] However, for SMAs designed to be used at much higher temperatures, above ~400°C, σ_y is often reduced to very low values, and shape memory behaviour becomes poor due to plastic accommodation of the phase transformation and operation of diffusional mechanisms.[74] As for the superelastic behaviour, higher test temperatures are accompanied by both reduction in σ_y and increase in σ_{SIM}. This is a detrimental combination and is the main reason that although superelasticity is ubiquitous at room temperature, very few materials show useful superelastic behaviour at higher temperatures. Not surprisingly, alloys that do show high temperature superelasticity all have very high yield strengths.

Most alloys also depend on non-equilibrium phases for their shape memory properties, and a tendency for equilibrium phase formation or precipitation at higher temperatures can be devastating to shape memory and superelastic behaviour. The equilibrium phases that precipitate during aging do not transform in most cases, and are usually either highly brittle, which causes loss of ductility, or highly plastic, which impairs recoverability. Oftentimes, the effective 'lifetime' and operating temperatures of many alloys are governed by the kinetics of second phase formation. For example, in Cu–Al–Ni alloys, the kinetics of equilibrium phase formation is slow even above A_f (~200°C), and several months are required for precipitation to occur. However, in Ni–Al alloys, the equilibrium phase forms almost instantly at temperatures below A_s (250–350°C), rendering shape memory recovery almost impossible.[2,178,222–225] On the other hand, some precipitates, if small enough, can be useful in improving shape memory behaviour by suppressing dislocation slip and enhancing creep resistance. Yet there is an insufficient number of studies on HTSMAs focusing on the beneficial precipitates, such as Ni_4Ti_3 precipitates in binary NiTi SMAs, to assess their affect on shape memory behavior in HTSMAs. Without a doubt, this is one area which requires urgent attention for accelerated inclusion of HTSMAs in applications.

Cyclic and thermal instabilities are not limited to HTSMAs but are quite commonplace in ordinary SMAs as well. Changes in shape memory behaviour during cycling are largely caused by the formation and evolution of dislocation structures and retained martensite, and are evident from changes in transformation temperatures during thermal cycling experiments both under stressed and stress free conditions. These changes stabilise in most alloys after 20–30 cycles, so that prior thermal cycling can be used to produce stable materials. Thermal instabilities refer to time dependent isothermal processes where samples are aged for long periods of time. These processes are diffusion driven and occur readily in many HTSMAs in the range of their transformation temperatures. Aging in a phase will stabilise it (i.e. aging above A_f will stabilise austenite), and manifests itself as a change in transformation temperature where martensite aging will increase A_s and A_f, while austenite aging will decrease M_s and M_f.

One explanation involves variations in vacancy concentration and the degree of long range order with aging time. Most alloys that were found to display this behaviour were water quenched resulting in large

amounts of quenched-in vacancies and a partially ordered to disordered state. During subsequent aging, the vacancy concentration decreases and ordering is gradually restored. The change in transformation temperatures between the ordered and disordered states can be quite large, such as up to 100°C differences were found in Cu–Al–Ni alloys.[2] In addition, mechanisms based on short range ordering of point defects, explained by the SC-SRO model provides a general description for martensite and austenite stabilisation, as discussed in Section II.2·2.

Recovery and recrystallisation are other issues in alloys with higher transformation temperatures. The activation of these mechanisms during basic operation of HTSMAs limits the opportunity to use thermomechanical treatments such as cold working to improve shape memory properties. Furthermore, creep begins to be a factor at temperatures where recovery and recrystallisation starts. Although available creep studies on HTSMAs are very limited, it would appear that if applied stress levels are high (>100 MPa), creep begins to be a serious concern even at temperatures around 400°C.[99] Furthermore, metals such as titanium are known to undergo creep and viscoelastic behaviour[346] even at room temperature. The kinetics are relatively slow, but the effects may be magnified if alloys are heated to slightly higher temperatures and dimensional requirements can be compromised as a result. Creep kinetics differs in different alloy systems, and no such studies have been performed on any alloy systems other than Ti–Ni–Pd.[99]

At the opposite extreme, many HTSMAs are limited by lack of plasticity or ductility in the polycrystalline state. In many alloy systems, such as Ni–Al, Ni–Mn–Ga and Co–Ni–Al/Ga, polycrystalline materials are reported to be so brittle in tension that experiments were performed almost exclusively in compression. Most other alloys also suffer from poor ductility with most exhibiting less than 5% elongation to failure at room temperature. This is a consequence of the ordered nature of intermetallics and lack of sufficient number of deformation systems, but several solutions exist. Boron additions in Ti–Ni–Pd,[77] have been marginally effective in increasing both ductility and tensile strength but the directly responsible mechanism was probably grain size refinement, which was due to the boron addition. Similar improvements have also been found in thin film studies of many alloys through grain refinement, which can be obtained in bulk alloys primarily through cold working or severe plastic deformation. Further research into these techniques could be quite beneficial, but fine grain sizes are usually metastable and will readily coarsen at moderately elevated temperatures. Alloying is also a powerful solution to the ductility problem, which can both improve the inherent ductility of the alloy and encourage the formation of more ductile second phases. However, this is almost always accompanied by equally powerful side effects including changes in transformation temperatures and/or deterioration of shape memory or superelastic effects.

For the most part, the environmental resistance of HTSMAs also has not been considered. Ni–Ti and other Ti based alloys have reasonable oxidation resistance up to ~600°C, placing an upper limit on the possible use of these alloys. The oxidation resistance of Ti–Ni–Pt appears to be better than binary Ni–Ti.[107] Ni–Ti–Ht has similar oxidation resistance to Ni–Ti, but the oxidation resistance of Ni–Ti–Zr and Zr–Cu–Co–Ni based alloys are much worse.[213] The Ru–Nb and Ru–Ta alloys have essentially no environmental resistance at temperatures where the martensitic transformation is observed, and have to be characterised and ultimately used only in vacuum. Other alloys such as those based on Ni–Al, however, would exhibit adequate environmental resistance up to at least 1000°C, but unfortunately suffer from other more serious problems such as thermal stability and ductility.

The raw material costs of many HTSMAs are very high, especially those containing precious metals. Unfortunately, Ti–Ni–Pd, which is the most mature and 'commercial ready' system is one of the most expensive due to the large amounts of palladium (~30 at-%) required. The high material cost can often be offset to a certain degree by the reduction in design and fabrication complexity offered by HTSMAs. However, processing also contributes to the overall cost of the material, and alloys such as Ni–Al are very difficult to process and can lead to very high overall cost despite very low costs of the raw materials.[136]

As with all materials, the issue of fabrication and processing must also be addressed. Given the often steep dependence of transformation temperatures to alloying additions and overall stoichiometry, compositional control during melting is a challenge. Of course each heat of material could be tested for actual transformation (use) temperatures, as is the practice with commercial Ni–Ti alloys, but this would be a prohibitively costly option with the precious metal containing alloys. Limited ductility in some of these high temperature systems also makes thermomechanical processing an ordeal, which is a concern since one of the most common forms that these HTSMAs would be used is wire form.

Finally, it should be obvious that our knowledge of HTSMAs is far from complete. In many alloy systems, optimisation efforts through work hardening and grain refinement are completely absent, effects of precipitation hardening are not clearly reported, and well structured alloy development and microalloying are almost nonexistent. Furthermore, compounding the lack of information on these systems in general are differences in the experimental approach and reporting style of various research groups. Oftentimes, tests for shape memory behaviour are conducted exclusively in tension in one system and in bending in another. Considering the effect of crystallographic texture and stress state on transformation strains,[184] it often does not make complete sense to compare reported recovery levels and transformation strains. Recovery is reported in total recovery ε_{rec} by some authors, while others report only specific strain components such as ε_{sme} or ε_{SE}. Compositions and processing procedures are almost never consistent and unfortunately even minor differences in testing procedures can mask the original effects being studied.[98] These inconsistencies provide tremendous difficulties in comparing the limited data from the same system let alone the cross-comparison of different alloy systems. Thus, there is definitely an urgent need for the development of testing standards, not only for HTSMAs, but indeed for all SMAs to circumvent future inconsistencies.

VI. Concluding remarks

From the present survey of available HTSMAs, summarised in Table 2 and 3 and Fig. 61, it is apparent

that a number of potential alloy systems are available for use in the 100–400°C range but very limited options are possible at higher temperatures. For actuator applications, it would have been more useful to compare work output or at least transformation strain at a given stress level during thermal cycling, however, these critical properties have only been determined for a limited number of the Ni–Ti based alloys. Furthermore, there is little relation between the stress free shape memory response and the work characteristics of an SMA 104 (this reference needs to be superscripted) so Figure 61 would provide little guidance other than the possible strain range and operating temperature range when trying to identify materials for actuator applications.

In general, this lack of critical engineering data is the biggest barrier to the utility of HTSMAs. While the origin and mechanism of shape memory is rather well understood in the high temperature alloys and the transformation temperatures well defined, most engineering aspects of these materials have not been determined. Almost no research has been done in identifying the operational limits of HTSMAs including the effects of temperature and stress on strain recovery, work output, and fatigue life. Furthermore, these new alloys will need to be more than just functional materials. They will have to be robust to handle the challenges associated with an elevated operating temperature including long term stability of the alloy together with its microstructure, phase structure, and resistance to oxidation.

Since actuators are usually highly loaded, relaxation and creep is also a concern. But the concern lies deeper than just holding dimensional tolerances. The recoverable strain and the amount of work that a shape memory actuator can perform depend directly on the materials resistance to dislocation mediated deformation. The higher the resistance the material has to dislocation motion, the greater the amount of work that can be performed during the martensite to austenite transformation. Additionally, anything done to strengthen the alloy against dislocation processes must be accomplished without affecting the properties giving rise to the shape memory affect, in other words, without significantly increasing the stress for reorientation/detwinning, stress induced martensitic transformation, and reversibility. This requirement is also coupled with the need for the material to possess adequate ductility and toughness to survive processing and typical damage during use. The gaps in Tables 2 and 3 are yet another indicator of the tremendous amount of research that must take place before HTSMAs become commonly accepted as an actuation alternative.

Finally, to further expedite commercialisation of HTSMAs, models that accurately describe the engineering aspects of HTSMAs should be developed. In addition to existing SMA models, the exposure to high temperature creates a series of new variables, such as creep and viscoplasticity, and the effects of extensive plasticity, must be accounted for.

While progress in developing HTSMAs in general has been slow, recent concentrated efforts on particular alloy systems such as the Ni–Ti–Pd and Ni–Ti–Pt have led to the development of specific alloys and microstructures with a reasonable balance of properties for use between 100 and 300°C. In addition, component demonstrations utilising these materials have shown, at first cut, that HTSMAs can be viable actuator materials.[95,323,324,327,329,331,340] While efforts are being made to optimise particular alloys in these systems, future research also needs to be focused on developing alternative systems composed of less costly raw materials. Furthermore, use of these alloys will begin to escalate once a commercial source of material is available and new applications will naturally evolve as engineers become accustomed to designing with these alternative, solid state actuation devices. Despite the fact that development of SMAs with an acceptable balance of properties for elevated temperature application is a daunting metallurgical challenge, interest in HTSMAs is growing in such areas as aerospace, automotive, fastening, and down hole energy exploration. This is because of the fact they fulfil a need for compact actuation that cannot be met by any other known system.

Acknowledgements

The corresponding author would like to acknowledge the financial support from: the NASA Fundamental Aeronautics Program, Subsonic Fixed Wing Project through cooperative agreement no. NNX07AB56A; National Science Foundation – Division of Chemical, Bioengineering, Environmental, and Transport Systems – Bioengineering Program, grant no. 0731133; and National Science Foundation – Division of Materials Research – Metallic Materials Program, grant no. 0805293, all of which were instrumental in the preparation of this review. RDN would like to acknowledge support from the NASA Fundamental Aeronautics Program, Supersonics and Subsonic Fixed Wing Projects.

References

1. C. Zhang, R. Zee and P. Thoma: *Intersoc. Energy Convers. Eng. Conf.*, 1996, **1**, 239.
2. J. van Humbeeck: *Trans. ASME*, 1999, **121**, 98.
3. K. Otsuka and X. Ren: *Intermetallics*, 1999, **7**, 511.
4. Yu. Koval: *Mater. Sci. Forum*, 2000, **327–328**, 271.
5. D. Grummon: *JOM*, 2003, **55**, 24.
6. G. Firstov, J. van Humbeeck and Yu. Koval: *J. Intell. Mater. Syst. Struct.*, 2006, **17**, 1041.
7. R. Noebe, T. Biles and S. Padula: in 'Advanced structural materials: properties, design optimization, and applications', (ed. W. Soboyejo and T. Srivastan), 145; 2007, Boca Raton, FL, CRC Press.
8. K. Bhattacharya and R. V. Kohn: *Acta Mater.*, 1996, **44**, 529.
9. K. Shimizu and T. Tadaki: in 'Shape memory alloys', (ed. H. Funakubo) 1–27; 1987, New York, Gordon and Breach.
10. Z. Nishiyama: 'Martensitic transformations'; 1978, New York, Academic Press.
11. L. Kaufman: *Prog. Met. Phys.*, 1958, **7**, 165.
12. K. Otsuka and X. Ren: *Prog. Mater. Sci.*, 2005, **50**, 511.
13. Y. T. Cheng and D. S. Grummon: in 'Micro and nano testing of materials and devices', (ed. F. Q. Yang and C. M. James), 71; 2008, New York, Springer.
14. R. W. Cahn: *Acta Metall.*, 1953, **1**, 49.
15. J. W. Christian and S. Mahajan: *Prog. Mater. Sci.*, 1995, **39**, 1.
16. M. S. Wechsler, D. S. Lieberman and T. A. Read: *Trans. AIME*, 1953, **197**, 1503.
17. J. K. Mackenzie and J. S. Bowles: *Acta Metall.*, 1957, **5**, 137.
18. H. Sehitoglu, I. Karaman, R. Anderson, X. Zhang, K. Gall, H. J. Maier and Y. Chumlyakov: *Acta Mater.*, 2000, **48**, 3311.
19. T. Saburi and S. Nenno: Proc. Int. Conf. on 'Solid–solid phase transformations', (ed. H. Aaronson *et al*), 1455; 1981, Warrendale, PA, AIME.

20. K. Otsuka: *Mater. Sci. Forum*, 1990, **56–58**, 393.
21. T. Saburi and C. M. Wayman: *Acta Metall.*, 1979, **27**, 979.
22. S. Miyazaki, K. Otsuka and C. M. Wayman: *Acta Metall.*, 1989, **37**, 1873.
23. J. M. Ball and R. D. James: *Arch. Ration. Mech. Anal.*, 1987, **100**, 13.
24. K. Madangopal: *Acta Mater.*, 1997, **45**, 5347.
25. P. K. Kumar and D. Lagoudas: in 'Shape memory alloys: modeling and engineering applications', (ed. D. Lagoudas), 1; 2008, New York, Springer.
26. I. Saburi and S. Nenno: *Scr. Metall.*, 1974, **8**, 1363.
27. Y. Liu, Y. Liu and J. van Humbeeck: *Acta Mater.*, 1999, **47**, 199.
28. S. Eucken and T. W. Duerig: *Acta Metall.*, 1989, **37**, 2245.
29. M. Nishida and T. Honma: *Scr. Metall.*, 1984, **18**, 1293.
30. J. Pons, M. Sade, F. C. Lovey and E. Cesari: *Mater. Trans.*, 1993, **34**, 888.
31. T. Fukuda, A. Deguchi, T. Kakeshita and T. Saburi: *Mater. Trans.*, 1997, **38**, 514.
32. K. Otsuka and X. Ren: *Mater. Sci. Eng. A*, 2001, **A312**, 207.
33. X. Ren and K. Otsuka: *Nature*, 1997, **389**, 579.
34. D. J. Hartl and D. Lagoudas: in 'Shape memory alloys: modeling and engineering applications', (ed. Lagoudas), 53; 2008, New York, Springer.
35. H. Sehitoglu, X. Y. Zhang, Y. I. Chumlyakov, I. Karaman, K. Gall and H. J. Maier: Proc. IUTAM Symp. on 'Mechanics of martensitic phase transformation in solids', (ed. Q. P. Sun), 101; 2002, Dordrecht, Kluwer Academic Press.
36. K. Bhattacharya, S. Conti, G. Zanzotto and J. Zimmer: *Nature*, 2004, **428**, 55.
37. K. Bhattacharya and R. V. Kohn: *Acta Mater.*, 1996, **44**, 529.
38. Y. Ma, C. Jiang, Y. Li, H. Xu, C. Wang and X. Liu: *Acta Mater.*, 2007, **55**, 1533.
39. J. Cui, Y. S. Chu, O. O. Famodu, Y. Furuya, J. Hattrick-Simpers, R. D. James, A. Ludwig, S. Thienhaus, M. Wuttig, Z. Zhang and I. Takeuchi: *Nature Mater.*, 2006, **5**, 286.
40. R. F. Hamilton, H. Sehitoglu, Y. Chumlyakov and H. J. Maier: *Acta Mater.*, 2004, **52**, 3383.
41. H. Sehitoglu, R. Hamilton, D. Canadinc, X. Y. Zhang, K. Gall, I. Karaman, Y. I. Chumlyakov and H. J. Maier: *Metall. Mater. Trans. A*, 2003, **34**, 5.
42. K. Gall, H. Sehitoglu, Y. I. Chumlyakov and I. V. Kireeva: *Acta Mater.*, 1999, **47**, 1203.
43. V. M. Segal: *Mater. Sci. Eng. A*, 1998, **A197**, 157.
44. V. M. Segal: *Mater. Sci. Eng. A*, 1999, **A271**, 322.
45. V. M. Segal: *Mater. Sci. Eng. A*, 2004, **A386**, 269.
46. M. E. Kassner and M. T. Perez-Prado: *Prog. Mater. Sci.*, 2000, **45**, 1.
47. S. Takeuchi and A. S. Argon: *J. Mater. Sci.*, 1975, **11**, 1542.
48. F. R. N. Nabarro and H. L. de Villers: 'The physics of creep'; 1995, London, Taylor & Francis.
49. G. Eggeler, J. Khalil-Allafi, K. Neuking and A. Dlouhy: *Z. Metall.*, 2002, **93**, 654.
50. C. Lexcellent, P. Robin, J. Bernardini, D. L. Beke and P. Olier: *Materialwiss. Werkst.*, 2005, **36**, 509.
51. A. K. Mukherjee: *J. Appl. Phys.*, 1968, **39**, 2201.
52. H. Kato, T. Yamamoto, S. Hashimoto and S. Miura: *Mater. Trans.*, 1999, **40**, 343.
53. S. M. Oppenheimer, A. R. Yung and D. C. Dunand: *Scr. Mater.*, 2007, **57**, 377.
54. D. Abu Judom, P. Thoma, M. Kao and D. Angst: 'High transformation temperature shape memory alloy', US patent no. 5114504, 1992.
55. Y. Au and C. M. Wayman: *Scr. Metall.* 1972, **6**, 1209.
56. Y. Kim and C. M. Wayman: *Scr. Metall. Mater.*, 1990, **24**, 245.
57. C. L. Chu, S. K. Wu and Y. C. Yen: *Mater. Sci. Eng. A*, 1996, **A216**, 193.
58. T. H. Nam, D. W. Chung, H. W. Lee, J. H. Kim and M. S. Choi: *J. Mater. Sci.*, 2003, **38**, 1333.
59. L. Zhang, C. Xie and J. Wu: *Mater. Charact.*, 2007, **58**, 471.
60. K. S. Kim, K. K. Jee, W. C. Kim, W. Y. Jang and S. H. Han: *Mater. Sci. Eng. A*, 2008, **A481**, 658.
61. J. H. Ko and D. B. Lee: *Mater. Sci. Forum*, 2005, **475–479**, 853.
62. S. Shabalovskaya: *Bio-Med. Mater. Eng.*, 2002, **12**, 69.
63. C. H. Xu, X. Q. Ma, S. Q. Shi and C. H. Woo: *Mater. Sci. Eng. A*, 2004, **A371**, 45.
64. C. M. Wayman: Proc. Int. Conf. on 'Martensitic transformation', (ed. K. Shimizu), 645; 1987, Nara, The Japan Institute of Metals.
65. T. Kakeshita, K. Shimizu, S. Nakamichi, R. Tanaka and S. Endo: *Mater. Trans.*, 1982, **33**, 1.
66. V. Khachin: *Rev. Phys. Appl.*, 1989, **24**, 733.
67. H. Donkersloot and J. van Vucht: *J. Less-Common Met.*, 1970, **20**, 83.
68. E. Eckelmeyer: *Scr. Metall.*, 1976, **10**, 667.
69. P. G. Lindquist and C. M. Wayman: in 'Engineering aspects of shape-memory alloys', (ed. T. W. Duerig *et al*), 58–68; 1990, London, Butterworth-Heinemann.
70. Y. Lo and S. Wu: *Scr. Metall. Mater.*, 1991, **27**, 1097.
71. D. Golberg, Y. Xu, Y. Murakami, K. Otsuka, T. Ueki and H. Horikawa: *Mater. Lett.*, 1995, **22**, 241.
72. Y. Xu, S. Shimizu, Y. Suzuki, K. Otsuka, T. Ueki and K. Mitose: *Acta Mater.*, 1996, **45**, 1503.
73. Y. Suzuki, Y. Xu, S. Morito, K. Otsuka and K. Mitose: *Mater. Lett.*, 1998, **36**, 85.
74. K. Otsuka, K. Oda, Y. Ueno and M. Piao: *Scr. Metall. Mater.*, 1993, **29**, 1355.
75. D. Golberg, Y. Xu, Y. Murakami, S. Morito, K. Otsuka, T. Ueki and H. Horikawa: *Scr. Metall. Mater.*, 1994, **30**, 1349.
76. S. Shimizu, Y. Xu, E. Okunishi, S. Tanaka, K. Otsuka and K. Mitose: *Mater. Lett.*, 1998, **34**, 23.
77. W. Yang and D. Mikkola: *Scr. Metall. Mater.*, 1993, **28**, 161.
78. G. Bigelow: "Effects of palladium Content, Quaternary Alloying, and Thermomechanical Processing on the Behavior of Ni-Ti-Pd Shape Memory Alloys For Actuator Applications," MSc thesis, Colorado School of Mines, Golden, CO, USA, June 2006.
79. Q. Tian, J. Wu and Y. Cheng: *J. Mater. Sci. Technol.*, 2003, **19**, 179.
80. K. C. Atli, I. Karaman, R. D. Noebe, A. Garg, Y. I. Chumlyakov and I. V. Kireeva: *Metall. Mater. Trans. A*, 2010, in press.
81. D. Golberg, Y. Xu, Y. Murakami, S. Morito and K. Otsuka: *Intermetallics*, 1995, **3**, 35.
82. H. C. Lin, S. K. Wu, T. S. Chou and H. P. Kao: *Acta Metall. Mater.*, 1991, **39**, 2069.
83. J. Wu and Q. Tian: *Intermetallics*, 2003, **11**, 773.
84. R. D. Noebe, S. A. Padula, G. S. Bigelow, O. Rios, A. Garg and B. Lerch: *Proc. SPIE*, 2006, **6170**, 617010.
85. Y. Shirakawa, Y. Morizono and M. Nishida: *Mater. Sci. Forum*, 2000, **327–328**, 171.
86. M. Nagasako, M. Nishida, Y. Murakami and D. Shindo: *Mater. Sci. Eng. A*, 2006, **A438–440**, 848.
87. X. Meng, W. Cai, F. Chen and L. Zhao: *Scr. Mater.*, 2006, **54**, 1599.
88. Q. Tian and J. Wu: *Mater. Sci. Eng. A*, 2002, **A325**, 249.
89. Q. Tian and J. Wu: *Intermetallic*, 2002, **10**, 675.
90. H. Xu, S. Hu and S. Gong: *Z. Metalkd*, 2000, **91**, 468.
91. W. Cai and K. Otsuka: *J. Mater. Sci. Technol.*, 2001, **17**, 359.
92. W. Cai, S. Tanaka and K. Otsuka: *Mater. Sci. Forum*, 2000, **327–328**, 279.
93. G. S. Bigelow, S. A. Padula II, A. Garg and R. D. Noebe: *Proc. SPIE*, 2007, **6526**, 65262B.
94. G. S. Bigelow, R. D. Noebe, S. A. Padula and A. Garg: 'Development and characterization of improved high temperature shape memory alloys by solid solution strengthening and thermomechanical processing of NiTiPd alloys', Proc. Int. Conf. on 'Shape memory and superelastic technologies', 113; 2008, Materials Park, OH, ASM International.
95. S. A. Padula, R. D. Noebe, G. S. Bigelow, D. Culley, M. Stevens, N. D. Penney Gaydosh, T. Quackenbush, B. Carpenter: Proc. 48th Conf. on 'Structures, structural dynamics, and materials', 2007–2196; 2007, Honolulu, HI, AIAA.
96. W. B. Cross, A. H. Kariotis and F. J. Stimler: 'NITINOL characterization study', NASA CR-1433, 1969.
97. T. W. Duerig, D. Stockel and A. Keeley: in 'Engineering aspects of shape memory alloys', (ed. T. W. Duerig et al.), 181; 1990, Boston, MA, Butterworth-Heinemann.
98. S. A. Padula, G. S. Bigelow, R. D. Noebe, D. Gaydosh and A. Garg: 'Challenges and progress in the development of high-temperature shape memory alloys based on NiTiX compositions for high-force actuator applications', Proc. Int. Conf. on 'Shape memory and superelastic technologies', 787; 2008, Materials Park, OH, ASM International.
99. P. Kumar and D. C. Lagoudas: *Acta Mater.*, 2101, **58**, 1618.
100. O. Rios, R. D. Noebe, T. Biles, A. Garg, A. Palczer, D. Scheiman, H. J. Seifert and M. Kaufman: *Proc. SPIE*, 2005, **5761**, 376–387.
101. P. G. Lindquist: "Structure and transformation behavior of martensitic Ti - (Ni,Pd) and Ti - (Ni,Pt) alloys," PhD thesis, University of Illinois, Urbana-Champaign, IL, USA, 1988.
102. L. L. Meisner and V. P. Sivokha: *Physica B, 2004*, **344B**, 93.
103. M. Hosoda, M. Tsuji, Y. Takahashi, T. Inamura, K. Wakashima, Y. Yamabe-Mitarai, S. Miyazaki and K. Inoue: *Mater. Sci. Forum*, 2003, **426–432**, 2333.

104. R. D. Noebe, D. Gaydosh, S. Padula, A. Garg, T. Biles and M. Nathal: *Proc. SPIE*, 2005, **5761**, 364–375.
105. R. D. Noebe, S. Draper, D. Gaydosh, A. Garg, B. Lerch, N. Penney, G. S. Bigelow, S. Padula and J. Brown: 'Effect of thermomechanical processing on the microstructure, properties, and work behavior of a $Ti_{50{\cdot}5}Ni_{29{\cdot}5}Pt_{20}$ high-temperature shape memory alloy', Proc. Int. Conf. on 'Shape memory and superelastic technologies', 409; 2008, Materials Park, OH, ASM International.
106. N. Morgan: ''The stability of NiTi shape memory alloys and actuator applications,'' PhD thesis, Cranfield University, England, UK, 1999.
107. J. L. Smialek, D. L. Humphrey and R. D. Noebe: 'Oxidation kinetics of a NiTiPt high temperature shape memory alloy', NASA/TM–2007-214697, 2007.
108. E. Quandt, C. Halene, H. Holleck, K. Feit, M. Kohl, P. Scholossmacher, A. Skokan and K. Skrobanek: *Sens. Actuators A*, 1996, **53A**, 434.
109. Y. Fu and H. Du: *J. Mater. Sci. Lett.*, 2003, **22**, 531.
110. J. Lee, B. Thomas and A. Rabiei: *Thin Solid Films*, 2006, **500**, 309.
111. M. Panduranga, D. Shin and G. Carman: *Thin Solid Films*, 2006, **515**, 1938.
112. P. Schlossmacher: *Mater. Lett.*, 1997, **31**, 119.
113. T. Sawaguchi, M. Sato and A. Ishida: *Mater. Sci. Eng. A*, 2002, **A332**, 47.
114. K. Mohanchandra, D. Shin and G. Carman: *Smart Mater. Struct.*, 2005, **14**, S31 G 2.
115. E. Baldwin, B. Thomas, J. Lee and A. Rabiei: *Surf. Coat. Technol.*, 2005, **200**, 2571.
116. E. Baldwin, A. Rabiei: *Proc. Mater. Res. Soc. Symp.*, 2004, **785**, 225.
117. B. Kockar: ''Shape memory behavior of ultrafine grained NiTi and TiNiPd shape memory alloys,'' PhD thesis, Texas A&M University, College Station, TX, USA, 2007.
118. D. Angst, P. Thoma and M. Kao: *J. Phys. IV*, 1995, **C8**, 747.
119. S. Besseghini, E. Villa and A. Tuissi: *Mater. Sci. Eng. A*, 1999, **A273–275**, 390.
120. Y. Wang, Y. Zheng, W. Cai and L Zhao: *Scr. Mater.*, 1999, **40**, 1327.
121. P. Olier, J. Brachet, J. Bechade, C. Foucher and G. Guenin: *J. Phys. IV*, 1995, **C8**, 741.
122. B. Kockar, I. Karaman, J. Kim and Y. Chumlyakov: *Scr. Mater.*, 2006, **54**, 2203.
123. J. Mulder: ''Investigation on high temperature shape memory alloys using Ni-Ti-Zr and Ni-Ti-Hf system,'' PhD thesis, University of Twente, Enschede, The Netherlands, 1994.
124. S. Hsieh and S. Wu: *Mater. Charact.*, 1998, **41**, 151.
125. Z. Pu, H. Tseng and K. Wu: *Proc. SPIE*, 1995, **2441**, 171.
126. P. Thoma and J. Boehm: *Mater. Sci. Eng. A*, 1999, **A273–275**, 385.
127. M. Zarinejad, Y. Liu and T. J. White: *Intermetallics*, 2008, **16**, 876.
128. Y. Tong, F. Chen, B. Tian, L. Li and Y. Zheng: *Mater. Lett.*, 2009, **63**, 1869.
129. S. Han, W. Zou, S. Jin, Z. Zhang and D. Yang: *Scr. Metall. Mater.*, 1995, **32**, 1441.
130. L. Meisner, V. Grishkov and V. Sivokha: Proc. Int. Symp. on 'Shape memory materials', 263; 1994, Beijing, International Academic Publishers.
131. X. Meng, Y. Zheng, Z. Wang and L. Zhao: *Scr. Mater.*, 2000, **42**, 341.
132. S. Hsieh and S. Wu: *J. Alloys Compd*, 1998, **266**, 276.
133. X. Meng, Y. Zheng, Z. Wang and L. Zhao: *Mater. Lett.*, 2000, **45**, 128.
134. V. Sivokha and L. Meisner: *Physica B*, 2001, **296B**, 329.
135. Z. Feng, B. Gao, J. Wang, D. Qian and Y. Liu: *Mater. Sci. Forum*, 2002, **394–395**, 365.
136. S. Russell and F. Sczerzenie: *Proc. Mater. Res. Soc. Symp.*, 1995, **360**, 455.
137. X. Meng, Y. Zheng, W. Cai and L. Zhao: *J. Alloys Compd*, 2004, **372**, 180.
138. S. Hsieh and W. Chang: *J. Mater. Sci.*, 2002, **37**, 2851.
139. T. Sawaguchi, M. Sato and A. Ishida: *Metall. Mater. Trans. A*, 2004, **35A**, 111.
140. S. Hsieh and S. Wu: *Mater. Charact.*, 2000, **45**, 143.
141. X. Meng, Y. Tong, K. Lau, W. Cai, L. Zhou and L. Zhao: *Mater. Lett.*, 2002, **57**, 452.
142. G. Firstov, J. van Humbeeck and Yu. Koval: *Scr. Mater.*, 2004, **50**, 243.
143. X. Meng, W. Cai, Y. Zheng, Y. Tong, L. Zhao and L. Zhou: *Mater. Lett.*, 2002, **55**, 111.
144. X. Meng, W. Cai, Y. Zheng and L. Zhao: *Mater. Sci. Eng. A*, 2006, **A438–440**, 666.
145. A. Sandu, K. Tsuchiya, S. Yamamoto, Y. Todaka and M. Umemoto: *Scr. Mater.*, 2006, **55**, 1079.
146. A. Sandu, K. Tsuchiya, M. Tabuchi, S. Yamamoto, Y. Todaka and M. Umemoto: *Mater. Trans.*, 2007, **48**, 432.
147. T. H. Nam, T. Saburi and K. Shimizu: *Mater. Trans.*, 1990, **31**, 959.
148. X. Meng, W. Cai, K. Lau, L. Zhao and L. Zhou: *Intermetallics*, 2005, **13**, 197.
149. F. Dalle, V. Kolomytsev, P. Ochin and R. Portier: *Scr. Mater.*, 2001, **44**, 929.
150. Y. Tong, Y. Liu, J. Miao and L. Zhao: *Scr. Mater.*, 2005, **52**, 983.
151. S. Sanjabi, Y. Cao and Z. Barber: *Sens. Actuators A*, 2005, **121A**, 543.
152. A. Manca, A. Shelyakov and G. Airoldi: *Mater. Trans.*, 2003, **44**, 1219.
153. R. Santamarta, C. Seguí, J. Pons and E. Cesari: *Scr. Mater.*, 1999, **41**, 867.
154. V. Kolomytsev, M. Babanly, R. Musienko, A. Sezonenko, P. Ochin, A. Dezellus, P. Plaindoux, R. Portier and P. Vermaut: *J. Phys. IV*, 2001, **11**, 457.
155. P. Ochin, V. Kolomytsev, A. Pasko, A. Sezonenko, P. Vermaut, F. Prima and R. Portier: *J. Alloys Compd*, 2007, **434–435**, 268.
156. A. Pasko, V. Kolomytsev, M. Babanly, A. Sezonenko, P. Ochin, R. Portier and P. Vermaut: *J. Phys. IV*, 2003, **112**, 1055.
157. G. Monastyrsky, V. Odnosum, J. Van Humbeeck, V. Kolomytsev and Yu. Koval: *Intermetallics*, 2002, **10**, 95.
158. G. Monastyrsky, J. van Humbeeck, V. Kolomytsev and Y. Koval: *Intermetallics*, 2002, **10**, 613
159. B. Bertheville: *J. Alloys Compd*, 2005, **398**, 94.
160. B. Bertheville and J. Bidaux: *J. Alloys Compd*, 2005, **387**, 211.
161. P. Swann and H. Warlimont: *Acta Metall.*, 1963, **11**, 511.
162. T. Tadaki: in 'Shape memory material', (ed. K. Otsuka and C. Wayman), 97; 1998, Cambridge, Cambridge University Press.
163. H. Kato, R. Stalmans and J. van Humbeeck: *Mater. Trans.*, 1998, **39**, 378.
164. G. Kannarpady and A. Bhattacharyya: *Mater. Sci. Eng. A*, 2006, **A438–440**, 719.
165. H. Sakamoto and K. Shimizu: *ISIJ Int.*, 1989, **29**, 395.
166. H. Morawiec, J. Lelatko, D. Stroz and M. Gigla: *Mater. Sci. Eng. A*, 1999, **A273–275**, 708.
167. N. Kuwano and C. M. Wayman: *Metall. Trans. A*, 1984, **15A**, 621.
168. V. Recarte, R. B. Perez-Saez, E. H. Bocanegra, M. L. No and J. San Juan: *Metall. Mater. Trans. A*, 2002, **33A**, 2581.
169. K. Otsuka, H. Sakamoto and K. Shimizu: *Acta Metall.*, 1979, **27**, 585.
170. M. Sade, C. Damiani, R. Gastien, F. C. Lovey, J. Malarria and A. Yawny: *Smart Mater. Struct.*, 2007, **16**, S126.
171. F. Dagdelen, T. Gokhan, A. Aydogdu, Y. Aydogdu and O. Adiguzel: *Mater. Lett.*, 2003, **57**, 1079.
172. M. Morris and T. Lipe: *Acta Metall. Mater.*, 1994, **42**, 1583.
173. J. van Humbeeck, D. van Hulle, L. Delaey, J. Ortin, C. Seguí and V. Torra: *Trans. Jpn Inst. Met.*, 1987, **28**, 383.
174. J. van Humbeeck, M. Chandrasekaran and L. Delaey: *ISIJ Int.*, 1989, **29**, 388.
175. J. Font, J. Muntasell, J. Pons and E. Cesari: *J. Mater. Res.*, 1997, **12**, 2288.
176. Y. Gao, M. Zhu and J. Lai: *J. Mater. Sci.*, 1998, **33**, 3579.
177. H. Morawiec and M. Gigla: *J. Phys. IV*, 1995, **C2**, 193.
178. C. Qingfu, I. Hurtado, R. Stalmans and J. van Humbeeck: *J. Phys. IV*, 1995, **C2–5**, 181.
179. K. Adachi, K. Shoji and Y. Hamada: *ISIJ Int.*, 1989, **29**, 378.
180. M. Morris: *Acta Metall. Mater.*, 1992, **40**, 1573.
181. K. Mukunthan and L. Brown: *Metall. Trans. A*, 1988, **19A**, 2921.
182. S. Euken, E. Kobus and E. Hornbogen: *Z. Metalkd*, 1991, **82**, 640.
183. E. Cingolani, J. van Humbeeck and M. Ahlers: *Metall. Mater. Trans. A*, 1999, **30A**, 493.
184. Y. Sutou, T. Omori, R. Kainuma, N. Ono and A. Ishida: *Metall. Mater. Trans. A*, 2002, **33A**, 2817.
185. J. Lelatko, H. Morawiec, Yu. Koval and V. Kolomytsev: *Met. Sci. Heat Treat.*, 1999, **41**, 351.
186. J. Lelatko and H. Morawiec: *J. Phys. IV*, 2001, **11**, 487.
187. J. Lelatko and H. Morawiec: *Mater. Chem. Phys.*, 2003, **81**, 472.
188. H. Morawiec, J. Lelatko, Y. Koval and V. Kolomytsev: *Mater. Sci. Forum*, 2000, **327–328**, 291.

189. J. Guilemany, J. Fernandez and R. Franch: *J. Phys. IV*, 1995, **C8-5**, 979.
190. J. Guilemany, J. Fernandez, R. Franch, A. Benedetti and A. Adorno: *J. Phys. IV*, 1995, **C2–5**, 361.
191. Y. Ma, C. Jiang, L. Deng and H. Xu: *J. Mater. Sci. Technol.*, 2003, **19**, 431.
192. H. Xu: *Mater. Sci. Forum*, 2002, **394–395**, 375.
193. R. Perez-Saez, V. Recarte, M. No, O. Ruano and J. San Juan: *Adv. Eng. Mater.*, 2000, **2**, 49.
194. Z. Li, Z. Pan, N. Tang, Y. Jiang, N. Liu, M. Fang and F. Zheng: *Mater. Sci. Eng. A*, 2006, **A417**, 225.
195. A. Ibarra, P. Rodriguez, V. Recarte, J. Perez-Landazabal, M. No and J. San Juan: *Mater. Sci. Eng. A*, 2004, **370A**, 492.
196. A. Ibarra, J. San Juan, E. Bocanegra, M. No: *Mater. Sci. Eng. A*, 2006, **A438–440**, 782.
197. T. Omori, W. Ito, K. Ando, K. Oikawa, R. Kainuma and A. Ishida: *Mater. Trans.*, 2006, **47**, 2377.
198. T. Omori, Y. Sutou, K. Oikawa, R. Kainuma and A. Ishida: *Mater. Sci. Eng. A*, 2006, **A438–440**, 1045.
199. T. Omori, Y. Sutou, K. Oikawa, R. Kainuma and A. Ishida: *Mater. Trans.*, 2003, **44**, 2732.
200. T. Omori, Y. Sutou, K. Oikawa, R. Kainuma and A. Ishida: *Scr. Mater.*, 2005, **52**, 565
201. K. Ando, T. Omori, J. Sato, Y. Sutou, K. Oikawa, R. Kainuma and A. Ishida: *Mater. Trans.*, 2006, **47**, 2381.
202. A. Sato, E. Chishima, K. Soma and T. Mori: *Acta Metall.*, 1982, **30**, 1177.
203. K. Oikawa, L. Wulff, T. Lijima, F. Gejima, T. Ohmori, A. Fujita, K. Fukumichi, R. Kainuma and K. Ishida: *Appl. Phys. Lett.*, 2001, **79**, 3290.
204. K. Oikawa, T. Ota, Y. Imano, T. Omori, R. Kainuma and K. Ishida: *J. Phase Equil. Diff.*, 2006, **27**, 75.
205. J. Liu, M. Xia, Y. Huang, H. Zheng and J. Li: *J. Alloys Compd*, 2006, **417**, 96.
206. H. Karaca, I. Karaman, D. Lagoudas, H. J. Maier and Y. Chumlyakov: *Scr. Mater.*, 2003, **49**, 831.
207. R. Hamilton, H. Sehitoglu, C. Efstathiou, H. Maier, Y. Chumlyakov and X. Zhang: *Scr. Mater.*, 2005, **53**, 131.
208. R. Hamilton, H. Sehitoglu, C. Efstathiou, H. Maier and Y. Chumlyakov: *Acta Mater.*, 2006, **54**, 587.
209. J. Dadda, H. Maier, I. Karaman, H. Karaca and Y. Chumlyakov: *Scr. Mater.*, 2006, **55**, 663.
210. J. Dadda, D. Canadinc, H. Maier, I. Karaman, H. Karaca and Y. Chumlyakov: *Philos. Mag.*, 2007, **87**, 2313.
211. V. Chernenko, J. Pons, E. Cesari and I. Zasimchuk: *Scr. Mater.*, 2004, **50**, 225.
212. J. A. Monroe, I. Karaman, H. E. Karaca, Y. I. Chumlyakov and H. J. Maier: *Scr. Mater.*, 2010, **62**, 368.
213. H. E. Karaca, I. Karaman, Y. Chumlyakov, D. C. Lagoudas and X. Zhang: *Scr. Mater.*, 2004, **51**, 261.
214. K. Enami and S. Nenno: *Metall. Trans.*, 1971, **2**, 1487.
215. R. Kainuma, H. Ohtani and K. Ishida: *Metall. Mater. Trans. A*, 1996, **27A**, 2445.
216. E. George, C. Liu, J. Horton, C. Sparks, M. Kao, H. Kunsmann and T. King: *Mater. Charact.*, 1997, **39**, 665.
217. S. Kim, M. Oh and D. Wee: *Metall. Mater. Trans. A*, 2003, **34A**, 2089.
218. K. Jee, P. Potapov, S. Song and M. Shin: *Scr. Mater.*, 1997, **36**, 207.
219. K. Ishida, R. Kainuma, N. Ueno and T. Nishizawa: *Metall. Trans. A*, 1991, **22A**, 441.
220. N. Ono, A. Tsukahara, R. Kainuma and K. Ishida: *Mater. Sci. Eng. A*, 1999, **A273–275**, 420.
221. K. Enami and S. Nenno: *Trans. Jpn Inst. Met.*, 1978, **19**, 571.
222. J. Yang and C. M. Wayman: *Intermetallics*, 1994, **2**, 121.
223. J. Yang and C. M. Wayman: *Intermetallics*, 1994, **2**, 111.
224. D. Schryvers and, Y. Ma: *J. Alloys Compd*, 1995, **221**, 227
225. S. Kositsyn, A. Valiullin, N. Kataeva and I. Kositsyna: *Phys. Met. Metall.*, 200, **102**, 391.
226. H. Kim and S. Miyazaki: *Scr. Mater.*, 2004, **50**, 237.
227. D. Schryvers and D. Holland-Moritz: *Mater. Sci. Eng. A*, 1999, **A273–275**, 697.
228. J. Horton, C. Liu and E. George: *Mater. Sci. Eng. A*, 1995, **A192–193**, 873.
229. K. Oikawa, Y. Tanaka, Y. Sutou, T. Omori, F. Luo, R Kainuma and K Ishida: *ISIJ Int.*, 2006, **46**, 1287.
230. R. Kainuma, H. Nakano and K. Ishida: *Metall. Mater. Trans. A*, 1996, **27A**, 4153.
231. K. Adachi and C. M. Wayman: *Metall. Trans. A*, 1985, **16A**, 1567.
232. R. Kainuma, M. Ise, K. Ishikawa, I. Ohnuma and K. Ishida: *J. Alloys Compd*, 1998, **269**, 173.
233. P. Potapov, N. Polyakova, V. Udovenko and E. Svistunova: *Z. Metalkd*, 1995, **87**, 33.
234. P. Potapov: *Met. Sci. Heat Treat.*, 1993, **35**, 520.
235. P. Potapov and V. Udovenko: *J. Phys. IV*, 1995, **C8-5**, 1059.
236. W. S. Yang and D. E. Mikkola: *Proc. Mater. Res. Soc. Symp.*, 1992, **246**, 135.
237. Z. He and J. Zhou: *Mater. Sci. Eng. A*, 2003, **360**, 183.
238. Z. He and J. Zhou: *J. Alloys Compd*, 2003, **358**, 245.
239. T Cheng: *Scr. Metall. Mater.*, 1994, **31**, 1187.
240. H. E. Karaca, I. Karaman, B. Basaran, Y. Chumlyakov and H. J. Maier: *Acta Mater.*, 2006, **54**, 233.
241. H. E. Karaca, I. Karaman, B. Barasan, D. C. Lagoudas, Y. Chumlyakov and H. J. Maier: *Acta Mater.*, 2007, **55**, 4253.
242. L. Manosa and A. Planes: in 'Advances in solid state physics', Vol. 40, 361; 2000, Berlin/Heidelberg, Springer.
243. O. Soderberg, I. Aaltio, Y. Ge, O. Heczko and S. P. Hannula: *Mater. Sci. Eng. A*, 2008, **A481–482**, 80.
244. V. Chernenko, J. Pons, C. Seguí and E. Cesari: *Acta Mater.*, 2002, **50**, 53.
245. C. Jiang, G. Feng, S. Gong and H. Xu: *Mater. Sci. Eng. A*, 2003, **A342**, 231.
246. V. Khovailo, T. Abe, V. Koledov, M. Matsumoto, H. Nakamura, R. Note, M. Ohtsuka, V. Shavrov and T. Takagi: *Mater. Trans.*, 2003, **44**, 2509.
247. T. Liang, C. B. Jiang, H. B. Xu: *Mater. Sci. Eng. A*, 2005, **A402**, 5.
248. H. Xu, Y. Ma and C. Jiang: *Appl. Phys. Lett.*, 2003, **82**, 3206.
249. Y. Lin, Y. Xin, C. Jiang and H. Xu: *Scr. Mater.*, 2004, **51**, 849.
250. Y. Li, Y. Xin, C. Jiang and H. Xu: *Mater. Sci. Eng. A*, 2006, **A438–440**, 978.
251. Y. Xin, L. Yan, L. Chai and H. Xu: *Scr. Mater.*, 2006, **54**, 1139.
252. Y. Ma, S. Yang, W. Jin and X. Liu: *J. Alloys Compd*, 2009, **471**, 570.
253. E. Cesari, J. Font, J. Muntasell, P. Ochin, J. Pons and R. Santamarta: *Scr. Mater.*, 2008, **58**, 259.
254. C. Seguí, J. Pons and E. Cesari: *Acta Mater.*, 2007, **55**, 1649.
255. J. Pons, V. A. Chernenko, R. Santamarta and E. Cesari: *Acta Mater.*, 2000, **48**, 3027.
256. Y. Ma, C. Jiang, G. Feng and H. Xu: *Scr. Mater.*, 2003, **48**, 365.
257. V. Chernenko, V. L'vov, J. Pons and E. Cesari: *J. Appl. Phys.*, 2003, **93**, 2394.
258. K. Tsuchiya, A. Tsutsumi, H. Ohtsuka and M. Umemoto: *Mater. Sci. Eng. A*, 2004, **A378**, 370.
259. Y. Ma, S. Yang, Y. Liu and X. Liu: *Acta Mater.*, 2009, **57**, 3232.
260. J. Sui, Z. Gao, H. Yu, Z. Zhang and W. Cai: *Scr. Mater.*, 2008, **59**, 874.
261. J. Wang and C. Jiang: *Scr. Mater.*, 2010, **62**, 298.
262. Y. Xin, Y. Li, L. Chai and H. Xu: *Scr. Mater.*, 2007, **57**, 599.
263. J. Wang, H. Bai, C. Jiang, Y. Li and H. Xu: *Mater. Sci. Eng. A*, 2010, **A527**, 1975.
264. V. Khovailo, T. Abe, V. Koledov, M. Matsumoto, H. Nakamura, R. Note, M. Ohtsuka, V. Shavrov and T. Takagi: *Mater. Trans.*, 2003, **44**, 2509.
265. C. Seguí, E. Cesari, J. Font, J. Muntasell and V. Chernenko: *Scr. Mater.*, 2005, **53**, 315.
266. C. Liu, W. Cai, X. An, L. X. Gao, Z. Y. Gao and L. C. Zhao: *Mater. Sci. Eng. A*, 2006, **A438–440**, 986.
267. S. Besseghini, E. Villa, F. Passaretti, M. Pini and F. Bonfanti: *Mater. Sci. Eng. A*, 2004, **A378**, 415.
268. E. Semenova and Y. Kudryavtsev: *J. Alloys Compd*, 1994, **203**, 165.
269. Yu. Koval, G. Firstov and A. Kotko: *Scr. Metall. Mater.*, 1992, **27**, 1611.
270. G. Firstov, Yu. Koval and J. van Humbeeck: *J. Phys. IV*, 1997, **C5**, 549.
271. Yu. Koval, G. Firstov, J. van Humbeeck, L. Delaey and W. Jang: *J. Phys. IV*, 1995, **C8**, 1103.
272. R. Waterstrat, J. Stalick, X. Meng-Burany, A. Curzon and M. Estermann: *Scr. Metall. Mater.*, 1995, **33**, 695.
273. G. Firstov, J. van Humbeeck and Yu. Koval: *J. Phys. IV*, 2001, **11**, 481.
274. Yu. Koval, G. Firstov, L. Delaey and J. van Humbeeck: *Scr. Metall. Mater.*, 1994, **31**, 799.
275. G. Firstov, J. van Humbeeck, Yu. Koval and R. Vitchev: *J. Phys. IV*, 2003, **112**, 1075.
276. G. Firstov, J. van Humbeeck and Yu. Koval: *Scr. Mater.*, 2004, **50**, 243.
277. G. Firstov, J. van Humbeeck and Yu. Koval: *Mater. Sci. Eng. A*, 2004, **378**, 2.

278. G. Firstov, Yu. Koval, J. van Humbeeck, R. Portier, P. Vermaut and P. Ochin: *Mater. Sci. Eng. A*, 2006, **A438–440**, 816.
279. T. Maeshima, S. Ushimaru, K. Yamauchi and M. Nishida: *Mater. Sci. Eng. A*, 2006, **A438**, 844.
280. H. Y. Kim, Y. Ohmatsu, J. I. Kim, H. Hosoda and S. Miyazaki: *Mater. Trans.*, 2006, **47**, 518.
281. H. Y. Kim, S. Hashimoto, J. I. Kim, H. Hosoda and S. Miyazaki: *Mater. Trans.*, 2004, **45**, 2443.
282. H. Y. Kim, Y. Ikehara, J. I. Kim, H. Hosoda and S. Miyazaki: *Acta Mater.*, 2006, **54**, 2419.
283. M. Ikeda, S. Y. Komatsu and Y. Nakamura: *Mater. Trans.*, 2004, **45**, 1106.
284. P. J. S. Buenconsejo, H. Y. Kim, H. Hosoda and S. Miyazaki: *Acta Mater.*, 2009, **57**, 1068.
285. D. L. Moffat: "Phase transformations in the titanium-niobium binary alloy system," PhD thesis, University of Wisconsin, Madison, WI, USA, 1985.
286. C. Baker: *Met. Sci. J.*, 1971, **5**, 92
287. H. Y. Kim, S. Hashimoto, J. I. Kim, T. Inamura, H. Hosoda and S. Miyazaki: *Mater. Sci. Eng. A*, 2006, **A417**, 120.
288. P. J. S. Buenconsejo, H. Y. Kim and S. Miyazaki: *Acta Mater.*, 2009, **57**, 2509.
289. D. Ping, Y. Mitarai and F. Yin: *Scr. Mater.*, 2005, **52**, 1287.
290. D. Ping, C. Cui, F. Yin and Y. Yamabe-Mitarai: *Scr. Mater.*, 2006, **54**, 1305.
291. R. Vandermeer, J. Ogle and W. G. Northcutt: *Metall. Trans. A*, 1981, **12A**, 733.
292. R. Vandermeer, J. Ogle and W. Snyder: *Scr. Mater.*, 1978, **12**, 243.
293. A. J. Clarke, R. D. Field, R. J. McCabe, C. M. Cady, R. E. Hackenberg and D. J. Thoma: *Acta Mater.*, 2008, **56**, 2638.
294. E. Semenova: *Powder Metall. MCeram.*, 1997, **36**, 394.
295. S. Wu and C. M. Wayman: *Metallography*, 1987, **20**, 359.
296. K. Enami, K. Morota, M. Hisa and K. Inoue: *Mater. Sci Forum*, 2000, **327–328**, 287.
297. T. Biggs, M. Cortie, M. Witcomb and L. Cornish: *Metall. Mater. Trans. A*, 2001, **32A**, 1881.
298. T. Kawamura, R. Tachi, T. Inamura, H. Hosoda, K. Wakashima, K. Hamada and S. Miyazaki: *Mater. Sci. Eng. A*, 2006, **A438–440**, 383.
299. S. Li, M. Nishida, Y. Murakami and D. Shindo: *J. Phys. IV*, 2003, **112**, 1035.
300. K. Enami, K. Horii and J. Takahashi: *ISIJ Int.*, 1989, **29**, 430.
301. Y. Xu, K. Otsuka, E. Furubayashi, T. Ueki and K. Mitose: *Mater. Lett.*, 1997, **30**, 189.
302. Y. Xu, K. Otsuka, E. Furubayashi and K. Mitose: *Mater. Lett.*, 1998, **34**, 14.
303. W. Cai and K. Otsuka: *Scr. Mater.*, 1999, **41**, 1311.
304. V. Solomon and M. Nishida: *Mater. Trans.*, 2002, **43**, 897.
305. T. Biggs, M. Cortie, M. Witcomb and L. Cornish: *Platin. Met. Rev.*, 2003, **47**, 142.
306. T. Biggs, M. Witcomb and L. Cornish: *Mater. Sci. Eng. A*, 1999, **A273–275**, 204.
307. Y. Yamabe-Mitarai, T. Hara and H. Hosoda: *Mater. Sci. Forum*, 2003, **426–432**, 2267.
308. Y. Yamabe-Mitarai, T. Hara, S. Miura and H. Hosoda: *Mater. Trans.*, 2006, **47**, 650.
309. B. H. Chen and H. F. Franzen: *J. Less Common Met.*, 1990, **157**, 37.
310. R. Fonda, H. Jones and R. Vandermeer: *Scr. Mater.*, 1998, **39**, 1031.
311. Z. He, J. Zhou and Y. Furuya: *Mater. Sci. Eng. A*, 2003, **A348**, 36.
312. K. Chastaing, A. Denquin, R. Portier and P. Vermaut: *Mater. Sci. Eng. A*, 2008, **A481–482**, 702.
313. Z. He, J. Zhou and Y. Furuya: *Rare Met. Mater. Eng.*, 2003, **33**, 703.
314. R. Fonda and H. Jones: *Mater. Sci. Eng. A*, 1999, **A273–275**, 275.
315. X. Gao, Y. Zheng, W. Cai, S. Zhang and L. Zhao: *J. Mater. Sci. Technol.*, 2004, **20**, 97.
316. Z. He, F. Wang and J. Zhou: *J. Mater. Sci. Technol.*, 2006, **22**, 634.
317. X. Gao, W. Cai, Y. Zheng and L. Zhao: *Mater. Sci. Eng. A*, 2006, **A438–440**, 862.
318. K. Otsuka and T. Kakeshita: *MRS Bull.*, Feb. 2002, 91.
319. J. van Humbeeck: *Mater. Sci. Eng. A*, 1999, **A273–275**, 134.
320. S. Hirose, K. Ikuta and Y. Umetani: *Adv. Robot.*, 1989, **3**, 3.
321. C. Mavroidis: *Res. Nondestruct. Eval.*, 2002, **14**, 1.
322. I. Ohkata, Y. Suzuki: in 'Shape memory materials', (ed. K. Otsuka and C. M. Wayman), 240; 1998, Cambridge, Cambridge University Press.
323. M. Kohl, D. Dittman, E. Quandt and B. Winzek: *Sens. Actuators A*, 2000, **83A**, 214.
324. W. Huang: *Mater. Des.*, 2002, **23**, 11.
325. J. Webster: *Proc. SPIE*, 2006, **6171**, 61710F.
326. E. Chau, C. Friend, D. Allen, J. Hora and J. Webster: *Mater. Sci. Eng. A*, 2006, **A438–440**, 589.
327. J. H. Mabe, F. T. Calkins and G. W. Butler: 'Boeing's variable geometry chevron, morphing, aerostructure for jet engine noise reduction,' Proc. 47th Conf. on 'Structures, structural dynamics, and materials', 2006–2142; 2006, Newport, RI, AIAA.
328. F. T. Calkins, J. H. Mabe and G. W. Butler: *Proc. SPIE*, 2006, **6171**, 61710O.
329. T. R. Quackenbush: 'High temperature smart structures technology for engine noise reduction', Contract no. NNC06CA03C, NASA Glenn Research Center, Cleveland, OH, USA, April 2008.
330. T. R. Quackenbush, B. F. Carpenter, A. H. Boschitsch and P. V. Danilov: *Proc. SPIE*, 2008, **6930**, 6930-25.
331. A. Stebner, S. A. Padula, R. D. Noebe and D. D. Quinn: *Proc. SPIE*, 2008, **6928**, 6928-36.
332. P. Barooah and N. Rey: *Proc. SPIE*, 2002, **4693**, 384–395.
333. J. H. Mabe, F. T. Calkins and M. B. Alkislar: *Proc. SPIE*, 2008, **6930**, 6930-29.
334. J. A. DeCastro, K. J. Melcher, R. D. Noebe and D. J. Gaydosh: *Smart Mater. Struct.*, 2007, **16**, 2080–2090.
335. J. A. DeCastro, K. J. Melcher and R. D. Noebe: Proc. 41st AIAA Conf., July 2005, Tucson, AZ, USA, AIAA, Paper AIAA-2005-3988.
336. L. Schetky: *Mater. Des.*, 1991, **12**, 29.
337. D. Stoeckel: *Mater. Des.*, 1990, **11**, 302.
338. J. G. Gore, L. Chandresekaran, A. R. Bowles, M. G. Maylin, D. Forsyth and M. Byers: *Proc. SPIE*, 2008, **6930**, 6930-25.
339. J. Gore, A. Bowles, M. Maylin, L. Chandrasekaran, D. Forsyth and M. Buyers: *Proc. SPIE*, 2008, **6930**, 69300R.
340. Y. Liu, M. Kohl, K. Okutsu and S. Miyazaki: *Mater. Sci. Eng. A*, 2004, **A378**, 205.
341. M. A. Huff, W. L. Bernard, F. J. Lisy and T. S. Prince: US patent no. 6622558, 2003.
342. K. Mizuuchi, K. Inoue, K. Hamada, K. Yamauchi, K. Enami, M. Sugioka, M. Itami and Y. Okanda: *Mater. Sci. Eng. A*, 2002, **A329–331**, 557.
343. J. van Humbeek: *J. Alloys Compd*, 2003, **355**, 58–64.
344. K. P. Duffy, S. A. Padula and D. A. Scheiman: *Proc. SPIE*, 2008, **6929**, 6929–48.
345. MIGA Motor Company: http://www.migamotors.com/Products.html.
346. R. Zeyfang, R. Martin and H. Conrad: *Mater. Sci. Eng.*, 1971, **8**, 134.